BNL 50536
ISA 76-13

9-29

A. 1155

135
6-23-77

MAGNETIC FIELDS FOR TRANSPORTING CHARGED BEAMS

G. PARZEN

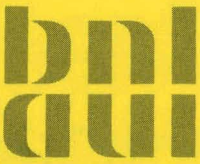

January 1976

BROOKHAVEN NATIONAL LABORATORY
ASSOCIATED UNIVERSITIES, INC.
UNDER CONTRACT NO. EY-76-C-02-0016 WITH THE
UNITED STATES ENERGY RESEARCH AND DEVELOPMENT ADMINISTRATION

DISCLAIMER

BNL 50536
ISA 76-13
(Particle Accelerators and High-Voltage
Machines - TID-4500)

MAGNETIC FIELDS FOR TRANSPORTING CHARGED BEAMS

G. PARZEN

January 1976

BROOKHAVEN NATIONAL LABORATORY
UPTON, NEW YORK 11973

NOTICE

Printed in the United States of America
Available from
National Technical Information Service
U.S. Department of Commerce
5285 Port Royal Road
Springfield, VA 22161

Price: Printed Copy $5.00; Microfiche $3.00

April 1977 575 copies

ABSTRACT

The transport of charged particle beams requires magnetic fields that must be shaped correctly and very accurately. During the last 20 years or so, many studies have been made, both analytically and through the use of computer programs, of various magnetic shapes that have proved to be useful. Many of the results for magnetic field shapes can be applied equally well to electric field shapes. This report gathers together the results that have more general significance and would be useful in designing a configuration to produce a desired magnetic field shape.

The field shapes studied include the fields in dipoles, quadrupoles, sextupoles, octupoles, septum magnets, combined-function magnets, and electrostatic septums. Where possible, empirical formulas are proposed, based on computer and analytical studies and on magnetic field measurements. These empirical formulas are often easier to use than analytical formulas and often include effects that are difficult to compute analytically. In addition, results given in the form of tables and graphs serve as illustrative examples.

The field shapes studied include uniform fields produced by window-frame magnets, C-magnets, H-magnets, and cosine magnets; linear fields produced by various types of quadrupoles; quadratic and cubic fields produced by sextupoles and octupoles; combinations of uniform and linear fields; and septum fields with sharp boundaries.

ACKNOWLEDGMENTS

I would like to thank Kurt Jellett for his help with many of the magnet computer studies. I am indebted to Brookhaven National Laboratory for granting me the leave during which this report was written and to Dr. Mark Barton and Dr. Harald Hahn for their cooperation and understanding. I also wish to thank Marion R. Davis for the particularly fine typing of the original manuscript and for her enthusiastic support during the writing of it.

CONTENTS

CONTENTS

1. BENDING MAGNETS

In a bending magnet the desired magnetic field is uniform across the magnet's aperture. There are two well-known two-dimensional current and iron configurations that give a uniform field. The first is the rectangular window-frame magnet (Figure 1.1-A), with rectangular current blocks having a uniform current density. The second is the circular cosine magnet (Figure 1.3-A), in which the current density varies as the cosine of the azimuthal angle. Bending magnets can be built by approximating the iron and current configurations in these two well-known solutions of Maxwell's equation.

One can also start with some other configuration, such as the H-magnet (Figure ... A), and gradually shape the iron pole by adding shims at its edge or by adding correction windings. Any reasonable iron and current configuration can probably be used; the field can be made as close as desired to a uniform field by adding a sufficient number of corrections. The problem of producing a magnet with a uniform field thus has many solutions.

The four most commonly used approaches, the window-frame magnet, the H-magnet, the cosine magnet, and the C-magnet, are described below.

1.1 Window-Frame Magnets

The window-frame magnet shown in Figure 1.1-A is a simple bending magnet or dipole magnet with a uniform magnetic field. For the case of iron with infinite permeability and a uniform current density in the rectangular conductors that completely fill the aperture, the problem can be solved analytically. On the median plane of the magnet, the vertical field B is found to be uniform until the conductor is reached, and there the field drops linearly to zero within the conductor.

1.1.1 Iron Saturation Effects in Window-Frame Magnets. If the permeability of the iron is not infinite, then even at low magnetic fields the field is not strictly uniform. The finite permeability causes the field to be lower at the center of the magnet.

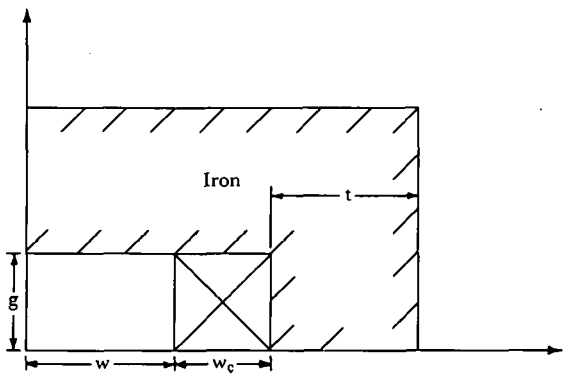

1.1-A. Window-frame magnet geometry.

One way to describe the field variation is to expand the vertical field in the median plane into its multipoles:

$$B = B_0(1 + b_1 x + b_2 x^2 + \ldots),$$

where x is the horizontal distance from the center of the magnet.

Because of the magnet symmetry, the odd b_n vanish and the sextupole term b_2 has a small positive value, which shows that the field increases with distance from the center of the magnet.

Computer studies show that b_2 varies linearly with γ ($\gamma = 1/\mu$, where μ is the permeability of the iron). The magnitude of b_2 can be roughly estimated from

$$g^2 b_2 \sim 0.2\gamma g/(w + w_c/2), \qquad (1.1.1\text{-}1)$$

where g is the vertical half-gap of the magnet, w is the horizontal half-width of the aperture, and w_c is the width of the coils. Equation (1.1.1-1) is an empirical rule which, as computer studies indicate, is good within a factor of ~ 2. This rule is verified in the two examples of window-frame magnets given below. Note that $g^2 b_2$ is the sextupole field at the pole tip in terms of B_0.

In the examples it can be seen that for window-frame magnets the sextupole dominates all other multipoles induced by iron saturation, and thus the sextupole term b_2 alone gives a fair description of how much the field B departs from being uniform. The amount of field variation caused by iron saturation can be computed by using Eq. (1.1.1-1). The result is valid only if the iron shield thickness is great enough that not much of the saturation effect is due to iron saturation in the iron backleg. Most of it is due to iron saturation in the iron pole, the iron directly above the center of the magnet.

Table 1.1.1-I

Computer Results for the BNL 18D72 Window-Frame Magnet

($g = 3.81$, $w = 3.81$, and $w_c = 1.905$ cm)

	B, kG			
	20.0	29.6	40.2	50.2
$g^2 b_2/10^{-2}$	0.40	5.2	9.8	
$g^4 b_4/10^{-2}$	0	0.43	0.99	...
$g^6 b_6/10^{-2}$	0	−0.28	−0.43	−0.55
$g^8 b_8/10^{-2}$	0	−0.03	−0.08	−0.11
NI, kA	122	200	308	436
$NI/NI_{\mu=\infty}$*	1.0	1.1	1.27	1.43
Stored energy, kJ/m	10.8	26.4	55.3	98.4
$\gamma(B)$	0.02	0.3	0.48	0.58

*$NI/NI_{\mu=\infty}$ is the ratio of the ampere turns needed to what would be needed if the iron had infinite permeability.

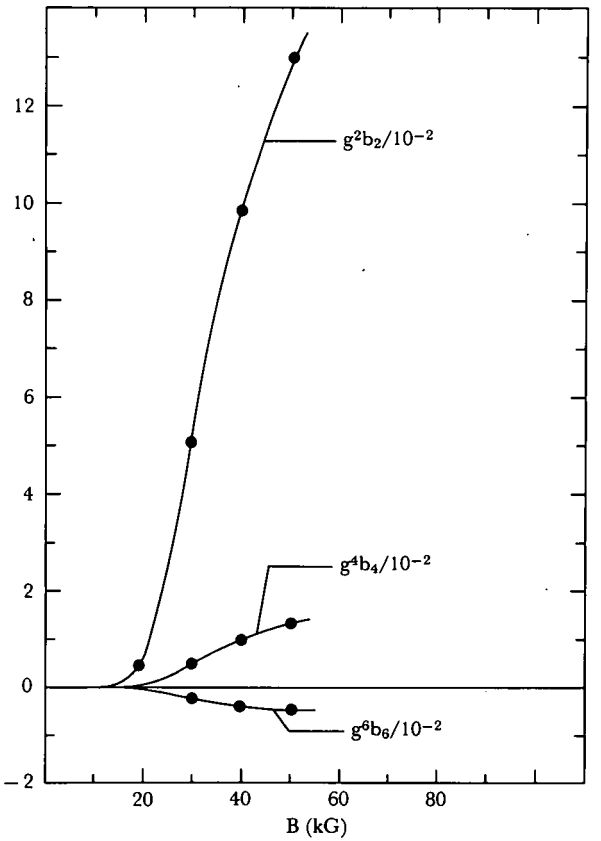

1.1.1-A. Field multipoles for a square window-frame magnet. $g=3.81$, $w=3.81$, and $w_c=1.905$ cm.

The first example for studying iron saturation effects is a window-frame magnet with a square aperture. Such magnets have been studied by Danby and co-workers [1.1.1-a] in considerable detail. A square-aperture magnet tends to have less iron saturation effect than the more usual rectangular window-frame magnet, whose horizontal aperture is about twice the vertical aperture. The magnet tends to improve as the vertical aperture increases. The coils also increase vertically and approach the situation of being two parallel infinite conductors that generate a uniform field between them. Thus at very high fields, where the iron behaves like air, the field is still quite uniform.

At 40 kG, the square window-frame magnet has a pole-tip field due to the iron-saturation induced sextupole of about $0.1B_0$. The corresponding quantity for the cosine magnet (Section 1.3) is about 20 times as small.

Table 1.1.1-I summarizes some characteristics of a square window-frame magnet whose half-gap g is 3.81 cm. The same results can be applied with reasonable

Table 1.1.1-II

Computed Results for a Window-Frame Magnet

($g=7.62$, $w=22.86$, $w_c=33.02$, and $t=48.89$ cm)

	B, kG		
	18.9	22.5	23.4
$g^2b_2/10^{-2}$	0.02	0.16	0.22
$\gamma(B)$	0.014	0.08	0.11
$NI/NI_{\mu=\infty}$	1.025	1.34	1.47

Table 1.1.1-III

Computed Results for the Function $F(B)$ of Eq. (1.1.1-2)

	B, kG						
	18.9	20.0	22.5	23.4	29.6	40.2	50.2
$F(B)/10^{-2}$	0.11	0.5	0.84	1.16	6.5	11.5	16.2

accuracy to other window-frame magnets with square apertures by scaling the results by the correct scale factor, or the correct power of g.

An interesting result is the degree to which the nonlinear field introduced by iron saturation effects is dominated by the sextupole term, which is ten times as large as the next largest multipole.

The effects of iron saturation depend on the kind of iron used. However, for high-field magnets operating near 40 kG, the kind of iron used does not affect the results greatly. The results in Table 1.1.1-I were obtained by using the permeability table for 1.8% Si steel (which has a magnetization $B-H=21.5$ kG) at 4.2 K [1.1.1-b].

Figure 1.1.1-A shows the dependence of the multipoles b_2, b_4, and b_6 on field level up to 50 kG. At higher field levels, the multipoles will level off and approach the values of the multipoles present when the iron is replaced by air. At 40 kG, the multipoles are already within about 20% of their iron-free values, so that they will not increase greatly at higher field levels.

The second example, a window-frame magnet that is rectangular in aper is the Brookhaven National Laboratory 18D72 bending magnet. This magnet has been extensively measured by Danby et al. [1.1.1-c] and also studied on the computer [1.1.1-d]. It has a vertical half-gap $g=7.62$ cm, a horizontal half-width $w=22.86$ cm, coil width $w_c=33.02$ cm, and iron thickness $t=48.89$ cm.

Table 1.1.1-II gives some results for the BNL 18D72 magnet. The sextupole pole-tip field g^2b_2 is given as a function of field from 18.9 to 23.4 kG; from this the field departure from uniformity can be estimated. The inverse permeability $\gamma=1/\mu$ can be used to test the empirical rule of Eq. (1.1.1-1). The iron used has a saturation magnetization $B-H=21$ kG.

An alternative way of presenting the empirical rule given by Eq. (1.1.1-1) is

$$g^2 b_2 = F(B) g/(w + w_c/2) , \qquad (1.1.1\text{-}2)$$

where $F(B)$ is a function of B only. $F(B)$ really depends on the inverse permeability, and thus on the type of iron. But for the accuracy claimed for Eq. (1.1.1-2) (a factor of 2 or 3), this dependence on the type of iron can be neglected. The function $F(B)$, computed from the results in Tables 1.1.1-I and 1.1.1-II, is given in Table 1.1.1-III.

If results for b_2 are known for a magnet at one field level, they can be scaled to higher field levels, since $F(B)$ is linear in $\gamma(B)$.

REFERENCES, SECTION 1.1.1

1.1.1-a. J. Allinger, G. Danby, B. Devito, H. Foelsche, S. Hsieh, J. Jackson, and A. Prodell, in *Proc. 9th Int. Conf. High Energy Accelerators, SLAC, Stanford University, 1974*, p. 198, CONF-740522, 1974; *IEEE Trans. Nucl. Sci.* **NS-20**, No. 3, 678 (1973); G. Danby, H. Foelsche, S. Hsieh, J. Jackson, and A. Prodell, in *Proc. 4th Int. Conf. Magnet Technology, Brookhaven, 1972*, p. 334, CONF-720908, 1972; J.E. Allinger, G.T. Danby, J.W. Jackson, and S.T. Lin, *Ibid.*, p. 637; J. Allinger, G. Danby, B. Devito, H. Foelsche, R. Gibbs, S. Hsieh, J. Jackson, A. Prodell, and A. Raag, *Ibid.*, p. 758.

1.1.1-b. A.D. McInturff and J. Clauss, BNL Internal Report No. AADD-162, 1974.

1.1.1-c. G.T. Danby, J.E. Allinger, and J.W. Jackson, in *Proc. 2nd Int. Conf. Magnet Technology, Oxford, 1967*, p. 87, H. Hadley, Editor, Rutherford Laboratory, 1967.

1.1.1-d. G. Parzen, BNL Internal Report No. AADD-155, 1969.

1.1.2 End Effects in Window-Frame Bending Magnets. End effects can contribute appreciably to the effective value of the various field multipoles. The relevant magnetic quantity in determining the orbits of particles passing through the magnets is usually the integrated value of the magnetic field over the longitudinal length of the magnet. If

$$\bar{B}(x,y) = \int_{-\infty}^{\infty} dz B(x,y,z) ,$$

where $B(x,y,z)$ is the vertical component of the field and z is along the longitudinal direction of the magnet, then in the median plane

$$\bar{B} = \bar{B}_0 (1 + \bar{b}_2 x^2 + \bar{b}_4 x^4 + \ldots) , \qquad (1.1.2\text{-}1)$$

where $\bar{B}_0$ is the integrated field along the central axis of the magnet.

The effect of the magnet ends is often described by measuring the effective dilength ΔL_B of the ends, which is defined by

$$\bar{B}(x,0) = B(x,0)[L_M + \Delta L_B(x)] , \qquad (1.1.2\text{-}2)$$

where $B(x,y)$ is the two-dimensional field that is valid near the longitudinal center of the magnet and L_M is the longitudinal length of the magnet iron.

The effect of the magnet ends on the various multipoles can also be described by writing $\bar{b}_n$ as

$$\bar{b}_n = b_n + \Delta b_n , \qquad (1.1.2\text{-}3)$$

where the b_n are the multipoles of the two-dimensional field $B(x,y)$ and Δb_n is the contribution of the ends to $\bar{b}_n$.

Table 1.1.2-I

Measured Results for the End Effects, ΔL_B and Δb_2, in Several Window-Frame Bending Magnets at Low Fields

	Magnet				
	ANL [1.1.2-a]	ANL [1.1.2-a]	BNL [1.1.2-b]	ANL [1.1.2-a]	ANL [1.1.2-a]
L_M, in.	30	72	72	72	7?
g, in.	3	3	3	3	
w, in.	7.5	9	9	15	1
w/g	2.5	3	3	5	5
$\Delta L_B/2g$	0.45	−0.017	1.3	–	0.45
$g^2\Delta b_2/10^{-4}$	−7.0	−8.4	−4.1	−0.63	−5.6
$gL_M\Delta b_2/(g/w)^2$	−0.044	−0.18	−0.087	−0.038	−0.34

Table 1.1.2-I lists the low-field end effects, ΔL_B and Δb_2, for various window-frame magnets measured at Argonne National Laboratory by Ratner and Lari [1.1.2-a] and at Brookhaven National Laboratory by Danby [1.1.2-b]. The ΔL_B given is that at the magnetic center, $x=0$.

Clearly, end effects depend critically on how the end coils are constructed and can vary greatly from magnet to magnet. However, these effects can be estimated on the basis of the results in Table 1.1.2-I, and a rough empirical rule for $\Delta L_B/2$, which is roughly the contribution to the effective length due to one end, is

$$\Delta L_B/2 \doteq 0.7g\,. \tag{1.1.2-4}$$

For Δb_2, it seems reasonable to assume that $g^2\Delta b_2=(g/L_M)f(g/w)$. The g/L_M factor indicates the relative longitudinal extent of the end effect, and the function $f(g/w)$ indicates that the end effects get smaller as the magnet becomes wider in the transverse direction. Using the data in Table 1.1.2-I, one may propose a rough empirical rule for Δb_2:

$$g^2\Delta b_2=0.1(g/L_M)(g/w)^2\,. \tag{1.1.2-5}$$

The values for $gL_M\Delta b_2/(g/w)^2$ in Table 1.1.2-I show how well the rule holds for the magnets listed.

As the magnet gets wider, for large values of w/g the single multipole Δb_2 not adequately describe the variation of $\bar{B}$ with x. However, Δb_2 alone does give an adequate description for $w/g\lesssim 3$; for $w/g=5$, high multipoles can increase the change in $\bar{B}$ with x by a factor of ~ 2 for $x/w\gtrsim 0.4$.

Effect of iron saturation. The above results for the end effects ΔL_B and Δb_2 are valid at low field levels. At higher fields, the end effects will change somewhat because of iron saturation.

The contribution of one end to the effective length, $\Delta L_B/2$, varies from $1.3g$ to $1.08g$ from low fields to 18.5 kG, or a change of 18%, for the magnet measured by Danby [1.1.2-b], which has $L_M=72$, $w=9$, and $g=2$ in.

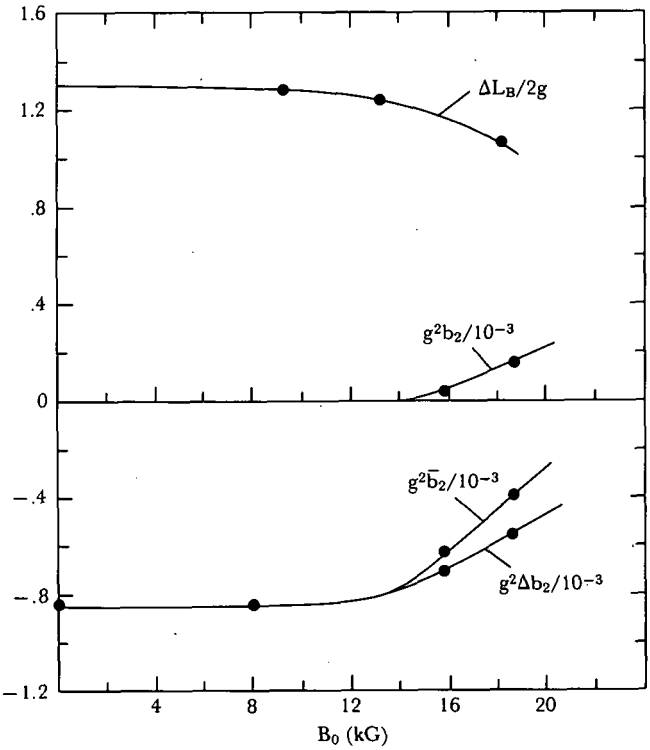

1.1.2-A. End effect on the sextupole multipole for a window-frame magnet. $g=3$, $w=9$, and $L_M=72$ in.

Figure 1.1.2-A shows the effect of iron saturation on Δb_2, the contribution of the end to the integrated sextupole b_2 for the window-frame magnet measured by Ratner and Lari [1.1.1-a], which has $L_M=72$, $w=9$, and $g=3$ in. It can be seen that b_2 is largely due to the end effect Δb_2, which changes by 33% as the field changes from low level fields to 18.6 kG. Note that for the window-frame magnet, Δb_2 and b_2 are of opposite sign, so that b_2 will go through zero at $B\simeq 22$ kG.

$\Delta L_B/2g$ is also shown in Figure 1.1.2-A as a function of the field. The result n for ΔL_B is that found for the magnet measured by Danby [1.1.2-b].

Studies of window-frame magnets have also been carried out by Ohayon, Penicaud, and de Sereville [1.1.2-c].

REFERENCES, SECTION 1.1.2

1.1.2-a. L.G. Ratner and R. J. Lari, *ANL User's Handbook,* Section 5, 1966.
1.1.2-b. G.T. Danby, BNL Internal Report No. GTD-2, 1961.
1.1.2-c. M. Ohayon, J.P. Penicaud, and B. de Sereville, in *Proc. 4th Int. Conf. Magnet Technology, Brookhaven, 1972*, p. 108, CONF-720908, 1972.

1.2 H-Magnets

One advantage of an H-magnet, such as that shown in Figure 1.2-A, is that the coils can be simple pancake coils, which need not be bent up at the end of the magnet, as must be done for a window-frame magnet, to prevent a beam passing through the magnet from striking the coils. A second advantage is that the coils are hidden by the pole and the field can be made insensitive to errors in the location of the coils. A disadvantage is that the field is not as uniform as that in a window-frame magnet, and to obtain a good uniform field region the H-magnet must be made larger than a corresponding window-frame magnet.

1.2.1 Effect of Pole Width, Infinite-Permeability Iron. Figure 1.2.1-A sh the field variation on the median plane for the case in which the half-pole w $w=4g$ (g is the vertical half-gap). The results clearly are the same for magnets having the same w/g, so this curve applies to any H-magnet with $w/g=4$ whose coil is hidden by the pole, whose iron return backleg is far enough away not to affect the field appreciably, and for $\mu=\infty$ iron. It can be seen that there is a flat region in the center. In Figure 1.2.1-B the region of good field in the median plane, Δx, is plotted versus the pole width w. $\Delta x_{0.01}$, or $\Delta x_{0.001}$, is the half-region of good field, given the criterion that the field not change by $>1\%$, or $>0.1\%$, respectively.

The relation between the region of good field and the width of the pole can be roughly described by

$$\Delta x_{0.01}=w-g\,,$$
$$\Delta x_{0.001}=w-2g\,. \qquad (1.2.1\text{-}1)$$

A gap width in the good field region is lost if 1% accuracy is required in the field, and two gap widths if 0.1% accuracy is required.

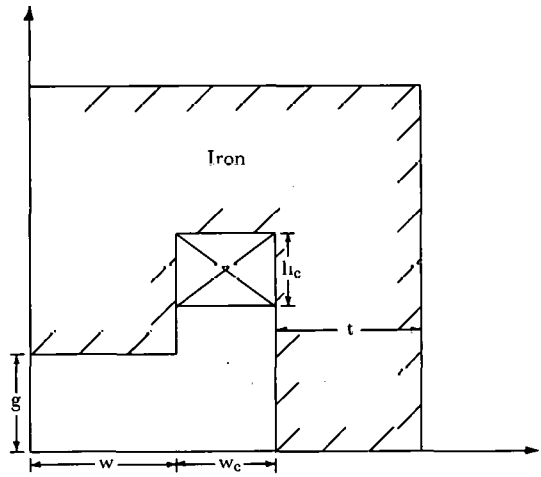

1.2 A. H magnet geometry. $w/g=4$.

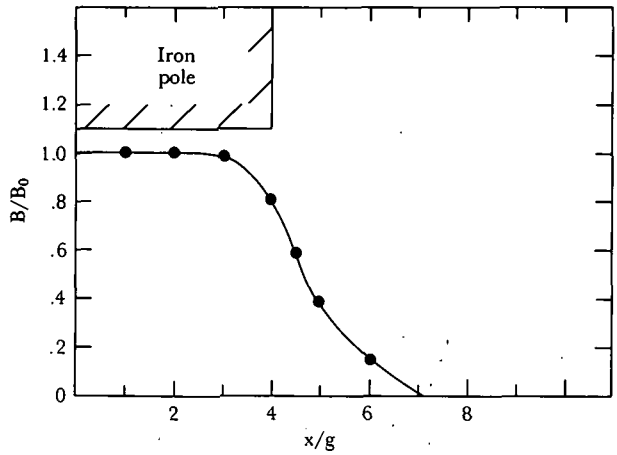

1.2.1-A. Median plane field for an H-magnet.

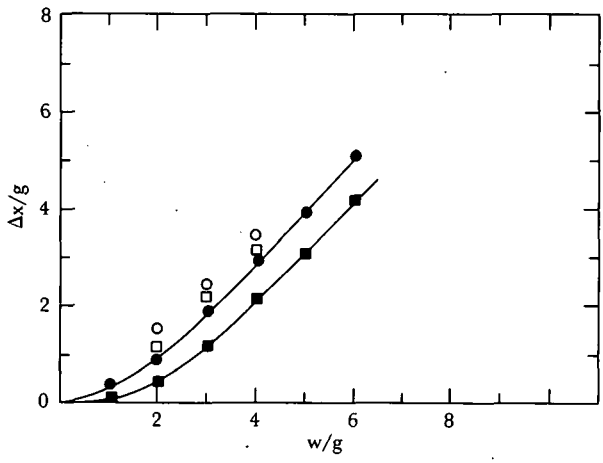

1.2.1-B. Good field aperture for H-magnets with and without shims.
●, $\Delta x_{0.01}$ without shim; ■, $\Delta x_{0.001}$ without shim; ○, $\Delta x_{0.01}$ with shim; □, $\Delta x_{0.001}$ with shim.

Figure 1.2.1-C shows the multipoles as a function of the pole width. The field at the pole face due to each multipole, $b_2 g^2$, $b_4 g^4$, $b_6 g^6$, $b_8 g^8$, is plotted against the pole width w/g. The pole-face field due to the sextupole term $b_2 g^2$ varies from 0.2 for $w/g = 1$ to 8×10^{-6} for $w/g = 4$. The multipoles decrease exponentially with the pole width. A rough relationship is

$$b_n \simeq \text{const} \times \exp(-2.5\, w/g)\,. \qquad (1.2.1\text{-}2)$$

For the wider poles, the multipoles do not provide a useful description of the field shape, since no one multipole is dominant.

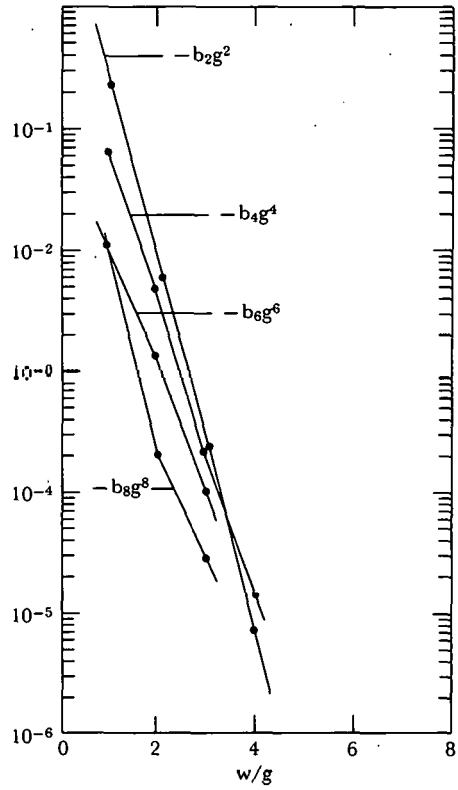

1.2.1-C. Field multipoles for H-magnets.

1.2.2 H-Magnet Shims. The region of good field in an H-magnet can be extended by adding a shim at the edge of the pole, as shown in Figure 1.2.2-A. The magnetic field without the shim tends to fall off with distance from the center. It seems reasonable to assume that the shim will oppose this tendency and increase the flat region in the center.

The case of the rectangular simple shim as shown in Figure 1.2.2-A has been studied by Rose [1.2.2-a]. More extensive calculations were done by Wilkins and Spurway [1.2.2-b], using conformal mapping techniques.

Figure 1.2.2-B shows the dimensions of the shim that will produce the la flat region as found by Wilkins and Spurway [1.2.2-b]. A somewhat larger shim causes the field to rise at the edge of the pole, and a somewhat smaller shim allows the field to drop more rapidly at the edge. The depth of the shim d is plotted against the width of the shims. Also plotted is the area of the shim, sd. The area curve is relatively flat for shims with $s/g \simeq 0.4$. A rough empirical rule can be proposed for the shim area:

$$\text{Shim area} = 0.021g^2\,, \tag{1.2.2-1}$$

which is fairly good for shims with $0.2 \leqslant s/g \leqslant 0.6$.

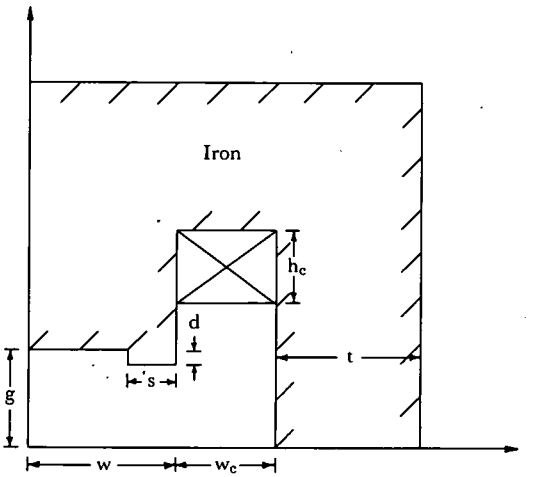

1.2.2-A. H-magnet geometry with shims.

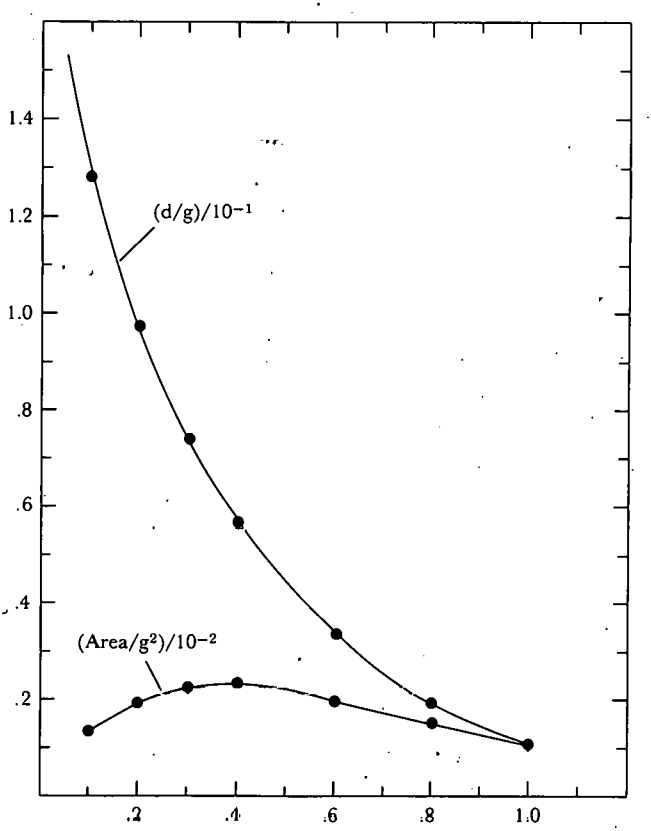

1.2.2-B. Shim dimensions to flatten field. See Figure 1.2.2-A for geometry.

The results shown in Figure 1.2.2-B were found analytically by conformal mapping techniques for an infinitely wide pole. Computer calculations for a more realistic pole have verified these results and show that the shim dimensions do not change much with the width of the pole.

Figure 1.2.1-B shows the increase in good aperture produced by the shim. To a first approximation it can be said that shims increase the good aperture $\Delta x_{0.01}$ by $0.5g$ and increase the good aperture $\Delta x_{0.001}$ by g. The shim gains one more aperture when the accuracy requirement for the field is greater.

Analytical treatments of shims are also given by B. Hedin [1.2.2-c], H. Brechna [1.2.2-d, -e], K. Halbach [1.2.2-f], and M. Foss [1.2.2-g].

REFERENCES, SECTION 1.2.2

1.2.2-a. M.E. Rose, *Phys. Rev.* 53, 715 (1958).
1.2.2-b. J.J. Wilkins and A.H. Spurway, Rutherford Laboratory Report NIRL/R/6, 1961.
1.2.2-c. B. Hedin, SLAC 16, May 1963.
1.2.2-d. H. Brechna, SLAC-28, May 1964.
1.2.2-e. H. Brechna, in *Proc. Int. Symp. Magnet Technology, SLAC, Stanford University, 1965*, p. 1, H. Brechna and H.S. Gordon, Editors, CONF-650922, 1965.
1.2.2-f. K. Halbach, in *Proc. 2nd Int. Conf. Magnet Technology, Oxford, 1967*, p. 47, H. Hadley, Editor, Rutherford Laboratory, 1967.
1.2.2-g. M. Foss, Carnegie Institute of Technology Report NYO-911, 1951.

1.2.3 Iron Saturation Effects in H-Magnets. One effect of introducing the pole in an H-magnet is that the field in the iron pole face directly above the center of the magnet is larger than that on the median plane by a considerable fraction, which leads to increased iron saturation effects.

In Figure 1.2.1-A it can be seen that the median-plane field extends past the edge of the pole and the effective half-width of the field is $w+g$. The flux that crosses the median plane is squeezed into the iron pole face with half-width w so that the field in the pole, B_{pole}, is increased by the fraction g/w, and

$$B_{\text{pole}} = B_0(1+g/w)\,. \qquad (1.2.3\text{-}1)$$

For a magnet with $w/g=4$, this can make the field in the pole larger than the median-plane magnetic field by 25%. Since the permeability is decreasing very rapidly with field at $B_0 \simeq 16$ kG, this effect can produce considerably greater iron saturation effects for the H-magnet.

Table 1.2.3-I lists results for an H-magnet with a gap of 4 cm and a pole v of 20 cm. For this magnet $g=2$, $w=10$, $w_c=12.5$, $h_c=11.5$, and $t=12.5$ cm, where h_c and w_c are the height and width of the coil and t is the thickness of the backleg. Of the multipoles induced by iron saturation, the sextupole multipole b_2 dominates, and the pole-tip field due to the sextupole term is more than 10 times as large as that due to the next stronger multipole, b_4. Thus the sextupole term alone gives a reasonable description of the field variation induced by iron saturation effects.

Note that the sextupole term is negative here. Iron saturation effects make the field higher at the center of the magnet, the opposite of what happens in the window-frame magnet. A possible explanation for the negative b_2 is that the magnetic field

Table 1.2.3-I

Computed Results for an H-Magnet

($g=2$, $w=10$, $t=12.5$, $w_c=12.5$, and $h_c=11.5$ cm)

	B, kG		
	12.4	14.0	15.9
$g^2b_2/10^{-4}$	−1.3	−3.28	−8.32
$g^4b_4/10^{-4}$	−0.12	−0.17	−0.34
$g^6b_6/10^{-4}$	0.003	−0.002	0.001
NI, kA	40.6	51	65
$NI/NI_{\mu=\infty}$	1.00	1.10	1.24
Stored energy, kJ/m	6.5	9.0	13.1
B_{pole}, kG	16	17.9	19.8
γ_{pole}	0.0025	0.008	0.021
$\gamma(B)$	0.00017	0.0008	0.0025
B_{pole}/B	1.29	1.28	1.24

in the iron pole near the coil is higher than that in the center of the pole. Thus the iron near the coil is more heavily saturated, and the field in the median plane drops as the coil is approached.

In the window-frame magnet, the magnetic field in the iron near the coils is smaller than that in the iron near the center of the magnet. The flux density is uniform as the lines of force enter the iron, but the lines near the coil start diverging faster than those at the center, which results in a lower field in the iron near the coil. This iron is less saturated, and the field in the median plane increases on approaching the coil.

The sextupole term, which is the dominant multipole, may be roughly estimated from the following empirical rule:

$$g^2b_2 = -0.2\left(\frac{5g}{w}\right)^2 \gamma_{\text{pole}} \frac{g}{w+g}, \qquad \text{(1.2.3-2a)}$$

in which γ_{pole} is the maximum value of γ along the center line of the pole. It can be estimated as the γ corresponding to the field B_{pole} that is given by Eq. (1.2.3-1).

Equation (1.2.3-2a) is a very rough rule, good within a factor of 2 or 3, for use imating the order of magnitude of the saturation effects to be expected. It appears to describe a limited number of H-magnets that have been computed. Data for two magnets for which this rule can be verified are given below. Equation (1.2.3-2a) should work fairly well for H-magnets that do not differ greatly from these two H-magnets.

Equation (1.2.3-2a) is written in a form to facilitate comparison with Eq. (1.1.1-1) for the window-frame magnet. It can be seen that the saturation b_2 in H-magnets has a much stronger dependence on the g/w ratio. H-magnets and window-frame magnets have about the same saturation effects when $g/w \simeq 1/5$ for the H-magnet.

Table 1.2.3-II

Computed Results for an H-Magnet

($g=3.81$, $w=11.43$, $w_c=11.43$, $h_c=8.89$, and $t=13.97$ cm)

	B, kG		
	2.5	16.3	18.2
$g^2b_2/10^{-3}$	−0.52	−3.92	−7.42
NI, kA	7.7	118	154
$NI/NI_{\mu=\infty}$	1.0	1.19	1.40
Stored energy, kJ/m	0.53	25.8	36.9
B_{pole}, kG	–	20.1	22.1
$\Delta x_{0.005}/g$	1.67	1.0	0.75
γ_{pole}	–	0.026	0.092
$\gamma(B)$	–	0.0038	0.0078
B_{pole}/B		1.23	1.21

Table 1.2.3-II lists results for an H-magnet with a half-gap of 3.81 cm and a pole half-width of 11.43 cm. This magnet has a w/g ratio of 3, compared with $w/g=5$ for the magnet described in Table 1.2.3-I. The magnet with the smaller w/g ratio has a considerably larger saturation effect, as shown by the $(g/w)^2$ factor in Eq. (1.2.3-2a). This factor probably crudely describes a more complicated saturation effect and may not be valid except for a limited range of H-magnets similar to the two presented here.

An alternative way of presenting the empirical rule given by Eq. (1.2.3-2a) is

$$g^2b_2 = -F(B_p)(5g/w)^2g/(w+g)\,, \qquad (1.2.3\text{-}2b)$$

where $F(B_p)$ is a function of B_p only and B_p is the field at the pole. $F(B_p)$ really depends on γ, the inverse permeability, and thus on the type of iron. But for the accuracy of a factor of 2 or 3 claimed for Eq. (1.2.3-2b), this dependence on the type of iron can be neglected. The function $F(B_p)$, computed from the results in Tables 1.2.3-I and -II, is given in Table 1.2.3-III.

If results for b_2 are known for a magnet for lower field levels, they can be scaled to higher field levels by realizing that $F(B_p)$ is linear in $\gamma(B_p)$.

Table 1.2.3-III

Computed Results for the Function $F(B_p)$ of Eq. (1.2.3-2b)

	B_p, kG				
	16	17.9	19.8	20.1	22.1
$F(B_p)/10^{-2}$	0.0778	0.196	0.498	0.564	1.07

REFERENCE, SECTION 1.2.3

1.2.3-a. W. J. Willis, G.T. Danby, H. Hahn, H. J. Halama, A.W. Maschke, M. Month, G. Parzen, and I. Polk, BNL Internal Report No. CRISP-74-6, 1974.

1.2.4 End Effects in H-magnets. As shown in Section 1.1.2, the end effects may be described by ΔL_B, the contribution of the ends to the effective length of the magnet, and by Δb_2, the contribution to the integrated sextupole $\bar{b}_2$ of the magnet. ΔL_B and Δb_2 can be expected to be roughly given by the same empirical rules as for the window-frame magnet. This is roughly true, as shown in Table 1.2.4-I, which gives the low-field end effects, ΔL_B and Δb_2, for several H-magnets measured at Argonne National Laboratory by Ratner and Lari [1.2.4-a]. On the basis of these results, the following rough empirical rules are proposed:

$$\Delta L_B/2 = 1.1g\,,$$

$$g^2\Delta b_2 = 0.3(g/L_M)(g/w)^2\,. \qquad (1.2.4\text{-}1)$$

To the accuracy claimed, these rules for the end effects in H-magnets are the same as those found for window-frame magnets in Section 1.1.2.

Effects of iron saturation. The above results for the end effects L_B and Δb_2 are valid at low field levels. At higher fields, they will change somewhat because of iron saturation.

$\Delta L_B/2$, the contribution of one end to the effective length, varies from $1.1g$ to $0.63g$, from low fields to 20.2 kG, or a change of 43%, for the first magnet in Table 1.2.4-I, and from $1.1g$ to $0.7g$, from low fields to 18.5 kG, or a change of 36%, for the second magnet.

Figure 1.2.4-A shows the effect of iron saturation on $\bar{b}_2$, the integrated sextupole for the first magnet in Table 1.2.4-I, which has $L_M = 36$, $g = 3$, and $w = 15$ in. The two-dimensional b_2 for the magnet measured was not available, and the b_2 shown in Figure 1.2.4-A is the b_2 computed for another magnet with the same g/w ratio. The integrated $\bar{b}_2$ for this H-magnet is about 10 times as large as that found for a win-

Table 1.2.4-I

Measured Results for the End Effects, ΔL_B and Δb_2, for Several H-Magnets at Low Fields

	Magnet	
	ANL [1.2.4-a]	ANL [1.2.4-a]
L_M, in.	36	20
g, in.	3	2.5
w, in.	15	10
w/g	5	4
$\Delta L_B/2g$	1.2	1.1
$g^2\Delta b_2/10^{-4}$	−7.3	−36.0
$L_M g\Delta b_2/(g/w)^2$	−0.22	−0.45

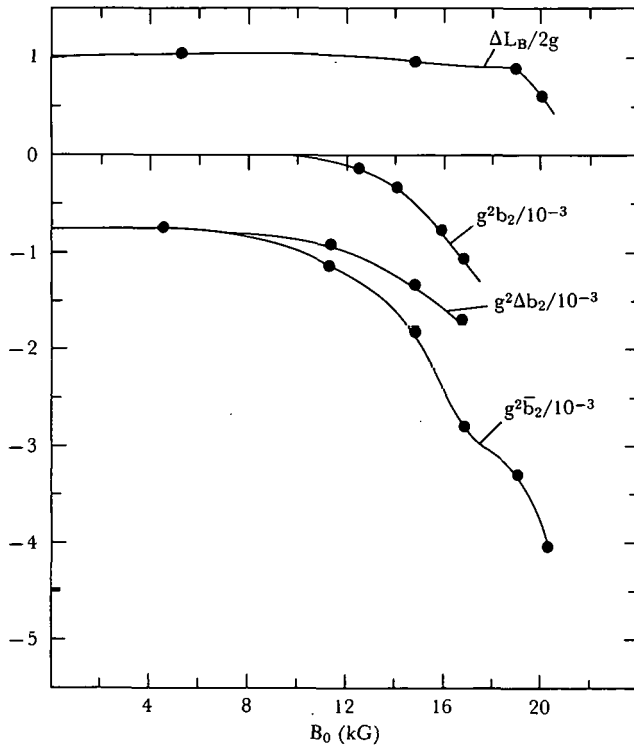

1.2.4-A. End effect on the sextupole multipole for an H-magnet. $g = 3$, $w = 15$, and $L_M = 36$ in.

dow-frame magnet in Section 1.1.2. Also, Δb_2, the contribution due to the ends, and b_2, the contribution of the center part of the magnet, contribute about equally at the higher fields. The results in Figure 1.2.4-A can be used for other magnets by scaling the result for Δb_2 by the factor $(g/L_M)(g/w)^2$. The curve shown here for Δb_2 vs B_0 for H-magnets is roughly the same as that in Section 1.1.2 for window-frame magnets and that in Section 1.4.1 for C-magnets when these curves are scaled according to the factor $(g/L_M)(g/w)^2$.

$\Delta L_B/2g$ is also shown in Figure 1.2.4-A as a function of field.

Studies of H-magnets have been carried out by Hoyer and Gunn [1.2.4-b] Perin [1.2.4-c].

REFERENCES, SECTION 1.2.4

1.2.4-a. L.G. Ratner and R. J. Lari, *ANL User's Handbook*, Section 5, 1966.

1.2.4-b. E. Hoyer and J. Gunn, in *Proc. 4th Int. Conf. Magnet Technology, Brookhaven, 1972*, p. 92, CONF-720908, 1972.

1.2.4-c. R. Perin, in *Proc. 3rd Int. Conf. Magnet Technology, Hamburg, 1970*, p. 304, G. Söhngen et al., Editors, Deutsches Elektronen-Synchrotron DESY, Hamburg, 1972.

1.3 Cosine Bending Magnets

A cosine dipole magnet is shown in Figure 1.3-A. It can be shown that a circular distribution of current, in which the current density is proportional to the cosine of the azimuthal angle, will produce a perfectly uniform field. The addition of a circular iron shield of infinite permeability which surrounds the current distribution will increase the magnitude of the magnetic field without affecting its uniformity [1.3-a].

The cosine dipole has received considerable attention since superconducting magnets became technologically feasible. Cosine dipoles have the property of giving -----ptionally uniform magnetic fields at both low and high field levels. At low levels, where the iron is not saturated and approaches infinite permeability, the uniform field is an exact solution for the ideal cosine magnet. At very high field levels (about 100 kG), the iron becomes very saturated and approaches the magnetic properties of air, and again the uniform field is an exact solution for the ideal cosine magnet. In practice, the worst departure from uniformity is found to occur at about 45 kG [1.3-b].

The continuous cosine current distribution can be approximated by using blocks of current within which the current density is constant, as shown in Figure 1.3-A. For the distribution shown, the total current in each block is chosen to be roughly proportional to the cosine of the azimuthal angle.

If the total current in each of the 6 blocks/quadrant (Figure 1.3-A) is exactly proportional to the cosine of the azimuthal angle, then it can be shown [1.3-c] that

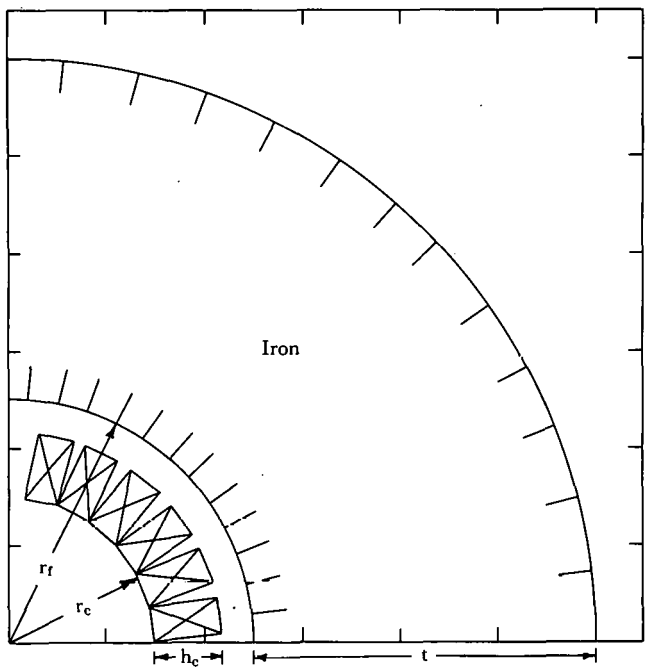

1.3-A. Cosine bending-magnet geometry with radial current blocks.

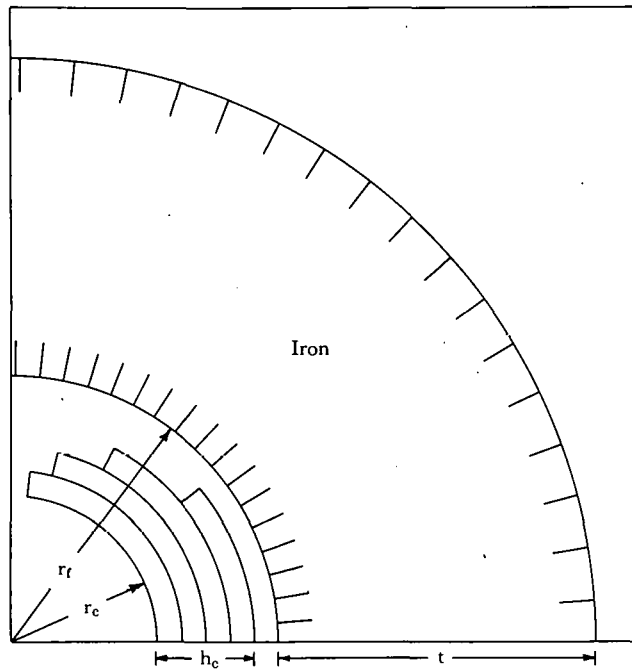

1.3-B. Cosine bending-magnet geometry with current shells.

the first 6 multipoles, which do not vanish because of symmetry, will vanish here. Thus, b_2, b_4, b_6, b_8, b_{10}, and b_{12} will be zero, and the first nonvanishing multipole is b_{14}.

The current blocks are usually wound of a conductor, either ribbon or rectangular shaped, and since each block must carry a whole number of turns of this conductor, the total current can be made only roughly proportional to the cosine of the azimuthal angle. However, the first 6 undesired multipoles can still be made to vanish by displacing each block a small amount azimuthally, as was shown by Morgan at BNL [1.3-d]. The azimuthal displacement of each of the 6 blocks gives 6 new variables that can be adjusted to make the first 6 undesired multipoles vanish. This calculation is usually done with a computer and requires solving 6 equations for 6 unknowns [1.3-e, -f].

A second approach to approximating the cosine distribution is to use cu shells, as shown in Figure 1.3-B. The results in this section were obtained by using radial current blocks rather than current shells. It is believed that most of the results given below apply equally well to both methods of approximating the cosine distribution.

REFERENCES, SECTION 1.3

1.3-a. H. Brechna, *Superconducting Magnet Systems*, p. 111, Springer-Verlag, Heidelberg and New York, 1973.

1.3-b. G. Parzen and K. Jellett, BNL Internal Report No. AADD-198, 1973.
1.3-c. R. Beth, BNL Internal Report No. AADD-135, 1967.
1.3-d. G.H. Morgan, BNL, Unpublished data.
1.3-e. P.F. Dahl, G.H. Morgan, and W.B. Sampson, BNL Internal Report No. CRISP 72-25, 1972.
1.3-f. G. Parzen and K. Jellett, in *Proc. 4th Int. Conf. Magnet Technology, Brookhaven, 1972*, p. 642, CONF-720908, 1972.

1.3.1 Number of Current Blocks. The number of current blocks used determines the region of good aperture at low field levels. Figure 1.3.1-A shows the gradi- across the aperture for a cosine magnet whose coil has an inner radius of 4 cm which has 6 blocks/quadrant. The field goes bad rather rapidly at $r = 2.7$ cm, or at about 67% of the coil inner radius. Since the lower multipoles b_2 to b_{12} all vanish, this blowup of the field quality is due to the higher multipoles. Thus, testing the field quality of a magnet by measuring only the lower multipoles may involve some risk.

The percentage of good aperture obtained depends on the number of current blocks and thus on the number of the lower harmonics made to vanish. Figure 1.3.1-B shows [1.3.1-a, -b] the percentage of good aperture versus the number of blocks per quadrant. Since blowup of the field occurs very rapidly, the results for the

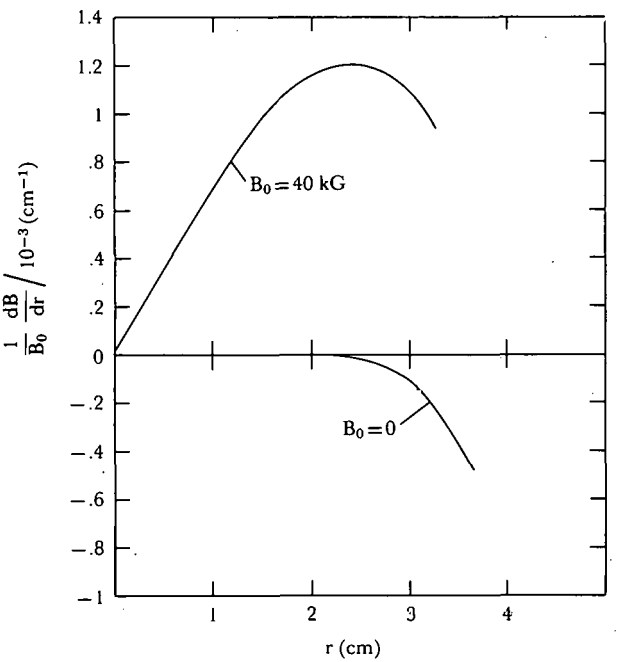

1.3.1-A. Median-plane field gradient for a cosine dipole. $r_c = 4$ cm; $r_f = 6.35$ cm.

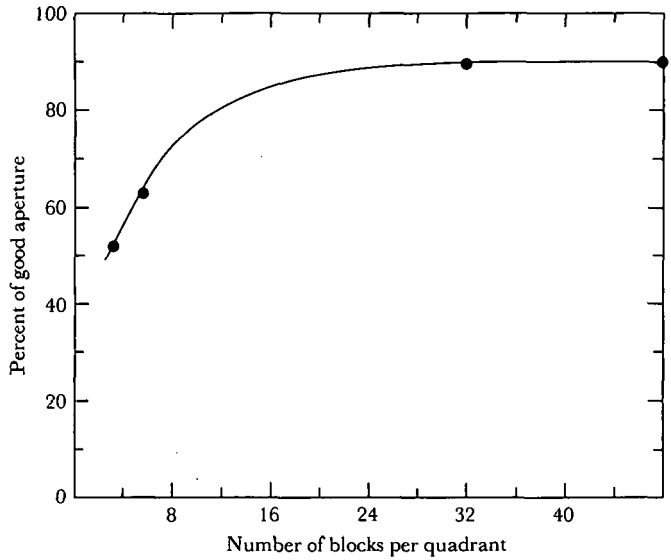

1.3.1-B. Good field aperture versus number of current blocks.

percentage of good aperture are not sensitive to the choice of criterion for considering the field unacceptable. The criterion used here was that $B''/B_0 \lesssim 1 \times 10^{-3}/\text{in.}^2$.

The calculations were done for current blocks with an inner radius of 3.8 cm and a radial thickness of 1.59 cm, but the results are probably not very sensitive to this choice of dimensions.

REFERENCES, SECTION 1.3.1

1.3.1-a. G. Parzen and K. Jellett, in *Proc. 4th Int. Conf. Magnet Technology, Brookhaven, 1972*, p. 642, CONF-720908, 1972.

1.3.1-b. G. Parzen and K. Jellett, BNL Internal Report No. AADD-188, 1972.

1.3.2 Iron Saturation Effects in Cosine Bending Magnets. Cosine bending magnets have remarkably small iron saturation effects. Up to 20 kG there is little saturation effect, but at 40 kG it is appreciable.

Figure 1.3.2-A shows that the saturation effect sets in at about 20 kG, peaks about 45 kG, and then slowly decreases. The sextupole field at the inner coil radius, $r_c^2 b_2$, is plotted against the dipole magnetic field up to 100 kG (r_c is the inner radius of the coil). The decapole field at the inner coil radius, $r_c^4 b_4$, is also plotted. The dimensions of the magnet considered here are those of the BNL 8-cm model superconducting dipole [1.3.2-a, -b] for which $r_c = 4$, $r_f = 6.35$, $h_c = 1.905$, and $t = 8.89$ cm. The iron used was 3.5% Si steel with a saturation magnetization of $B - H = 19.93$ kG. The maximum value of the sextupole field occurring near $B = 45$ kG is $r_c^2 b_2 = 6 \times 10^{-3}$. The amount of nonuniformity introduced into the field by the sextupole term is not large, but it is appreciable for accelerator magnets.

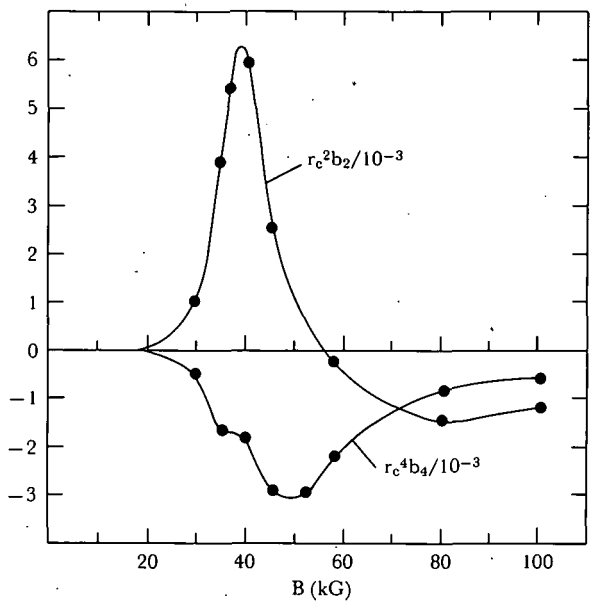

1.3.2-A. Field multipoles for a cosine bending magnet. $r_c = 4$ cm; $r_f = 6.35$ cm.

Table 1.3.2-I

Computed Results for a Cosine Bending Magnet

($r_c = 4$, $r_f = 6.35$, $h_c = 1.905$, and $t = 8.9$ cm; B_{leak} is the leakage field)

	B, kG					
	5	20	30.2	35.3	39.4	57.3
$r_c^2b_2/10^{-3}$	–	–	0.99	3.9	5.95	−0.3
$r_c^4b_4/10^{-3}$	–	–	−0.5	−1.7	−1.8	−2.2
$r_c^6b_6/10^{-3}$	–	–	−0.01	0.15	0.54	0.46
NI (kA)	48.5	194	294	348	395	651
Stored energy (kJ/m)	0.87	14	31.8	44.0	55.5	130.8
$\theta = 0$), kG	0.000	0.001	0.044	0.172	0.398	2.67
$\theta = 90°$), kG	0.000	0.000	0.007	0.042	0.114	1.33
$I_{\mu=\infty}$	1.00	1.00	1.00	1.02	1.03	1.17

The type of iron used can vary the magnitude of the sextupole field due to iron saturation by a factor of ~2. The type of iron does not greatly affect the size of the saturation effects.

Some results for the 8-cm-aperture magnet are listed in Table 1.3.2-I. For this magnet the presence of the iron increases the field obtained for a given current by a factor of 1.60. For an ideal magnet, with a very thin coil and the iron very close to the coil, this factor would be 2.0.

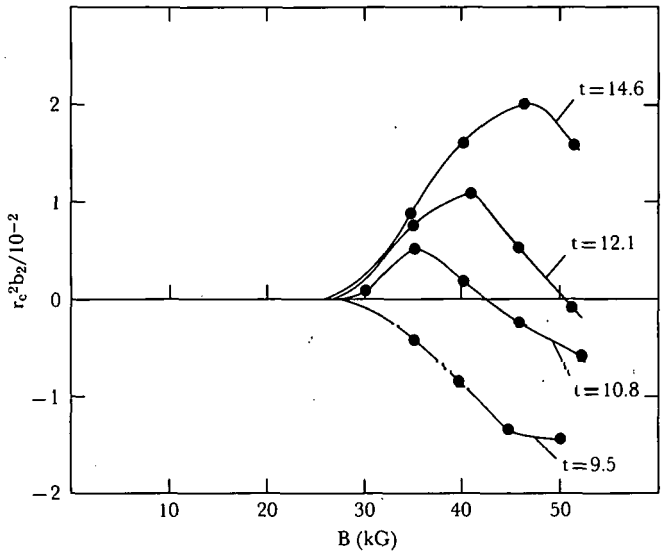

1.3.2-B. Field multipoles for a cosine bending magnet for various thicknesses of the iron shield. $r_c=6$ cm; $r_f=8.25$ cm.

Table 1.3.2-II

Computed Results for a Cosine Bending Magnet

($r_c=6$, $r_f=8.25$, $h_c=1.70$, and $t=12.1$ cm)

	B, kG			
	34.8	40.8	45.7	51.1
$r_c^2b_2/10^{-2}$	0.75	1.13	0.49	−0.08
$r_c^4b_4/10^{-2}$	−0.35	−0.29	−0.58	−0.61
$r_c^6b_6/10^{-2}$	−0.006	−0.03	−0.04	−0.03
$r_c^8b_8/10^{-2}$	0.02	−0.03	−0.05	−0.01
NI, kA	452	544	642	755
Stored energy (kJ/m)	81.4	114	151	
$B_{\text{leak}}(\theta=0)$, kG	0.12	0.52	1.4	
$NI/NI_{a=\infty}$	1.01	1.04	1.10	

The iron saturation effects are sensitive to the thickness of the iron shield. Figure 1.3.2-B shows the sextupole field $r_c^2b_2$ plotted against the field B for various choices of the iron shield thickness, t, for a 12-cm-aperture dipole, with $r_c=6$, $r_f=8.25$, and $h_c=1.70$ cm. It can be seen that there is a critical thickness of the iron shield, for which the sextupole field, b_2, remains flat over a larger range of field levels [1.3.2-c]. This critical thickness may be estimated from the empirical rule

$$t_c \doteq 1.23\, r_f\,. \tag{1.3.2-1}$$

For the 12-cm dipole for which data are given in Figure 1.3.2-B, the critical thickness is $t_c = 10$ cm. However, this thickness gives a large leakage field outside the iron shield. For the 12-cm dipole at 40 kG, the leakage field would be 1.8 kG just outside the iron on the median plane. It may be preferable to use a larger iron thickness to reduce the leakage field and also to reduce the current required to excite the magnet to 40 K, which is made larger by the heavy saturation of the iron.

The 12-cm dipole considered here is similar to the dipole magnet for the proposed ISABELLE accelerator [1.3.2-d], and a likely choice of iron thickness is 12.1 cm, which gives a leakage field of 0.4 kG. The maximum sextupole field, $r_c^2 b_2$, for this thickness occurs near $B = 40$ kG and has the value $r_c^2 b_2 = 0.01$.

Some results for the 12-cm-aperture magnet are listed in Table 1.3.2-II. For this magnet, the presence of the iron shield increases the field obtained for a given current by a factor of 1.70. The iron used is 1.8% Si steel with a saturation magnetization $B - H = 21.5$ kG.

It can be seen from Figure 1.3.2-C that the peak value of the sextupole term increases as the iron shield thickness increases above the critical thickness t_c. For sufficiently thick iron shields, the peak value of $r_c^2 b_2$ reaches a maximum. For the 12-cm-aperture magnet, $(r_c^2 b_2)_{\max} = 0.02$; it is reached for thicknesses > 15 cm and occurs at a dipole field of about 45 kG. This maximum value can be used as a measure of the saturation effect in a given magnet and can be computed from the empirical rule

$$(r_c^2 b_2)_{\max} = 0.032\,(r_c/r_f)^2\,. \qquad (1.3.2\text{-}2)$$

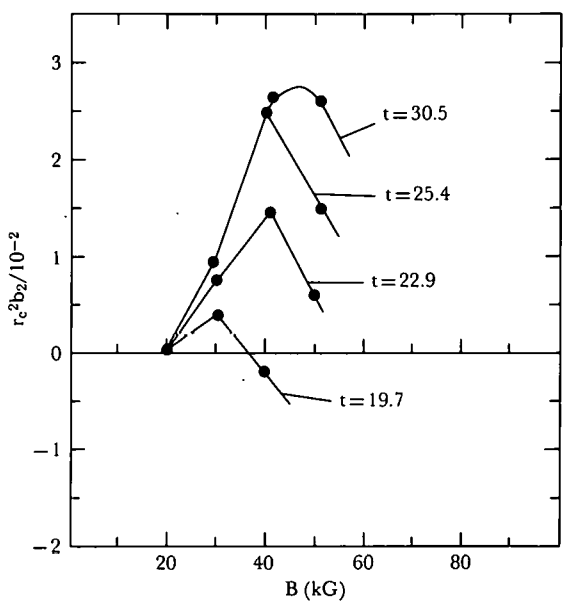

1.3.2-C. Field multipoles for a cosine bending magnet for various thicknesses of the iron shield. $r_c = 12.7$ cm; $r_f = 15.2$ cm.

Table 1.3.2-III

Computed Results for a Cosine Bending Magnet

($r_c = 12.7$, $r_f = 15.2$, $h_c = 2.03$, and $t = 22.9$ cm)

	B, kG			
	19.5	30.0	40.7	49.5
$r_c^2 b_2/10^{-2}$	0.01	0.75	1.52	0.55
$r_c^4 b_4/10^{-2}$	−0.002	−0.02	−0.027	–
$r_c^4 b_6/10^{-2}$	0.000	0.000	0.001	
NI, kA	468	724	1054	1400
Stored energy, kJ/m	96.5	228	450	726
$B_{leak}(\theta = 0)$, kG	–	0.045	0.93	2.3
$NI/NI_{\mu=\infty}$	1	1.008	1.08	1.18

This rule can be verified for the two examples given above. The factor $(r_c/r_f)^2$ shows that as the iron is moved away from the coil, the saturation effects decrease. This is a complicated effect which can be described adequately by $(r_c/r_f)^2$ only for a limited range of magnets similar to those discussed in this section.

As a third example, Table 1.3.2-III and Figure 1.3.2-C give data for a cosine dipole with a rather large aperture of 25.4 cm. This magnet has the parameters $r_c = 12.7$, $r_f = 15.2$, $h_c = 2.03$, and $t = 22.9$ cm and is being built for use on the experimental floor of the AGS at BNL [1.3.2-e]. The iron shield thickness $t = 22.9$ cm is not far from the critical thickness $t_c = 19$ cm; it gives somewhat smaller sextupole fields and somewhat larger leakage fields.

Other studies on various aspects of cosine bending magnets include those of Coupland [1.3.2-f], Coupland, Simkin, and Randle [1.3.2-g], Lee and Snowdon [1.3.2-h], Turowski, Coupland, and Perot [1.3.2-i], Berruyer, Blondet, Bronca, Genevey, Kircher, and Perot [1.3.2-j], Bronca, Genevey, Kircher, Perot, Pouillange, and Prost [1.3.2-k], Coupland and Baynham [1.3.2-l], Sampson, Dahl, McInturff, and Morgan [1.3.2-m], Gilbert, Meuser, Volker, Kilpatrick, Eaton, Toby, and Acker [1.3.2-n], Reardon, Strauss, Sutter, McCracken, Richied, and Ostravka [1.3.2-o], Sampson, Britton, Morgan, Dahl, and Blewett [1.3.2-p], and Brechna and Perot [1.3.2-q].

REFERENCES, SECTION 1.3.2

1.3.2-a. P.F. Dahl, R. Damm, D.D. Jacobus, C. Lasky, A.D. McInturff, G.H. Morgan, G. Parzen, and W.B. Sampson, in Proc. 1973 Particle Accelerator Conf., *IEEE Trans. Nucl. Sci.* **NS-20**, No. 3, 688 (1973).

1.3.2-b. G. Parzen and K. Jellett, BNL Internal Report No. AADD-198, 1973.

1.3.2-c. G. Parzen and K. Jellett, in Proc. 1971 Particle Accelerator Conf., *IEEE Trans. Nucl. Sci.* **NS-18**, No. 3, 646 (1971).

1.3.2-d. A.D. McInturff, P.F. Dahl, R. Damm, C. Lasky, K. Robins, and W.B. Sampson, in Proc. 1975 Particle Accelerator Conf., *IEEE Trans. Nucl. Sci.* **NS-22**, No. 3, 1133 (1975).

1.3.2-e. G. Morgan, J. Aggus, J. Bamberger, D. Brown, P. Dahl, R. Damm, H. Hahn, D. Kassner, C. Lasky, G. Parzen, A. Schlafke, and W. Sampson, *Ibid.*, 1164.
1.3.2-f. J.H. Coupland, Rutherford Laboratory Report RL-73-105, 1973.
1.3.2-g. J.H. Coupland, J. Simkin, and T.C. Randle, *Nucl. Instrum. Methods* **106**, 595 (1973).
1.3.2-h. W.W. Lee and S.C. Snowdon, p. 726 in ref. [1.3.2-a].
1.3.2-i. P. Turowski, J.H. Coupland, and J. Perot, in *Proc. 9th Int. Conf. High Energy Accelerators, SLAC, Stanford University, 1974*, p. 174, CONF-740522, 1974.
1.3.2-j. A. Berruyer, R. Blondet, G. Bronca, P. Genevey, F. Kircher, J. Perot, and J.P. Pouillange, in *Proc. 4th Int. Conf. Magnet Technology, Brookhaven, 1972*, p. 316, CONF-720908, 1972.
1.3.2-k. G. Bronca, P. Genevey, F. Kircher, J. Perot, J.P. Pouillange, and G. Prost, *Ibid.*, p. 203.
l. J.H. Coupland and D.E. Baynham, *Ibid.*, p. 737.
m. W.B. Sampson, P.F. Dahl, A.P. McInturff, and G.H. Morgan, *Ibid.*, p. 752.
1.3.2-n. W.S. Gilbert, R.B. Meuser, F. Volker, R.A. Kilpatric, W.F. Eaton, F.L. Toby, and R.C. Acher, p. 683 in ref. [1.3.2-a].
1.3.2-o. P.J. Reardon, B.P. Strauss, D. Sutter, R. McCracken, P. Richied, and M.A. Otavka, p. 744 in ref. [1.3.2-a].
1.3.2-p. W.B. Sampson, R.B. Britton, G.H. Morgan, P.F. Dahl, and J.P. Blewett, *IEEE Trans. Nucl. Sci.* **NS-16**, No. 3, 720 (1969).
1.3.2-q. H. Brechna and J. Perot, in *Proc. 3rd Int. Conf. Magnet Technology, Hamburg, 1970*, p. 3, G. Söhngen et al., Editors, Deutsches Elektronen-Synchrotron DESY, 1972.

1.3.3 End Effects in Cosine Bending Magnets. As described in Section 1.1.2, the ends of the cosine bending magnet will contribute an amount Δb_n to the integrated multipole $\bar{b}_n$, and we can write

$$\bar{b}_n = b_n + \Delta b_n ,$$

where b_n is the two-dimensional multipole valid near the center of the magnet and Δb_n gives the contribution of the ends.

Table 1.3.3-I lists the low field results for the contribution of the ends to the multipole for a cosine bending magnet measured at BNL [1.3.3-a] which has $r_c = 4$,

Table 1.3.3-I

Measured Results for the End Effects, Δb_n, for Two Cosine Bending Magnets at Low Fields

	Magnet	
	BNL [1.3.3-a]	RHEL [1.3.3-b]
L_M, cm	100	55
r_c, cm	4	4.65
r_f, cm	6.35	8.38
L_M/r_c	25	11.8
$r_c^2 \Delta b_2/10^{-2}$	−1.2	0.06
$r_c^4 \Delta b_4/10^{-2}$	−1.1	−0.2
$r_c^6 \Delta b_6/10^{-2}$	−0.03	0.4
$r_c^8 \Delta b_8/10^{-2}$	−0.14	0.3

Table 1.3.3-II

Measured Results for the End Effects, Δb_n,
for the Rutherford Laboratory Cosine Magnet [1.3.3-b]

($r_c = 4.65$ and $L_M = 55$ cm)

	B_0, kG	
	17	39
$r_c^2 \Delta b_2 / 10^{-2}$	0.06	0.00
$r_c^4 \Delta b_4 / 10^{-2}$	−0.2	−0.32
$r_c^6 \Delta b_6 / 10^{-2}$	0.46	0.56
$r_c^8 \Delta b_8 / 10^{-2}$	0.30	0.24

and $L_M = 100$ cm, and for a cosine bending magnet measured at Rutherford Laboratory [1.3.3-b] which has $r_c = 4.65$ and $L_M = 55$ cm. In comparing the results for the two magnets, it should be kept in mind that the Δb_n should scale like r_c/L_M, which differs between the two magnets by a factor of ~ 2.

The effect of the ends on the integrated multipole, b_n, depends strongly on the end geometry. It is known that the end geometry of the coil can be adjusted to make the $\Delta b_n = 0$ [1.3.3-c to -f]. It would be useful, however, to have an empirical rule for estimating the Δb_n when the ends are not especially designed to make them vanish. On the basis of the results in Table 1.3.3-I one may propose the empirical rule

$$r_c^2 \Delta b_2 = \pm 0.3 \, (r_c/L_M) \,,$$

$$r_c^4 \Delta b_4 \simeq r_c^2 \Delta b_2 \,,$$

$$r_c^6 \Delta b_6 \simeq 0.2 r_c^2 \Delta b_2 \,,$$

$$r_c^8 \Delta b_8 \simeq 0.2 r_c^2 \Delta b_2 \,. \qquad (1.3.3\text{-}1)$$

Effect of iron saturation. It appears reasonable to expect that the Δb_n present will change by an appreciable fraction as the field changes from low level to about 40 kG. Table 1.3.3-II gives the Δb_n measured for the Rutherford Laboratory magnet (see Table 1.3.3-I) for $B_0 = 17$ kG and 39 kG. Note that for this magnet Δb_2 was small at low fields and remains small at 39 kG.

REFERENCES, SECTION 1.3.3

1.3.3-a. P.F. Dahl, R. Damm, D.D. Jacobus, C. Lasky, A.D. McInturff, G.H. Morgan, G. Parzen, and W.B. Sampson, *IEEE Trans. Nucl. Sci.* **NS-20**, No. 3, 688 (1973).

1.3.3-b. J.H. Coupland, Rutherford Laboratory Report RL-73-105, 1973.

1.3.3-c. J.H. Coupland, Rutherford Laboratory, Report RHEL/R 230, 1970.

1.3.3-d. F.E. Mills and G. Morgan, *Part. Accel.* 5, No. 4, 227 (1973).

1.3.3-e. B.B. Goodman, *Nucl. Instrum. Methods* **89**, 4 (1970).

1.3.3-f. R.B. Meuser, *IEEE Trans. Nucl. Sci.* **NS-18**, No. 3, 677 (1971).

1.4 C-Magnets

One advantage of a C-magnet such as that shown in Figure 1.4-A is the easy accessibility of the space between the poles. The C-magnet can be thought of as an H-magnet with one backleg removed. All the flux is forced to return through the remaining backleg, which needs to be made correspondingly larger.

Most of the results given in Section 1.2 for H-magnets can be expected to apply to C-magnets also.

The empirical rule for the region of good field in the absence of iron saturation effects [Eqs. (1.2.1-1)] should apply:

$$\Delta x_{0.01} = w - g\,,$$

$$\Delta x_{0.001} = w - 2g\,,$$

where $\Delta x_{0.01}$, or $\Delta x_{0.001}$, is the half-region of good field, given the criterion that the field not change by $>1\%$, or $>0.1\%$, respectively.

The region of good field can probably be extended by adding a shim (dimensions given in Figure 1.2.2-B) at the two edges of the pole, and the area of the rectangular shim that will flatten the field is given roughly by Eq. (1.2.2-1):

$$\text{Shim area} = 0.021 g^2\,,$$

where g is the half-gap and the shims increase the good aperture $\Delta x_{0.01}$ or $\Delta x_{0.001}$ by $0.5g$ and g, respectively.

The sextupole term due to iron saturation effects will probably be the dominant multipole and may be roughly estimated from Eq. (1.2.3-2a):

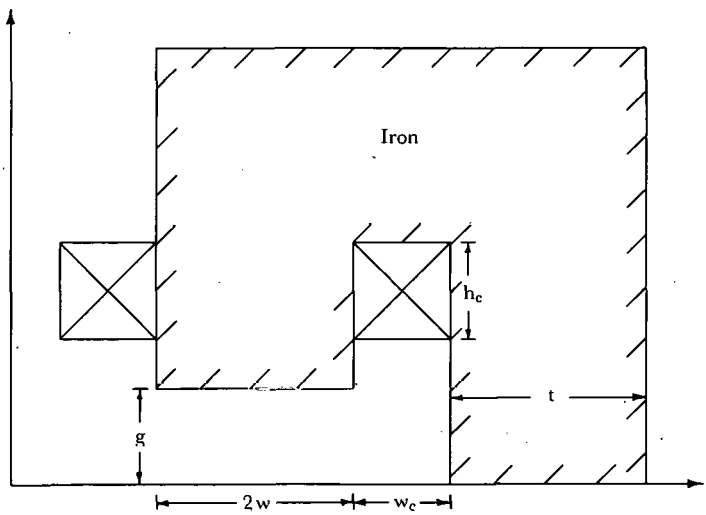

1.4-A. C-magnet geometry.

Table 1.4-I

Computed Results for a C-Magnet

($g=12.7$, $w=25.4$, $w_c=17$, and $h_c=25.4$ cm)

	B, kG		
	3.3	13.2	16.5
$g^2b_2/10^{-2}$	−1.0	−1.9	−3.0
NI, kA	67.2	336	526
$NI/NI_{\mu=\infty}$	1	1.25	1.57
$\Delta x_{0.01}/g$	0.74	–	–

$$g^2b_2 = -0.2\left(\frac{5g}{w}\right)^2 \gamma_{\text{pole}} \frac{g}{w+g},$$

where γ_{pole} is the maximum value of γ along the center line of the pole.

Table 1.4-I gives some results for a C-magnet with $g=12.7$, $w=25.4$, $w_c=17$, and $h_c=25.4$ cm, which was built at the Zero Gradient Synchrotron at ANL [1.4-a]. The data are consistent with the empirical rules given above within a factor of 2.

The C-magnet differs from the H-magnet in that it is not symmetrical around the center of the magnet. As a result, iron saturation effects introduce appreciable odd multipoles, b_1, b_3, ..., into the median-plane magnetic field.

Table 1.4-II gives results for the multipoles introduced by iron saturation for the Japanese 12-GeV proton accelerator main-ring bending magnet (KEK) [1.4-a, -b]. The dimensions of this C-magnet are $g=2.8$, $w=14$, $w_c=12$, $h_c=9.7$, and $t=29.5$ cm. The magnet has a rounded end and a shim to extend the good field region. The results given here are for nonoriented steel. These calculations by Endo and Kihara [1.4-b] also show that a similar H-magnet has about the same sextupole term, b_2, as the C-magnet.

REFERENCES, SECTION 1.4

1.4-a. L.G. Ratner and R.J. Lari, *ANL User's Handbook*, Section 5, 1966.

1.4-b. K. Endo and M. Kihara, in *Proc. 4th Int. Conf. Magnet Technology, Brookhaven, 1972*, p. CONF-720908, 1972.

1.4-c. T. Kasuga, E. Takasaki, T. Igaraski, A. Araki, A. Ando, K. Endo, and M. Kihara, in *Proc. 5th Int. Conf. Magnet Technology, Rome, 1975*, p. 14, CONF-750444, 1975.

1.4.1 End Effects in C-Magnets. As shown in Section 1.1.2, the end effects may be described by ΔL_B, the contribution of the ends to the effective length of the magnet, and by Δb_2, the contribution of the ends to the integrated sextupole, $\bar{b}_2$, of the magnet.

The two quantities describing the end effects, ΔL_B and Δb_2, are expected to be roughly given by the same empirical rules as were found for the H-magnet. This is

Table 1.4-II

Computed Results for a C-Magnet
(the Japanese 12-GeV Proton Accelerator Bending Magnet [1.4-a, -b])

($g=2.8$, $w=14$, $w_c=12$, $h_c=9.7$, and $t=29.5$ cm)

	B, kG				
	15	16	17	18	19
$.0^{-4}$	2.8	4.2	5.0	5.3	3.5
10^{-4}	0.78	1.6	1.96	2.7	3.9
$g^3b_3/10^{-4}$	0.025	0.040	0.055	0.064	0.049

roughly true, as shown in Table 1.4.1-I, which lists the low-field end effects, ΔL_B and Δb_2, for several C-magnets measured by Ratner and Lari [1.4.1-a] and by Endo and Kihara and by Kasuga et al. [1.4.1-b]. On the basis of the results in Table 1.4.1-I, one may propose the rough empirical rules

$$\Delta L_B/2 = 0.75g\,,$$

$$g^2\Delta b_2 = 0.36(g/L_M)(g/w)^2\,. \qquad (1.4.1\text{-}1)$$

To the accuracy claimed, these empirical rules for the end effects in C-magnets are the same as those found for H-magnets in Section 1.2.4 and for window-frame magnets in Section 1.1.2.

Effects of iron saturation. The above results for the end effects, ΔL_B and Δb_2, are valid at low field levels. At higher fields, the end effects will change because of iron saturation.

$L_B/2$, the contribution of one end of the magnet to the effective length, varies from 0.8 to $0.51g$, from low fields to 16.5 kG, or a change of 38% for the first magnet in Table 1.4.1-I.

Table 1.4.1-I

Measured Results for the End Effects, ΔL_B and Δb_2, for Several C-Magnets at Low Fields

	Magnet	
	ANL [1.4.1-a]	KEK [1.4.1-b]
L_M, cm	76.2	322
g, cm	12.7	2.8
w, cm	25.4	14
w/g	2	5
$\Delta L_B/2g$	0.8	0.7
$g^2\Delta b_2/10^{-4}$	−42	0.91
$L_M g\Delta b_2/(g/w)^2$	0.46	0.27

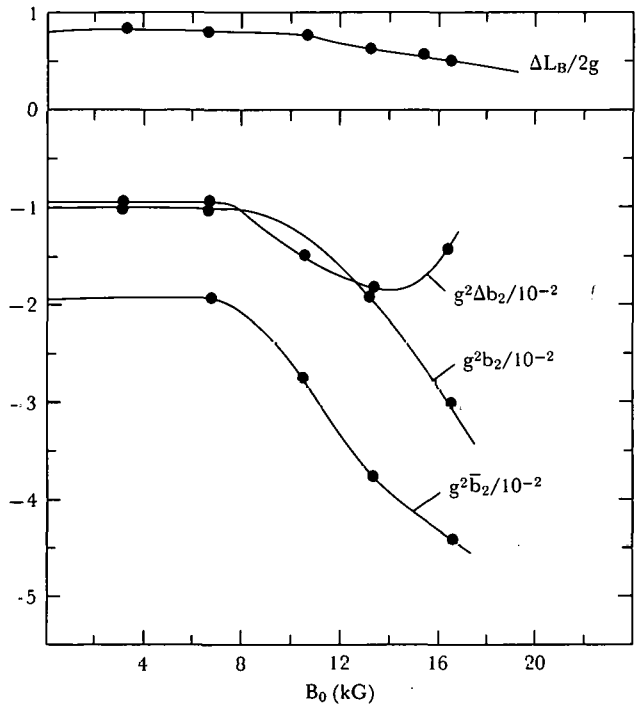

1.4.1-A. End effect on the sextupole multipole for a C-magnet. $g=5$, $w=10$, and $L_M=30$ in.

Figure 1.4.1-A shows the effect of iron saturation on Δb_2, the contribution of the ends to the integrated sextupole b_2, for the first magnet in Table 1.4.1-I, which has $L_M=30$, $g=5$, and $w=10$ in. For this magnet, Δb_2 and b_2, the contribution of the central part of the magnet, contribute about equally at the higher fields.

The results for Δb_2 shown in Figure 1.4.1-A can be used for other C-magnets by scaling by the factor $(g/L_M)(g/w)^2$. The curve in Figure 1.4.1-A for Δb_2 versus B_0 for C-magnets is roughly the same as the curve in Section 1.1.2 for window-frame magnets and that in Section 1.2.4 for H-magnets when these curves are scaled according to the factor $(g/L_M)(g/w)^2$.

$\Delta L_B/2g$ is also plotted in Figure 1.4.1-A as a function of field.

REFERENCES, SECTION 1.4.1

1.4.1-a. L.G. Ratner and R. J. Lari, *ANL User's Handbook*, Section 5, 1966.

1.4.1-b. K. Endo and M. Kihara, in *Proc. 4th Int. Conf. Magnet Technology, Brookhaven, 1972*, p. 363, CONF-720908, 1972; T. Kasugo, E. Takasaki, T. Igarashi, A. Araki, A. Ando, K. Endo, and M. Kihara, in *Proc. 5th Int. Conf. Magnet Technology, Rome, 1975*, p. 74, CONF-750444, 1975.

1.5 FNAL Bending Magnet

A bending magnet that may be considered a hybrid between the window-frame and H-magnets has been developed for use in the main rings of the FNAL and CERN high energy proton accelerators. The simple version of this magnet shown in Figure 1.5-A can be thought of as an H-magnet with a square pole, with some of the ampere turns put underneath the pole.

At low field levels, assuming $\mu = \infty$, the current I_2 underneath the poles produces a uniform field in the aperture, whereas the current I_1 generates a field similar to that of an H-magnet, where the field drops somewhat with distance from the center of the magnet on the median plane. This dropping of the field can be corrected by leaving a space of width δ between the coils underneath the pole and the pole. This space acts as a negative correction current I_c [1.5-a], occupying the space vacated, and produces a rising field which can be adjusted to compensate for the dropping field. The effective correction current depends on δ and on R, the ratio of the current underneath the pole to the total current $[R = I_2/(I_1 + I_2)]$. One can write

$$I_c \cong (\delta/g) I_2$$

or

$$I_c \cong \delta \frac{R}{1-R} I_1 .$$

There is then a range of solutions depending on the parameters δ and R, which flatten the field and improve the range of the good field aperture. In practice R can have only certain values, since it is determined by the ratio of the number of coil turns underneath the gap to the total number of turns. The field can also be flattened by shaping the pole [1.5-b, -c].

At the high field end, around 18 kG, an interesting effect occurs. As noted in Sections 1.1 and 1.3, the iron saturation effects in window-frame and H-magnets are

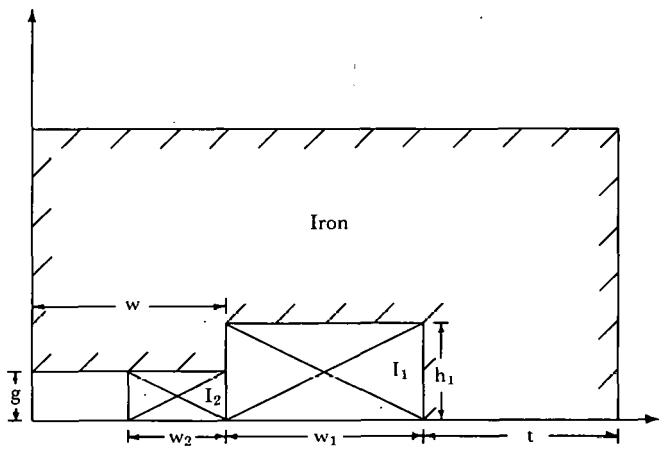

1.5-A. FNAL magnet geometry.

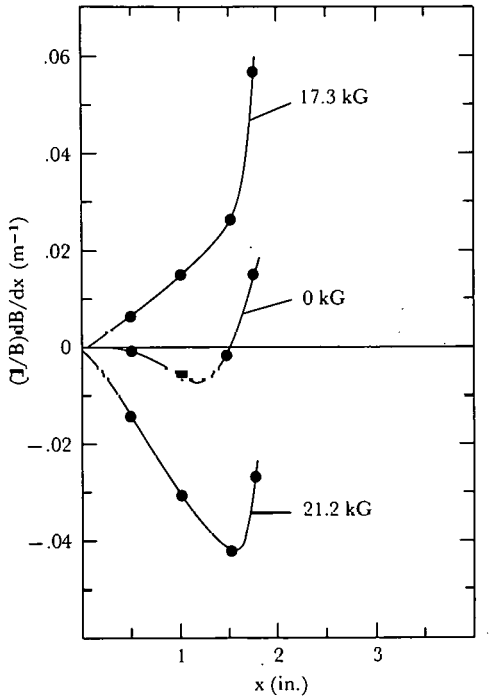

1.5-B. Median-plane field gradient in a square-pole FNAL magnet.

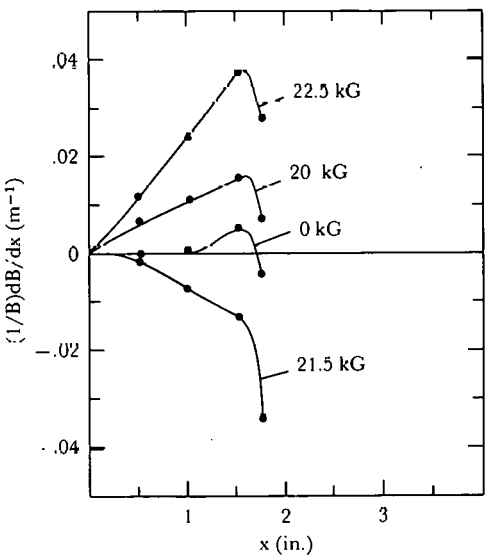

1.5-C. Median-plane field gradient in an FNAL magnet with shaped and tapered pole.

in opposite directions: for the window-frame magnet, the field rises with distance from the magnet center, whereas for the H-magnet, the field drops. These two effects appear to compete in a complicated and sensitive manner, so that the iron saturation effects rise and fall as the field is increased, instead of simply increasing monotonically. This is shown in Figure 1.5-B, where the gradient $(1/B_0)dB/dx$ is plotted against r for various field levels, for the square-pole magnet (Figure 1.5-A) with $w=4$, $w_2=2$, $g=1$, $h_1=2$, and $t=5$ in.

The competing effect at the high field end is sensitive to the shaping and tapering of the pole and to variation of the width of the pole which can be used to improve the field at the high field end. Figure 1.5-C shows the field shape obtained by FNAL B_2 magnet [1.5-c, -d], whose dimensions are roughly those of the square-pole magnet described above. However, the pole is shaped and tapered [1.5-c].

Results for the CERN magnet are given in refs. [1.5-e, -f].

REFERENCES, SECTION 1.5

1.5-a. R. J. Lari and L.C. Teng, *IEEE Trans. Nucl. Sci.* **NS-16**, No. 3, 667 (1969).

1.5-b. B. McD. Bingham, FNAL Report TM-194, 1969.

1.5-c. R. Yamada, C.S. Schmidt, R. Juhala, and R. Lari, in *Proc. 4th Int. Conf. Magnet Technology, Brookhaven, 1972*, p. 423, CONF-720908, 1972.

1.5-d. H. Hinterberger, J. Satti, C. Schmidt, R. Sheldon, and R. Yamada, *IEEE Trans. Nucl. Sci.* **NS-18**, No. 3, 853 (1971).

1.5-e. *The 300-GeV Programme*, CERN/1050, 1972.

1.5-f. R. Billinge, in *Proc. 5th Int. Conf. Magnet Technology, Rome, 1975*, p. 3, CONF-750444, 1975.

2. QUADRUPOLES

In a quadrupole the desired magnetic field varies linearly across the aperture of the magnet on the median plane. An almost linear field can be generated by a magnet configuration such as that in Figure 2.1-A in which the pole surface is a hyperbola. The field would be exactly linear if the coil size were to shrink to zero. However, the coils must have a nonzero size to carry the current needed to produce the desired gradient. Ending the hyperbola at some point in order to leave room for the coils limits the quality of the linear field obtainable.

The quadrupole often has a fourfold symmetry, as in Figure 2-A. In this the symmetry requires that the only multipoles present are b_1, b_5, b_9, etc., and can write the median plane field as

$$B = B_0'(x + b_5x^5 + b_9x^9 + \ldots), \tag{2-1}$$

where B_0' is the gradient at the center of the quadrupole.

Equation (2.1-1) shows that any quadrupole with fourfold symmetry will have a region in which the field is linear, no matter what pole shape is used, since the first nonlinear multipole is b_5x^5. Thus quadrupoles can be built with poles that are circles or straight lines, which are simpler to construct.

As shown later, the dimensions of the pole can be chosen to make b_5 vanish, which will give a fairly good quadrupole. This can be done if the pole surface is a hyperbola, a circle, a straight line, or probably any other reasonable curve.

By a more complicated shaping of the pole surface, both b_5 and b_9 can be made to vanish. It seems likely that this process can be carried as far as desired and the quadrupole made as linear as desired by shaping the iron pole surface [2-a].

It is apparent that the hyperbolic pole is just the first step in approximating a quadrupole. General rules can be given for pole profiles that make b_5 vanish. It is more difficult to give general solutions for more accurate quadrupoles, which require the elimination of even higher multipoles.

In the quadrupoles described so far, the field is determined primarily by the shape of the iron profile. It is also possible to construct quadrupoles in which the field is determined primarily by the shape of the current distribution. An example is the cosine quadrupole with a cosine current distribution (see Section 2.5).

2.1 Quadrupoles With Hyperbolic Poles

A quadrupole with a hyperbolic pole is shown in Figure 2.1-A. The hyperbolic part of the pole is cut off at the angle $\theta = \theta_1$, where θ is measured relative to the center of the pole. At $\theta = \theta_1$, in the design shown in Figure 2.1-A, the pole is continued along a radius. The manner in which the pole is ended is usually not a sensitive factor. The equation of the hyperbola may be written as

$$r^2 \cos 2\theta = r_0^2, \tag{2.1-1}$$

where r_0 is the radius to the center of the pole and θ is the azimuthal angle relative to the pole center.

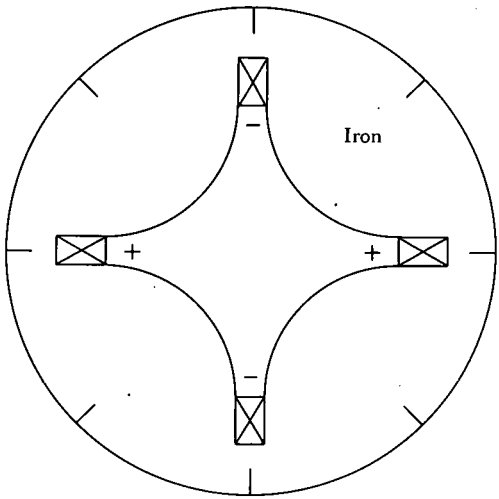

2-A. Quadrupole geometry.

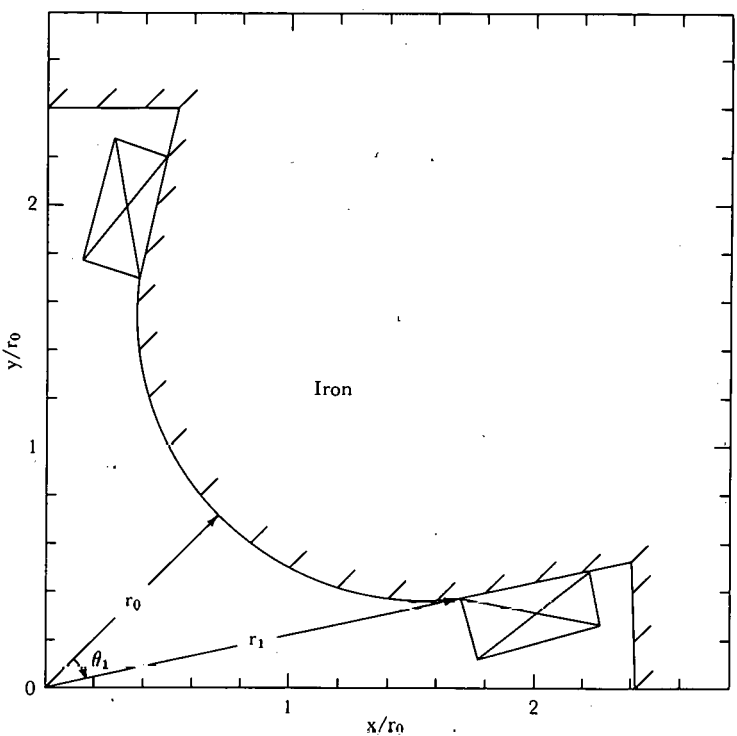

2.1-A. Quadrupole with a hyperbolic pole.

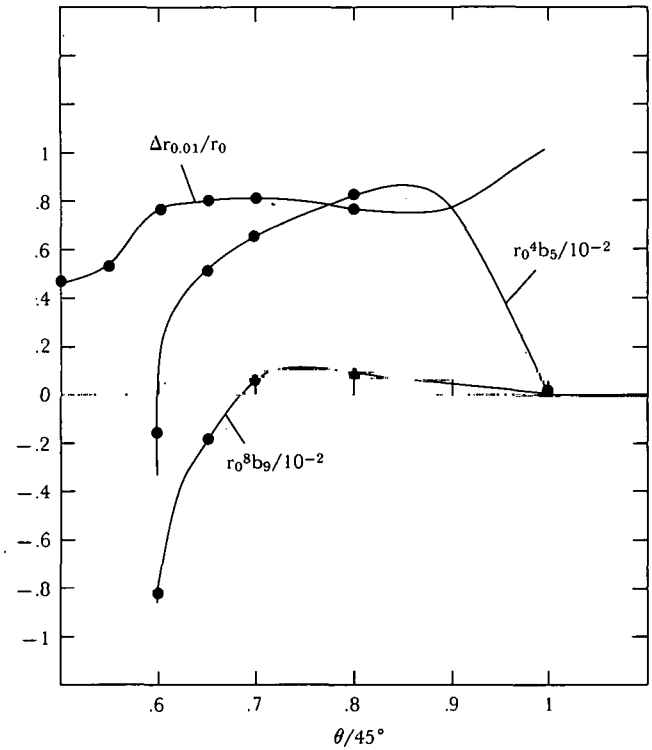

2.1-B. Field multipoles and good aperture for a quadrupole with a hyperbolic pole.

Figure 2.1-B shows how the size of the nonlinear multipoles b_5 and b_9 depends on the cutoff angle of the hyperbola, θ_1. There is a cutoff angle θ_1 at which the first undesired multipole, b_5, vanishes. This happens at

$$\theta_1 = 27.0°\,, \quad \theta_1/45° = 0.60\,;$$

$$r_1/r_0 = 1.122\,. \tag{2.1-2}$$

In Figure 2.1-B, $r_0^4 b_5$ is the field at the pole due to the b_5 multipole relative to due to the gradient term, which is $B_0' r_0$. In the same way $r_0^8 b_9$ represents the fie the pole due to the b_9 multipole.

Figure 2.1-B also shows the good aperture achieved, $\Delta r_{0.01}$. The criterion used in calculating $\Delta r_{0.01}$ is that the gradient not change by $>1\%$ in any direction. When b_5 vanishes, the size of $\Delta r_{0.01}$ is limited by the remaining b_9 multipole. It can be seen from Figure 2.1-B that for the cutoff angle that makes b_5 vanish, a good field aperture of 80% can be achieved.

Considerably more good field aperture is often obtained in one direction, the horizontal, for example, as compared with the vertical. The various multipoles may cancel each other in the horizontal direction but strengthen each other in the vertical.

The good field aperture $\Delta r_{0.01}$ has been computed from b_5 and b_9 by using the same 0.01 criterion and finding the good aperture limit due to the b_5 term alone, and that due to the b_9 term alone, and then taking the smaller of the two limits. This procedure gives an aperture limit that is achieved to a pretty good approximation in all directions. The b_5 and b_9 data in Figure 2.1-B can also be used to compute the good field aperture on the basis of some other criterion, such as requiring that the field gradient not change by $>.1\%$.

It can be seen in Figure 2.1-B that the maximum in the good field aperture $\Delta r_{0.01}$ is fairly broad and that the 80% good field aperture can be obtained for a range of cutoff angles. One advantage of the hyperbolic pole is that it is not tive to the cutoff angle. A second is that it gives somewhat more good aperture.

Several assumptions are made in obtaining the data shown in Figure 2.1-B. One is that the coil is sufficiently hidden by the pole that the field quality is not affected. This is the case if no part of the coil is closer than r_1, the radial position of the hyperbola at the cutoff angle θ_1. In addition, the results in the range $0.8 < \theta_1/45° < 1$ were found by extrapolation because of difficulties in studying this region with a magnet computer program.

2.2 Quadrupoles With Circular Poles

A quadrupole with a circular pole of radius R is shown in Figure 2.2-A. The circle part of the pole is cut off at the angle θ_1, where the pole is continued along a radius. It is possible to choose the circle radius R and the cutoff angle so that the lowest undesired multipole, b_5, vanishes. In this study, the radius R is related to the cutoff angle θ_1 in such a way that the radius r_1, drawn to the cutoff point on the circle, is tangent to the circle at that point. It is found that R and θ_1 are related by

$$R = r_0 \sin\theta_1/(1-\sin\theta_1) \; ;$$

$$r_1 = (R+r_0)\cos\theta_1 \; . \qquad (2$$

Figure 2.2-B shows how the multipoles b_5 and b_9 depend on the cutoff angle of the circle, θ_1. The first undesired multipole, b_5, vanishes at

$$\theta_1 = 31.5^\circ \; , \quad \theta_1/45^\circ = 0.70 \; ;$$

$$r_1/r_0 = 1.785 \; , \quad d/r_0 = 0.417 \; ;$$

$$R/r_0 = 1.094 \; , \quad w/r_0 = 0.932 \; . \qquad (2.2\text{-}2)$$

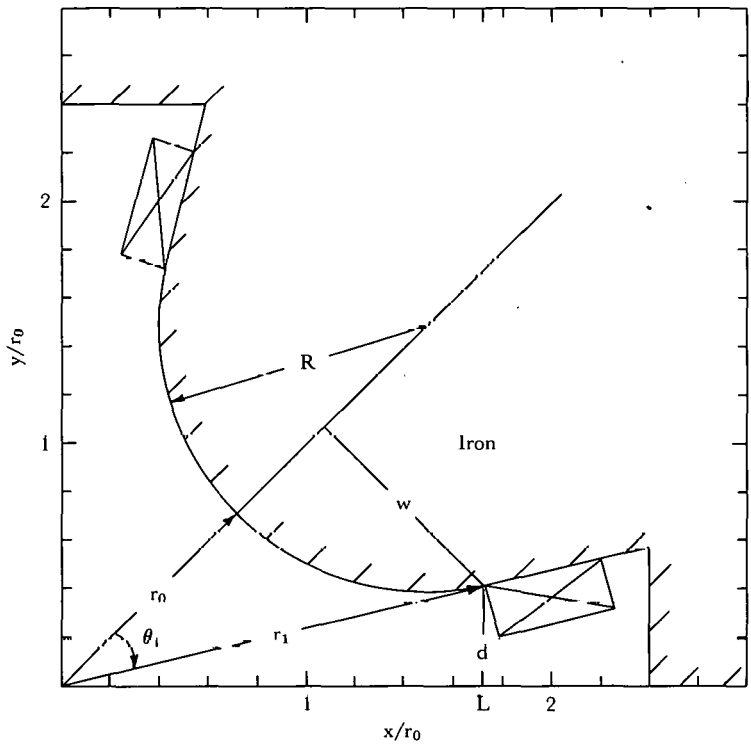

2.2-A. Quadrupole with a circular pole.

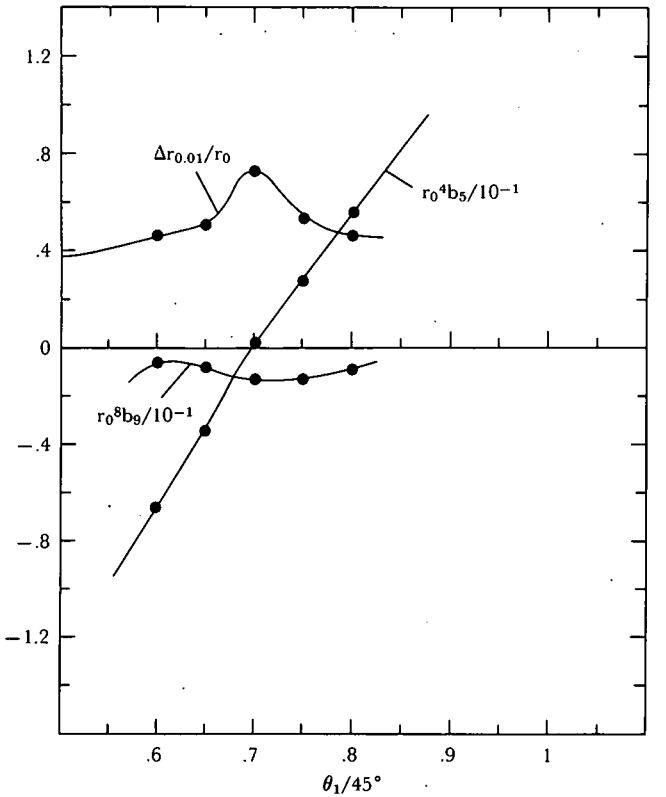

2.2-B. Field multipoles and good aperture for a quadrupole with a circular pole.

Also shown in Figure 2.2-B is the good field aperture, $\Delta r_{0.01}$, that is achieved. By choosing θ_1 to make b_5 vanish, one obtains the largest good aperture, which is 73% of r_0, compared with 80% for the hyperbolic pole.

As for the hyperbolic pole, it has been assumed that the coil is sufficiently hidden by the pole that the field quality is not affected. This is the case if no part of the
s closer to the center than r_1, the radial position of the circle at the cutoff
, θ_1.

The pole profile shown in Figure 2.2-A corresponds to the case in which b_5 vanishes.

The above solution should make it possible to design smaller quadrupoles with essentially the same good field aperture, $\Delta r_{0.01}/r_0 = 0.73$. The distance to the coil from the magnet center is given by $r_1/r_0 = 1.785$, which is about 2.4 times as large as the good aperture. A larger value of r_1, the coil position, has two disadvantages: the quadrupole is correspondingly larger, and the maximum field reached on the pole surface is also larger, being proportional to r_1. One way to make the quadrupole smaller is to start with the above solution and then move the coil toward the center.

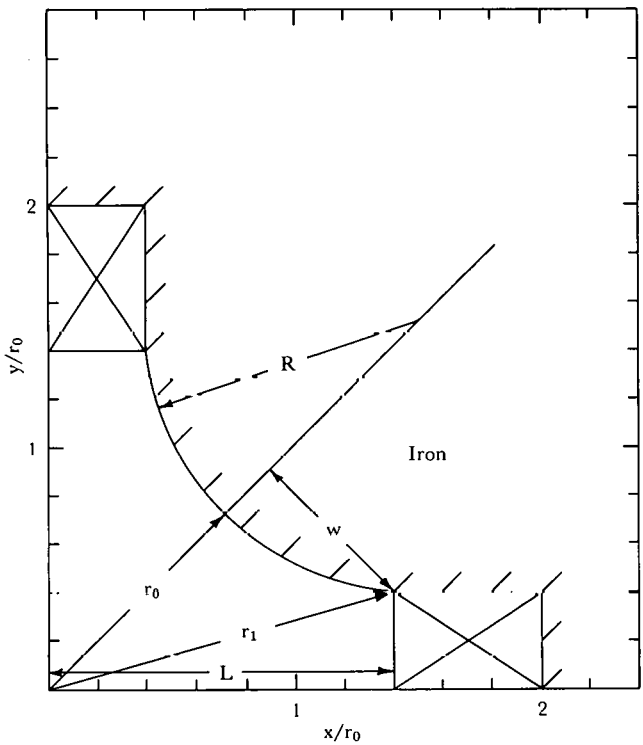

2.2-C. Quadrupole with a circular pole. (See refs. [2.2-a, -b].)

The b_5 produced will be different from zero and can be canceled by changing the radius R of the circular pole. A disadvantage of this approach is that the field becomes sensitive to the position and shape of the coil. A second way to make the quadrupole smaller is to start with the above solution and then shim or shape the ends of the pole near the coil to increase the good aperture (see Section 2.4 below). This approach involves a considerable amount of study and computation.

Studies have been carried out by Kobayashi [2.2-a] and by Bellendir and Lari [2.2-b] on the fields of quadrupoles with circular poles whose geometry is shown in Figure 2.2-C. The computational method was developed by Bellendir and Lari, applied it to one case. A more elaborate study using the same method was ca out by Kobayashi. This quadrupole geometry leads to smaller quadrupoles than the solution given previously and essentially corresponds to moving the coil closer in. The field is then likely to be sensitive to the coil position.

In the study by Kobayashi, for each value of L/r_0, the horizontal distance to the coil (see Figure 2.2-C), the radius R of the circular pole was varied to make $b_5 = 0$. Figure 2.2-D shows the dependence of the multipoles b_5 and b_9 on the cutoff angle of the pole, θ_1, for the case $L/r_0 = 1.4$. For this geometry, R and θ_1 are uniquely related for a given L/r_0, and R is also plotted in Figure 2.2-D. It can be seen from Figure 2.2-D that b_5 can be made to vanish when

$$L/r_0 = 1.4\,;$$

$$\theta_1 = 29.84^\circ\,, \quad \theta_1/45^\circ = 0.663\,;$$

$$r_1/r_0 = 1.449\,, \quad d/r_0 = 0.379\,;$$

$$R/r_0 = 1.137\,, \quad w/r_0 = 0.721\,. \tag{2.2-3}$$

The b_9 multipole for this case determines the good aperture, which is $\Delta r_{0.01} = 0.73 r_0$, the same as in the previous solution. This quadrupole is about 20% smaller.

Kobayashi gives results for even smaller quadrupoles for $L/r_0 = 1.4$ to $L/r_0 = 0.8$. One should be exercised in using the solutions corresponding to smaller values of L/r_0 because of the increased sensitivity of the field to the coil position and shape and because the higher multipoles in the field, past the b_9 multipole, become increasingly important. Table 2.2-I lists the solutions found that make $b_5 = 0$ for various values of L/r_0.

Lee-Whiting and Yamazaki [2.2-c] and Lee-Whiting and Keech [2.2-d] have studied circular poles analytically. They find that b_5 is made to vanish by choosing

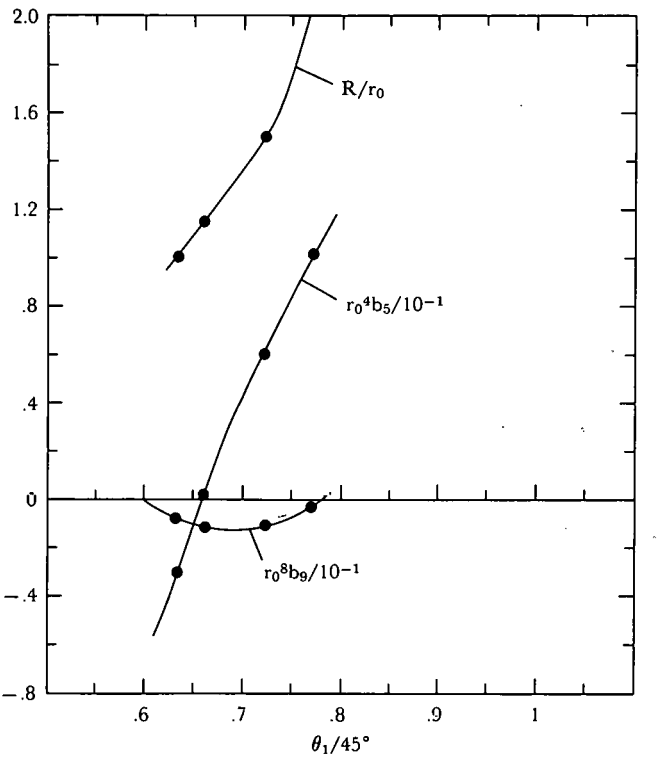

2.2-D. Field multipoles and circle radius for a quadrupole with circular pole. (See refs. [2.2a, -b].)

Table 2.2-I

Parameters of Quadrupoles With Circular Poles That Cause b_5 to Vanish [2.2-a]

(See Figure 2.2-C for geometry)

	L/r_0			
	0.8	1.0	1.2	1.4
R/r_0	1.009	1.063	1.114	1.137
d/r_0	0.624	0.499	0.420	0.379
r_1/r_0	1.015	1.118	1.271	1.449
$\theta_1/45°$	0.298	0.465	0.594	0.663

$R/r_0 = 1.145$, $d/r_0 = 0.372$, and $\theta_1/45° = 0.717$, and that the corresponding $r_0^8 b_9$ is -0.0122. This is to be compared with the results found here of $R/r_0 = 1.094$, $d/r_0 = 0.417$, $\theta_1/45° = 0.70$, and $r_0^8 b_9 = -0.0122$. The differences may be due to the difference in the way the circular pole is terminated.

Dayton et al. [2.2-e], Grivet and Septier [2.2-f], and Septier [2.2-g] have studied circular poles experimentally. They find that b_5 is made to vanish by choosing $R/r_0 = 1.15$, $w/r_0 = 1$, and $\theta_1/45° = 0.717$, and that the corresponding $r_0^8 b_9$ is -0.0125. This is to be compared with the results found here of $R/r_0 = 1.094$, $w/r_0 = 0.932$, $\theta_1/45° = 0.717$, and $r_0^8 b_9 = -0.0122$. Again, the difference may be due to the way in which the circular pole is terminated. Note that the results given here are two dimensional. Appreciable end effects are present (see Section 2.7 below), and these are more important than the inaccuracy that may be present in the above results.

REFERENCES, SECTION 2.2

2.2-a. M. Kobayashi, Institute of Nuclear Study, University of Tokyo, Report SJC-A-71-4, 1971.

2.2-b. G.J. Bellendir and R.J. Lari, ANL Report GJB/RJL-1, 1965.

2.2-c. G.E. Lee-Whiting and L. Yamazaki, *Nucl. Instrum. Methods* **94**, 319 (1971).

2.2-d. G.E. Lee-Whiting and G.H. Keech, Atomic Energy of Canada Limited Report AECL-3253, 1969.

2.2-e. I.E. Dayton, F.C. Shoemaker, and R.F. Mozley, *Rev. Sci. Instrum.* **25**, 485 (1954).

2.2-f. P. Grivet and A. Septier, *Nucl. Instrum. Methods* **6**, 126 (1960).

2.2-g. A. Septier, *Adv. Electron. Electron Phys.* **14**, 85 (1961).

2.3 Quadrupoles With a Straight-Line Pole

A quadrupole with a straight-line pole is shown in Figure 2.3-A. The straight line is cut off at the angle θ_1, where the pole is continued along a radius. It is possible to choose the cutoff angle θ_1 so that the lowest multipole, b_5, vanishes.

Figure 2.3-B shows how the multipoles b_5 and b_9 depend on the cutoff angle θ_1. The first undesired multipole, b_5, vanishes at

$$\theta_1 = 20.11°\,, \quad \theta_1/45° = 0.447\,;$$

$$r_1/r_0 = 1.064\,.$$

Also shown in Figure 2.3-B is the good field aperture, $\Delta r_{0.01}$, that is achieved. By choosing θ_1 to make b_5 vanish, one obtains the largest good aperture, which is 53% of r_0. This is considerably less than that obtained with the circular or hyperbolic pole.

The problem can be solved analytically. Sakudo and Hayashi [2.3-a] give results for the cutoff angle θ_1 that makes b_5 vanish for the two cases in which the angle

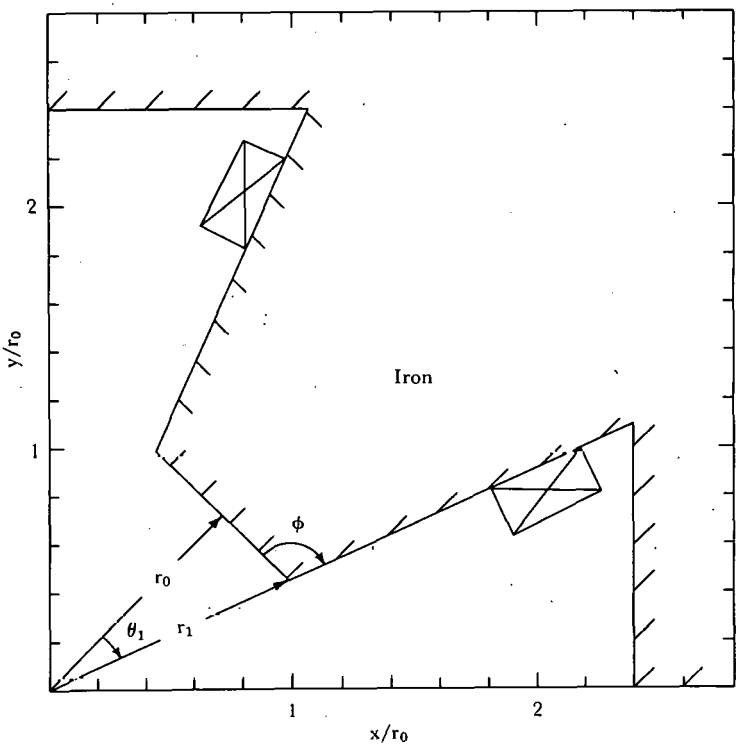

2.3-A. Quadrupole with a straight-line pole.

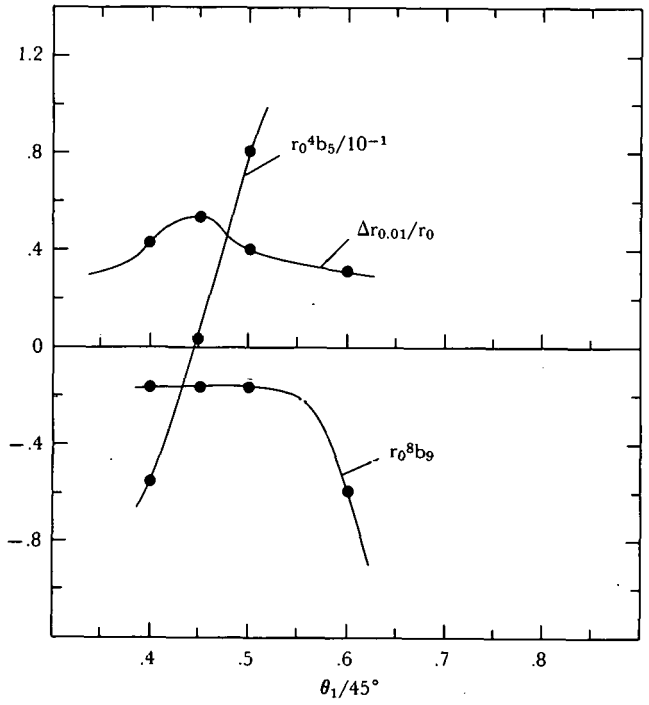

2.3-B. Field multipole and good field aperture for a quadrupole with a straight-line pole.

between the two lines at the edge of the pole, ϕ, is 90° and 135° (see Figure 2.3-A). Their results for θ_1 are

$$\phi = 90°, \quad \theta_1/45° = 0.494, \quad r_1 = 1.080;$$

$$\phi = 135°, \quad \theta_1/45° = 0.413, \quad r_1 = 1.055.$$

This can be compared with the result found here in computer studies: for $\phi = 110.1°$, $\theta_1/45° = 0.447$.

REFERENCE, SECTION 2.3

2.3-a. N. Sakudo and T. Hayashi, *Rev. Sci. Instrum.*, **46**, No. 8, 1060 (1975).

2.4 Pole Quadrupoles With Higher Corrections

The preceding three sections have presented pole profiles that can be adjusted to make the b_5 multipole vanish. Numerous quadrupoles have been designed to make the higher multipoles, such as b_9 and b_{13}, vanish, or to further improve the field gradient shape without using the multipole method of describing the field.

No simple rules seem to exist for shaping the pole to make the higher multipoles (b_9, b_{13}, etc.) vanish. Analytical solutions leading to a rather complicated set of equations to solve have been described by Snowdon [2.4-a]. Of course, any profile that includes higher corrections is a solution of the problem, since this profile can be scaled to any desired size, as long as iron saturation effects are not important. Three such quadrupoles are listed in Table 2.4-I, but precise descriptions of the profiles do not appear to be available in the literature.

One procedure often used is to start with a more or less hyperbolic pole profile and then shape the edges of the pole to get the desired region of acceptable field. Often the field requirements are different in the horizontal and vertical directions, and the pole edges can then be shaped differently in these two directions. This shaping can be done with a magnet computer program. Analytical calculations appear to do well also.

The pole edges are often shaped so as to extend the region where the field gradient is acceptable rather than to cancel the lower undesired multipoles. A larger region of acceptable field gradient is usually obtained by letting the multipoles cancel each other to some extent, instead of making one multipole vanish. Note that canceling multipoles in one direction will not cancel them in another and will produce a smaller aperture in that other direction. However, a larger aperture is often required in the horizontal direction than in the vertical. Canceling multipoles also means that while the field gradient may be acceptable, the multipoles can produce nonlinear fields, which may be troublesome in some applications.

Table 2.4-I lists the good aperture, $\Delta r_{0.01}/r_0$, achieved in four quadrupoles [2.4-b to -e] for both the horizontal and vertical directions. By shaping the pole edges properly one can achieve a good aperture of about $\Delta r_{0.01}/r_0 = 1.5$ in the horizontal direction, about $\Delta r_{0.01}/r_0 = 0.75$ in the vertical direction, or about $\Delta r_{0.01}/r_0 = 1$ in both directions.

Table 2.4-I

Good Field Aperture Achieved in Some Quadrupoles

	Quadrupole type			
	Elliptical (Japan [2.4-d])	Elliptical (FNAL [2.4-b])	Circular (CERN [2.4-c])	Circular (FNAL [2.4-e])
$\Delta r_{0.01}/r_0$, horizontal	1.60	1.50	1.50	1.1
$\Delta r_{0.01}/r_0$, vertical	0.80	0.75	–	1.1
r_0, cm	5	4.17	4.4	3.81

Two of the magnets listed in Table 2.4-I are not circular but elliptical; that is, the pole profile is terminated differently in the horizontal direction than in the vertical direction. The elliptical quadrupole does not have fourfold symmetry, which allows multipoles of lower order than b_5 to appear and allows the magnet to be smaller.

REFERENCES, SECTION 2.4

2.4-a. S.C. Snowdon, FNAL Report FN-253, p. 2221, 1973; *IEEE Trans. Nucl. Sci.* **NS-18**, No. 3, 848 (1971).

2.4-b. H. Hinterberger, S. Pruss, J. Satti, J. Schivell, C. Schmidt, and R. Sheldon Proc. 1971 Particle Accelerator Conf., *IEEE Trans. Nucl. Sci.* **NS-18**, No. 3, 857 (1971)

2.4-c. *The 300-GeV Programme*, CERN/1050, 1972.

2.4-d. K. Endo and M. Kihara, in *Proc. 4th Int. Conf. Magnet Technology, Brookhaven, 1972*, p. 363, CONF-720908, 1972.

2.4-e. F. Ascolese, R. Billinge, H. Edwards, W. Hanson, A. Maschke, J. Michelassi, P. Reardon, and S.C. Snowdon, *Ibid.*, p. 407.

2.4.1 A Stepped Quadrupole. One solution presented in the literature is the Danby-Jackson quadrupole [2.4.1-a], shown in Figure 2.4.1-A. It is a modification of the straight-line quadrupole described in Section 2.3. Two more straight-line steps have been introduced into the profile, and both b_5 and b_9 are made to nearly vanish

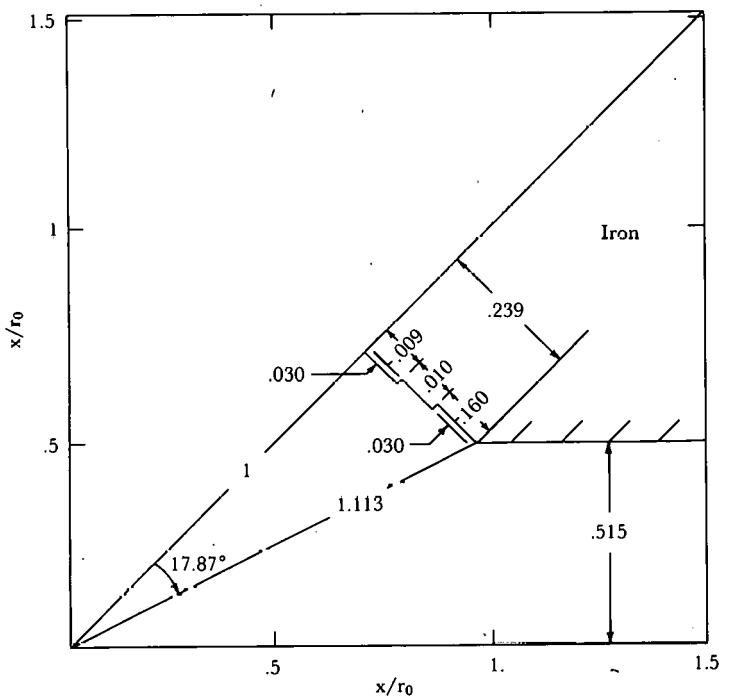

2.4.1-A. Geometry of a stepped quadrupole (Danby-Jackson pole).

by choosing the proper dimensions of the small steps. The step dimensions were determined by experimental measurement of the fields.

The dimensions of this pole profile are shown in Figure 2.4.1-A in units of r_0, the radius to the center of the pole. The remaining multipoles were found to be

$$r_0^4 b_5 = 0.12 \times 10^{-2} ;$$

$$r_0^8 b_9 = -0.43 \times 10^{-2} ;$$

$$r_0^{12} b_{13} = 2.6 \times 10^{-2} . \qquad (2.4.1\text{-}1)$$

If the good field aperture, $\Delta r_{0.01}/r_0$, due to each of the above multipoles is considered separately, the smallest aperture is found to be due to the b_{13} multipole, and there is a good field aperture of 75% in all directions.

By removing both the b_5 and b_9 multipoles, the Danby-Jackson quadrupole produces a good field aperture that is about the same as that achieved with either the hyperbolic or the circular poles adjusted to make b_5 vanish. However, it does allow more room for the coils.

One complication is the contribution of the ends of the quadrupole to the gradient, which may be appreciable if the magnet is not too long longitudinally. For a quadrupole based on making just b_5 vanish, the width of the pole can be adjusted to cancel the end contributions to the integrated value of b_5. If b_9 is also required to vanish, it may be more difficult to deal with the contributions due to the ends.

REFERENCE, SECTION 2.4.1

2.4.1-a. G. Danby and J. Jackson, in Proc. Particle Accelerator Conf., *IEEE Trans. Nucl Sci.* **NS-14**, No. 3, 414 (1967).

2.5 Cosine Quadrupoles

A cosine quadrupole similar to the cosine dipoles described in Section 1.3 can be built. The only difference is that the current density for the quadrupole must be proportional to $\cos 2\theta$, where θ is the azimuthal angle relative to the median plane. Most of the remarks on the cosine dipole (Section 1.3) also apply to the cosine quadrupole. The continuous $\cos 2\theta$ current distribution can be approximated by using blocks of current within which the current density is constant (Figure 2.5-A). For the quadrupole, the current density repeats, except for changes in sign, in every octant. Given three current blocks per octant, then by suitable small azimuthal displacements the first three multipoles, b_5, b_9, and b_{13}, can be made to vanish [2.5

The $\cos 2\theta$ current distribution can also be approximated by using current sl of the type shown in Figure 1.3-B.

REFERENCE, SECTION 2.5

2.5-a. P.F. Dahl and T.M. Taylor, BNL Internal Report No. AADD 74-8, 1974.

2.5.1. Number of Current Blocks. The region of good aperture obtained depends on the number of current blocks per octant, and thus on the number of the

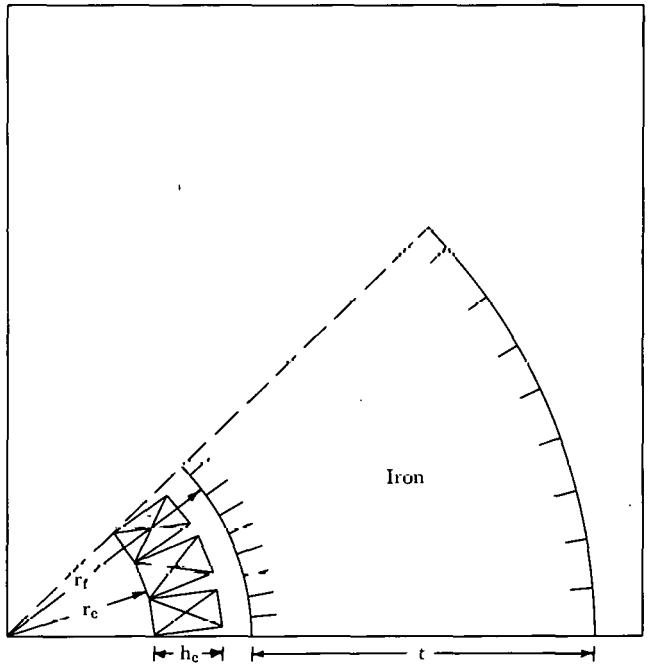

2.5-A. Geometry for a cosine quadrupole.

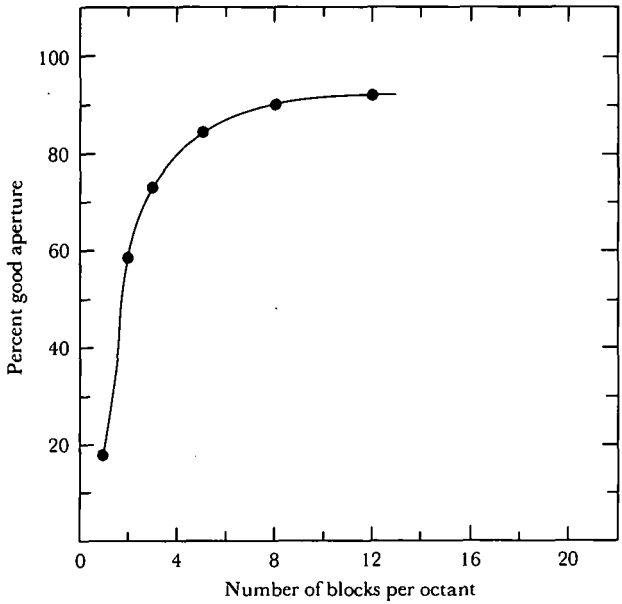

2.5.1-A. Percent good aperture versus number of current blocks in a cosine quadrupole.

lower harmonics that can be made to vanish. Figure 2.5.1-A [1.3.1-a] shows the percentage of good aperture versus the number of blocks per octant. It can be seen that three blocks per octant give about 75% good aperture. This calculation was done for current blocks with an inner radius of 3.8 cm and a radial thickness of 1.59 cm. The results do not seem to be very sensitive to the choice of block dimensions.

REFERENCE, SECTION 2.5.1

2.5.1-a. G. PARZEN AND K. JELLETT, in *Proc. 4th Int. Conf. Magnet Technology, Brookhaven 1972*, p. 612, CONF-720908, 1972.

2.5.2 Iron Saturation Effects in Cosine Quadrupoles. Iron saturation effects in cosine quadrupoles are similar in many respects to those found in cosine dipoles (Section 1.3.2). Results are given below for a quadrupole with a 12-cm aperture and one with a 25.4-cm aperture. Results for these two examples are given in Tables 2.5.2-IV and 2.5.2-II.

The iron saturation effects are sensitive to the thickness of the iron shield. Figure 2.5.2-A shows the decapole field, $r_c^4 b_5$, plotted against the field gradient B' for various choices of iron shield thickness, t, for a 12-cm aperture quadrupole with $r_c = 6$, $r_f = 8.25$, and $h_c = 1.70$ cm.

Table 2.5.2-I

Computed Results for a Cosine Quadrupole

($r_c=6$, $r_f=8.25$, $h_c=1.70$, and $t=7.62$ cm)

	B', kG/cm			
	5.14	5.82	6.67	7.50
$r_c^4 b_5/10^{-2}$	0.42	0.77	1.1	1.?
$r_c^8 b_9/10^{-2}$	−0.063	−0.032	0.040	0
NI, kA	258	296	345	396
Stored energy, kJ/m	22	29	39	50
B_{leak}, kG	0.006	0.021	0.111	0.146
$NI/NI_{\mu=\infty}$	1	1.01	1.03	1.05

Table 2.5.2-II

Computed Results for a Cosine Quadrupole

($r_c=12.7$, $r_f=15.2$, $h_c=2.03$, and $t=11.43$ cm)

	B', kG/cm			
	1.59	2.36	2.99	3.50
$r_c^4 b_5/10^{-2}$	0.01	0.85	1.4	1.0
$r_c^8 b_9/10^{-2}$	−0.006	−0.25	−0.14	−0.19
NI, kA	285	427	569	714
Stored energy, kJ/m	32	71	119	175
B_{leak}, kG	0.001	0.09	0.97	2.31
$NI/NI_{\mu=\infty}$	1.0	1.02	1.07	1.14

It can be seen in Figure 2.5.2-A that there is a critical thickness t_c of the iron shield [2.5.2-a] for which the decapole field b_5 remains flat over a larger range of field levels. This critical thickness may be estimated from the empirical rule

$$t_c=0.59r_f\,. \qquad (2.5.2\text{-}1)$$

Comparing the result of Eq. (2.5.2-1) with the corresponding result for cosine poles [Eq. (1.3.2-1)], it is apparent that the numerical coefficients differ by alr exactly a factor of 2.

Figure 2.5.2-B shows the decapole field variation for a 25.4-cm quadrupole with $r_c=12.7$, $r_f=15.2$, and $h_c=2.03$ cm. Comparison of Figures 2.5.2-A and -B shows that the peak value of the decapole term increases as the iron shield thickness is increased from the critical thickness, t_c. For sufficiently thick iron shields, the peak value of $r_c^4 b_5$ reaches a maximum when the field at the coils, $B'r_c$, is near 45 kG. For the 12-cm and 25.4-cm quadrupoles, this maximum is $(r_c^4 b_5)_{max}=0.011$ and 0.025 respectively. This maximum for the peak in $r_c^4 b_5$ can be used as a measure of the saturation effect in a given magnet, and it can be computed from the empirical rule

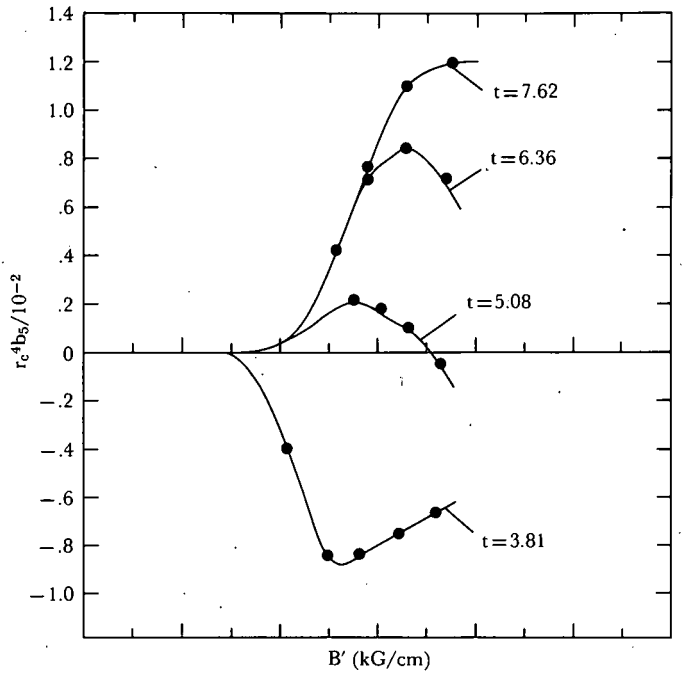

2.5.2-A. Field multipoles for 12-cm cosine quadrupole for various thicknesses of the iron shield. $r_c = 6$ cm; $r_f = 8.25$ cm.

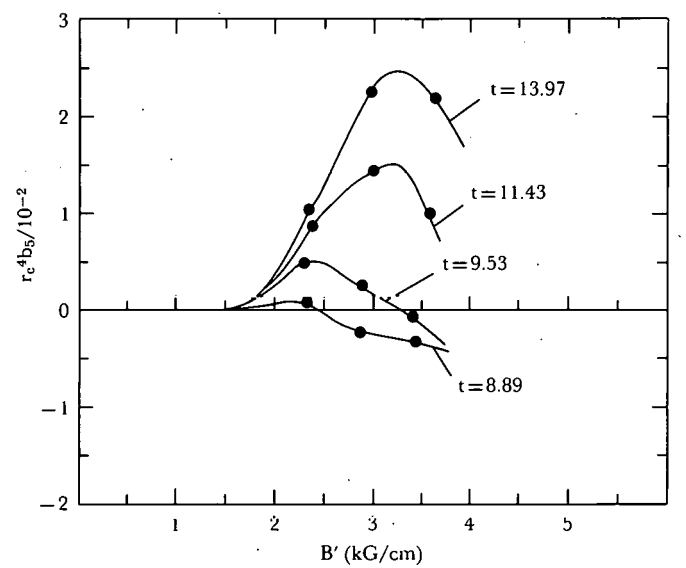

2.5.2-B. Field multipoles for a 25.4-cm cosine quadrupole for various thicknesses of the iron shield. $r_c = 12.7$ cm; $r_f = 15.2$ cm.

$$(r_c^4 b_5)_{\max} = 0.060\left(\frac{r_c}{r_f}\right)^5 . \qquad (2.5.2\text{-}2)$$

Comparison of this result with that for the $(r_c^2 b_2)_{\max}$ of cosine dipoles [Eq. (1.3.2-2)] shows that the numerical coefficient is almost exactly a factor of 2 larger, and the (r_c/r_f) factor occurs with the fifth power instead of the second. This suggests that this rule, with obvious generalizations of the coefficients, may apply to any cosine multipole magnet (cosine sextupoles, cosine octupoles, etc.).

There is no apparent dependence on γ, the inverse permeability, because γ varies only by about 25%, which is within the accuracy claimed for this empirical rule for most kinds of iron at these high fields. The qualifying remarks made for the empirical rule in the case of the cosine dipole also apply here.

Other studies on various aspects of cosine quadrupoles include those of Coupland, Simkin, and Randall [2.5.2-a], Asner and Leroy [2.5.2-b], Gilbert, Meuser, Voelker, Kilpatrick, Eaton, Toby, and Acker [2.5.2-c], and Brechna and Perot [2.5.2-d].

REFERENCES, SECTION 2.5.2

2.5.2-a. J.H. Coupland, J. Simkin, and T.C. Randall, *Nucl. Instrum. Methods* **106**, 595 (1973).

2.5.2-b. A. Asner and D. Leroy, in *Proc. 4th Int. Conf. Magnet Technology, Brookhaven, 1972*, p. 164, CONF-720908, 1972.

2.5.2-c. W.S. Gilbert, R.B. Meuser, F. Voelker, R.A. Kilpatrick, W.F. Eaton, F.L. Toby, and R.C. Acker, *IEEE Trans. Nucl. Sci.* **NS-20**, No. 3, 683 (1973).

2.5.2-d. H. Brechna and J. Perot, in *Proc. 3rd Int. Conf. Magnet Technology, Hamburg, 1970*, p. 3, G. Söhngen et al., Editors, Deutsches Elektronen-Synchrotron DESY, Hamburg, 1972.

2.6 Iron Saturation Effects in Quadrupoles With Poles

In quadrupoles whose field shape is determined by the shape of an iron pole such as that described in Sections 2.1 to 2.3, the field in the iron may become considerably larger than it does for a circular cosine quadrupole with the same field gradient. In a quadrupole, the magnitude of the field varies linearly with distance from the center of the quadrupole. The field at a point on the pole surface that is a distance r from the center is given by $B_0'r$, where B_0' is the quadrupole field gradient. The field at the center of the pole profile is given by $B_0'r_0$ (r_0 is the radius of the inscribed circle), while points on the pole surface near the edge of the pole, being much her from the center, will see fields that are as much as twice as large.

As a rough rule for many quadrupoles, the field in the iron, which determines whether appreciable iron saturation effects are present, is given by $2B_0'r_0$. .

For a circular quadrupole with fourfold symmetry, a rough empirical rule is that the iron saturation effects can be described by the b_5 multipole, and $r_0^4b_5$ is a function only of the pole-tip field at the center of the pole, $B_p = B_0'r_0$, or

$$r_0^4b_5 = F(B_p)\,. \tag{2.6-1}$$

Equation (2.6-1) is a rough rule for estimating the iron saturation effects within a factor of 2 or 3. Within this approximation, the field in the iron is determined by the pole-tip field, B_p, and the differences in permeability of various kinds of iron can be neglected.

The function $F(B_p)$ can be found from Table 2.6-I. In Table 2.6-I $r_0^4b_5$, as computed for four different quadrupoles, is shown as a function of B_p. The results in Table 2.6-I may be extrapolated to higher field levels by assuming that $r_0^4b_5$ rises linearly with γ_{max}, where γ_{max} is the value of γ, the inverse permeability, corresponding to the largest field in the iron, which can be estimated as $2B_p$.

The Japan and FNAL magnets in Table 2.6-I are elliptical. However, it was assumed that for rough estimation of the gradient variation, the iron saturation effects can be described by the b_5 multipole.

REFERENCE, SECTION 2.6

2.6-a. G.T. Danby and J.W. Jackson, BNL Internal Report No. GTD/JWJ-2, 1963.

Table 2.6-I

Results for Iron Saturation Effects in Some Iron Pole Dominated Quadrupoles

	CERN [2.4-c]	Japan [2.4-d]	FNAL [2.4-b]	BNL [2.6-a]	FNAL [2.4-b]	BNL [2.6-a]
B_p, kG	8.8	9.0	10.4	10.9	13.0	16.3
$r_0^4b_5/10^{-3}$	0.7	0.3	0.7	0.2	4.0	1.6
r_0, cm	4.4	5.0	4.17	10.2	4.17	10.2
B_0', kG/cm	2	1.8	2.5	1.07	3.12	1.6

2.7 End Effects in Quadrupoles

The results in the previous sections are for the most part two-dimensional results, valid near the longitudinal center of the magnet but not near the ends in the longitudinal direction. If the pole face is adjusted so that b_5 vanishes and the field shape is good near the magnet center, the magnet field may still be unacceptable because of the b_5 contribution due to the edge fields. As pointed out by Taylor [2.7-a], this limits the usefulness of the results found by two-dimensional calculations. It appears likely that three-dimensional results for the edge fields will soon be available. At present, there are several ways to compensate for the edge field effects. These methods require measurement of the integrated fields and are thus outside scope of this report, but some description of them seems warranted.

The relevant magnetic quantity in determining the orbits of the particles passing through a magnet is usually the integrated value of the magnetic field over the longitudinal length of the magnet. It can be shown that the integrated vertical component of the field,

$$\int_{-\infty}^{\infty} B(r,\theta,z)dz\,,$$

also obeys Laplace's equation and can be expanded in multipoles, so that in the median plane

$$\int_{-\infty}^{\infty} dzB(r,\theta,z)=\bar{B}_1(r+\bar{b}_5r^5+\bar{b}_9r^9+\ldots)\,, \tag{2.7-1}$$

and the integrated gradient is then

$$\int_{-\infty}^{\infty} dz\frac{\partial}{\partial r}B(r,\theta,z)=\bar{B}_1(1+5\bar{b}_5r^4+9\bar{b}_9r^8+\ldots)\,, \tag{2.7-2}$$

where $\bar{B}_1$ is the integrated gradient along the central axis of the quadrupole ($r=0$).

For a very long quadrupole, $\bar{b}_5=b_5$, where b_5 is the two-dimensional multipole measured near the longitudinal center. For quadrupoles with the finite iron length L,

$$\bar{b}_5=b_5+\Delta b_5\,, \tag{2.7-3}$$

where Δb_5 represents the contribution due to the ends of the quadrupole.

An estimate of how large Δb_5 is would be useful. Table 2.7-I gives the results of measurements of Δb_5 made by Taylor [2.7-a], Hassenzahl (2.7-b), and Danby and Jackson [2.7-c]. One may propose the empirical rule for the end effect Δb_5,

$$r_0^4\Delta b_5=Er_0/L\,, \tag{2.7-4}$$

where E is a constant that depends only on the geometry of the ends. It can be seen in Table 2.7-I that E varies from -0.062 to $+0.036$ for the quadrupoles measured. Δb_5 appears to be a very sensitive function of the end geometry. Measurements of b_5 along the axis of the magnet [2.7-a, -b] show that b_5 becomes strongly negative just before the end of the magnet and then swings strongly positive just after the end of the magnet. The net Δb_5 is due to the cancellation between these two peaks in b_5 near the end, and this may explain the sensitivity of Δb_5 to the end geometry.

Table 2.7-I

Results for the End Effect in Quadrupoles at Low Fields

	Magnet						
	LASL [2.7-b]	BNL [2.7-c]	BNL [2.7-c]	BNL [2.7-c]	SLAC [2.7-a]	SLAC [2.7-a]	SLAC [2.7-a]
r_0, cm	7.62	10.2	10.2	15.24	19.4	14.0	14.0
b	9.67	6	12	5	6.55	7.27	14.5
$/10^{-2}$	−0.03	0.60	0.60	0.54	0.050	−0.11	0.12
$_5/10^{-2}$	−0.64	0.50	0.28	0.71	−0.23	0.25	−0.015
E*	−0.062	0.030	0.034	0.036	−0.015	0.018	−0.002
$\Delta L_G/2r_0$	0.36	0.5	0.5	–	–	–	–

*E is defined by Eq. (2.7-2)

For purposes of estimating Δb_5, one may use $E=\pm 0.1$ and the empirical rule

$$r_0^4 \Delta b_5 = \pm 0.1 r_0/L \,. \tag{2.7-5}$$

For cosine quadrupoles it is known that the current winding can be adjusted to make $E=0$ [2.7-d to -g].

Using the estimate of the end effects given by Eq. (2.7-5), the length-to-aperture ratio, L/r_0, at which the end effects become troublesome, can be estimated. To obtain a good aperture of $\Delta r_{0.01}/r_0=0.75$, that is, the gradient should not vary by $>1\%$ over 75% of the aperture, then $r_0^4 b_5 \leqslant 6.3\times 10^{-3}$ is required and end effects become appreciable for $L/r_0 \leqslant 8.2$. For the requirement that the gradient should not vary by $>0.1\%$ over 75% of the aperture, end effects become appreciable for $L/r_0 \leqslant 82$.

One method of compensating for the end effects is to choose the pole profile so that b_5, the multipole present near the central region, is not zero but is just the right size to cancel Δb_5, the contribution to the integrated multipole b_5 due to the ends [2.7-h]. This requires experimental knowledge of the size of Δb_5.

A second method is to make $b_5 \simeq 0$ for the central region and to modify the pole profile at the ends so as to cancel Δb_5. This can be done by adding an iron shim on lat end of the pole or by using an adjustable field clamp [2.7-i], or by chamfer- r rounding the end of the pole [2.7-b, -j, -k].

The chamfer on the pole used by Hassenzahl [2.7-b] makes a 45° angle with the flat end of the pole and has the length c. Hassenzahl proposes the empirical rule for the effect of the introduction of the chamfer of a contribution to b_5:

$$b_{5\,\text{chamfer}} = -(1/0.194)(c/r_0)\Delta b_5 \,,$$

so that the chamfer $c/r_0=0.194$ will cancel Δb_5.

Effective gradient length at low fields. The effect of the magnet ends is often described by measuring the effective gradient length ΔL_G of the ends, which is defined by

Table 2.7-II

Effect of Iron Saturation on the Contribution of the Ends to b_5 for a Quadrupole With $r_0 = 10.2$ cm, $L_M/r_0 = 6$ [2.7-c]

	B_p, kG		
	5.4	10.9	16.3
$r_0^4 b_5/10^{-2}$	0.56	0.58	0.71
$r_0^4 \Delta b_5/10^{-2}$	0.5	0.5	0.25
$r_0^4 \bar{b}_5/10^{-2}$	10.6	10.8	0.96
ΔL_G, cm	10.2	9.4	6.35

$$\int_{-\infty}^{\infty} dz \frac{\partial}{\partial r} B(r,\theta,z) = B_1(L + \Delta L_G) . \tag{2.7-6}$$

B_1 is the two-dimensional gradient measured near the longitudinal center of the magnet, and L is the length of the magnet iron. ΔL_G includes the effect of both ends of the magnet. $\Delta L_G/2$ gives the effect of one end if both ends are identical.

Table 2.7-I lists $\Delta L_G/2$ for the quadrupoles for which data were available. On the basis of these data, a rough empirical rule for $\Delta L_G/2$ at low field levels is

$$\Delta L_G/2 = 0.43\, r_0 . \tag{2.7-7}$$

Effect of iron saturation on the end effects. At high field levels, saturation of the iron will affect Δb_5, the contribution to $\bar{b}_5$ due to the ends, and will also affect b_5, the two-dimensional multipole. Table 2.7-II shows the effect of iron saturation on b_5, Δb_5, and $\bar{b}_5$ as a function of B_p, the pole-tip field, for a quadrupole measured by Danby and Jackson. Note the considerable change in $r_0^4 \Delta b_5$, from 0.5×10^{-2} to 0.25×10^{-2}, as B_p goes from 5.4 to 16.3 kG. The variation in $\bar{b}_5$ is much less, because the change in Δb_5 is compensated for by the change in b_5.

Table 2.7-II also shows the effect of iron saturation on the effective gradient length due to the ends: ΔL_G drops from $1.0 r_0$ to $0.62 r_0$ as the pole-tip field varies from 5.4 to 16.3 kG.

The results in Table 2.7-II for Δb_5 can be used for other quadrupoles by scaling them according to the factor r_0/L_M.

All conclusions in this section are based on results for pole-dominated quadrupoles. It seems likely that they apply to cosine quadrupoles.

REFERENCES, SECTION 2.7

2.7-a. E.A. Taylor, in *Proc. 2nd Int. Conf. Magnet Technology, Oxford, 1967*, p. 241, H. Hadley, Editor, Rutherford Laboratory, 1967

2.7-b. W.V. Hassenzahl, in *Proc. 4th Int. Conf. Magnet Technology, Brookhaven, 1972*, p. 469, CONF-720908, 1972.

2.7-c. G.T. Danby and J.W. Jackson, BNL Informal Report No. GTD/JWJ-2, 1963; M.H. Blewett and G.T. Danby, in *Proc. Int. Conf. High Energy Accelerators, Dubna, USSR, 1963*, p. 767, A.A. Kolomensky et al., Editors, Atomizdat, Moscow, 1964.

2.7-d. J.H. COUPLAND, Rutherford Laboratory Report RHEL/R-230, 1970.
2.7-e. F.E. MILLS AND G. MORGAN, *Part. Accel.* **5**, No. 4, 227 (1973).
2.7-f. B.B. GOODMAN, *Nucl. Instrum. Methods* **89**, 4 (1970).
2.7-g. R.B. MEUSER, *IEEE Trans. Nucl. Sci.* **NS-18**, No. 3, 677 (1971).
2.7-h. R. PERIN, CERN Report IBR-MA/70-16; in *Proc. 3rd Int. Conf. Magnet Technology, Hamburg, 1970*, p. 304, G. Söhngen et al., Editors, Deutsches Elektronen-Synchrotron DESY, Hamburg, 1972.
2.7-i. K. HALBACH, *Nucl. Instrum. Methods* **119**, 327 (1974).
2.7-j. A. HARVEY, AND R.D. TURNER, *IEEE Trans. Nucl. Sci.* **NS-18**, No. 3, 892 (1971).
2.7-k. A. HARVEY, in *Proc. 4th Int. Conf. Magnet Technology, Brookhaven, 1972*, p. 456, CONF-720908, 1972.

2.8 SOME QUADRUPOLE REFERENCES

Listed below are some papers on quadrupoles which, in addition to those mentioned earlier, may be of interest in relation to quadrupole design.

Analytical approaches to quadrupole profile design, based on conformal transformations, have been given by, among others, Snowdon [2.8-a], Hardt [2.8-b], Perin [2.8-c], and Jaidane [2.8-d].

Hand and Panofsky [2.8-e] have proposed a rectangular quadrupole (see Figure 2.8-A) for which the linear quadrupole field is an exact solution. An improvement of this quadrupole was proposed by Morpugo [2.8-f to -h], who suggested reducing the amount of unused aperture by adding iron whose surface is everywhere perpendicular to the lines of force, since this does not change the shape of the field. Figure-of-eight quadrupoles, which have smaller horizontal dimensions, were suggested by Wilson [2.8-i] and studied by Asner [2.8-g]; a similar quadrupole was also suggested by Danby [2.8-j].

Studies of quadrupoles have been carried out by Ascolese, Billinge, Edwards, Hanson, Juhala, Maschke, Michelassi, Reardon, and Snowdon [2.8-k], Lou, Hauptman, and Walter [2.8-l], Taylor [2.8-m], and Perin [2.8-n].

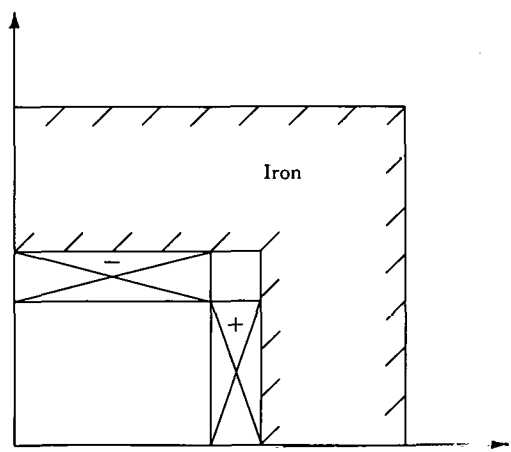

2.8-A. Geometry for Panofsky quadrupole.

REFERENCES, SECTION 2.8

2.8-a. S.C. SNOWDON, *IEEE Trans. Nucl. Sci.* **NS-18**, No. 3, 848 (1971).

2.8-b. W. HARDT, DESY Report DESY-A1.5, 1959.

2.8-c. R. PERIN, CERN Report AR/Int SG/64, 1964.

2.8-d. S. JAIDANE, CEA-R-3238 SACLAY, 1968.

2.8-e. L.N. HAND AND W.K.H. PANOFSKY, *Rev. Sci. Instrum.* **30**, 927 (1959).

2.8-f. M. MORPUGO, CERN 65-34, 1965.

2.8-g. A. ASNER, in *Proc. Int. Symp. Magnet Technology, Stanford University, 1965*, p. 218, H. Brechna and H.S. Gordon, Editors, CONF-650922, 1965.

2.8-h. A. ASNER, G. PETRUCCI, AND L. RESIGOTTI, in *Proc. 2nd Int. Conf. Magnet Technology, O: 1967*, p. 3, H. Hadley, Editor, Rutherford Laboratory, 1967.

2.8-i. E.J.N. WILSON, CERN Report MPS/INT/EP 2-60; CERN Report MPS/EP-29.

2.8-j. G. DANBY AND J. JACKSON, *IEEE Trans. Nucl. Sci.* **NS-14**, No. 3, 414 (1967).

2.8-k. F. ASCOLESE, R. BILLINGE, H. EDWARDS, W. HANSON, R. JUHALA, A. MASCHKE, J. MICHELASSI, P. REARDON, AND S.C. SNOWDON, in *Proc. 4th Int. Conf. Magnet Technology, Brookhaven, 1972*, p. 407, CONF-720908, 1972.

2.8-l. K.H. LOU, J.M. HAUPTMAN, AND J.E. WALTER, *IEEE Trans. Nucl. Sci.* **NS-16**, No. 3, 730 (1969).

2.8-m. E.A. TAYLOR, in *Proc. Int. Symp. Magnet Technology, SLAC, Stanford University, 1965*, p. 208, H. Brechna and H.S. Gordon, Editors, CONF-650922, 1965.

2.8-n. R. PERIN, in *Proc. 3rd Int. Conf. Magnet Technology, Hamburg, 1970*, p. 304, G. Söhngen et al., Editors, Deutsches Elektronen-Synchrotron DESY, Hamburg, 1972.

3. SEXTUPOLES

In a sextupole, the desired magnetic field varies as r^2 across the aperture of the magnet on the median plane, r being the distance from the magnet center. A sextupole field can be generated by a magnet pole shape like that in Figure 3.1-A, in which the pole surface is given by $r^3 \cos 3\theta = \text{const}$, where θ is the azimuthal angle measured from the pole center. However, the $r^3 \cos 3\theta$ pole has to end somewhere, to allow room for the exciting coils, and this limits the quality of the field achieved.

The sextupole often has a 6-fold symmetry, as in Figure 3-A. In this case the symmetry requires that the only multipoles present are b_2, b_8, and b_{14}, and the median plane field can be written as

$$B = \tfrac{1}{2} B_0''(r^2 + b_8 r^8 + b_{14} r^{14} + \ldots),$$
$$B'' = B_0''(1 + 28 b_8 r^6 + 91 b_{14} r^{12} + \ldots), \tag{3-1}$$

where B_0'' is the field second derivative at the center of the sextupole.

The remarks in Section 2 on quadrupoles apply here also. Because of the high symmetry, any sextupole with 6-fold symmetry will have some region in which the field is quadratic, no matter what pole shape is used, since the first undesired multipole is $b_8 r^8$. It is usually possible to choose the pole dimensions to make b_8 vanish, as shown below for the $r^3 \cos 3\theta$ pole and a circular pole.

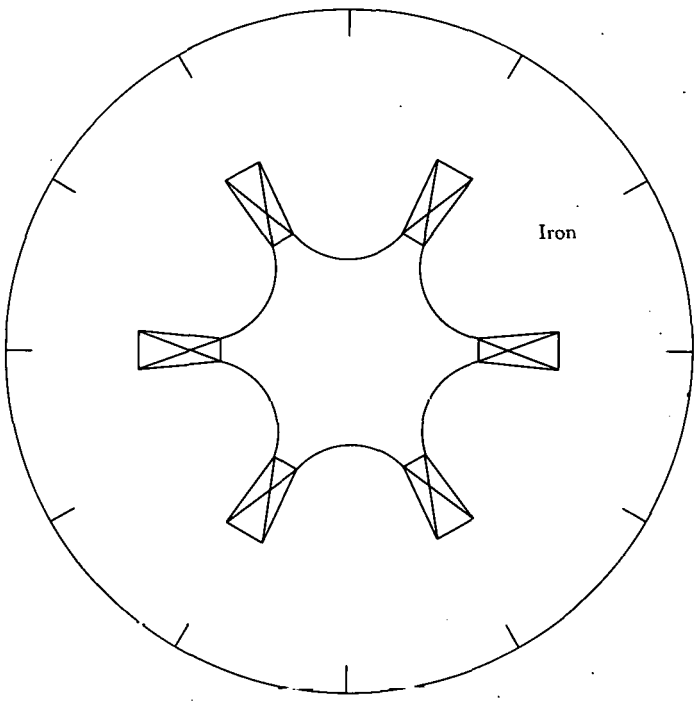

3-A. Geometry of a sextupole.

3.1 Sextupoles With $r^3 \cos 3\theta$ Poles

A sextupole with an $r^3 \cos 3\theta$ pole is shown in Figure 3.1-A. The $r^3 \cos 3\theta$ part of the pole is cut off at the angle $\theta = \theta_1$, where θ is measured relative to the center of the pole. At $\theta = \theta_1$, the pole is continued along a radius from the magnet center. The manner in which the pole is ended is usually not a sensitive factor. The equation of the pole surface may be written as

$$r^3 \cos 3\theta = r_0^3 , \tag{3.1-1}$$

where r_0 is the radius to the center of the pole.

Figure 3.1-B shows how the size of the undesired multipoles b_8 and b_{14} depe on the cutoff angle θ_1. The first undesired multipole, b_8, vanishes at

$$\theta_1 = 18.6^\circ , \quad \theta_1/30^\circ = 0.62 ;$$

$$r_1/r_0 = 1.212 .$$

In Figure 3.1-B, $r_0^6 b_8$ is the field at the pole due to the b_8 multipole relative to that at the pole due to the quadratic term, which is $0.5\, B_0'' r_0^2$. In the same way $r_0^{12} b_{14}$ represents the field at the pole due to the b_{14} multipole.

Also shown in Figure 3.1-B is the good aperture achieved, $\Delta r_{0.01}$, which is defined by requiring that B'' not vary by $>1\%$ in any direction. When b_8 vanishes, the size of $\Delta r_{0.01}$ is limited by the presence of the b_{14} multipole. It can be seen in Figure

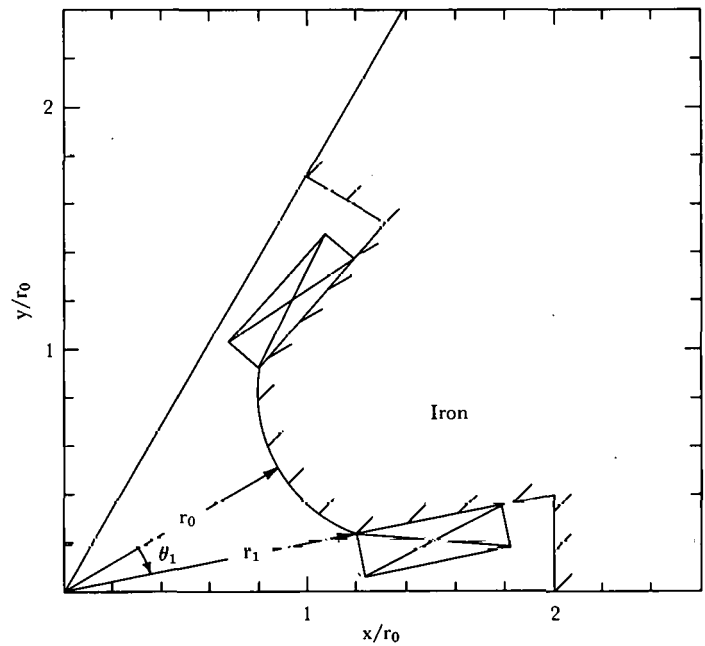

3.1-A. Sextupole with an $r^3 \cos 3\theta$ pole.

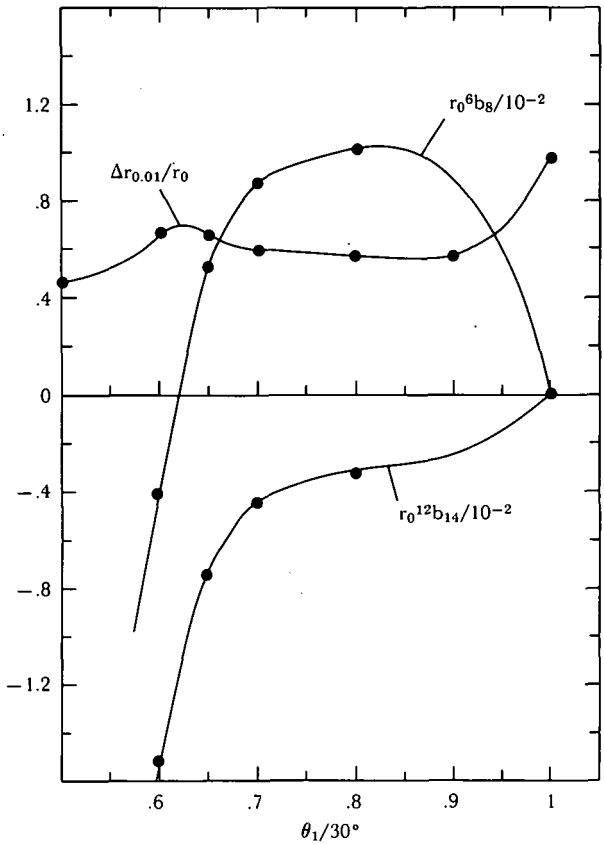

3.1-B. Field multipoles and good aperture for a sextupole with an $r^3 \cos 3\theta$ pole.

3.1-B that for the cutoff angle θ_1 for which b_8 vanishes, a good field aperture of 70% of r_0 can be achieved.

Many of the observations made in Section 2.1 regarding quadrupoles with hyperbolic poles also apply to the sextupole. It has been assumed in the above that the coil is sufficiently hidden by the iron pole that the field quality is not affected. This
e case if no part of the coil is closer to the magnet center than r_1, the radial posi-
of the $r^3 \cos 3\theta$ curve at the cutoff angle θ_1.

Figure 3.1-A represents the case in which the choice of θ_1 makes b_8 vanish.

3.2 Sextupoles With Circular Poles

A sextupole with a circular pole of radius R is shown in Figure 3.2-A. The circle part of the pole is cut off at the angle θ_1, where the pole is continued along a radius tangent to the circle. Since the radius is tangent at $\theta=\theta_1$, R and θ_1 are related by

$$R=r_0 \sin\theta_1/(1-\sin\theta_1)\,. \tag{3.2-1}$$

Figure 3.2-B shows how the multipoles b_8 and b_{14} depend on the cutoff angle of the circle, θ_1. The first undesired multipole, b_8, vanishes at

$$\theta_1=20.55°\,,\quad \theta_1/30°=0.685\,;$$
$$r_1/r_0=1.4428,$$
$$R/r_0=0.5409\,. \tag{3.2-2}$$

Also shown in Figure 3.2-B is the good field aperture $\Delta r_{0.01}$. For the cutoff angle θ_1 that makes b_8 vanish, a good aperture of 66% of r_0 is obtained. This is to be compared with 70% for the $r^3\cos 3\theta$ pole.

Again, as for the $r^3\cos 3\theta$ pole, it has been assumed that the coil is sufficiently hidden by the pole that the field is not greatly affected. This is the case if no part of

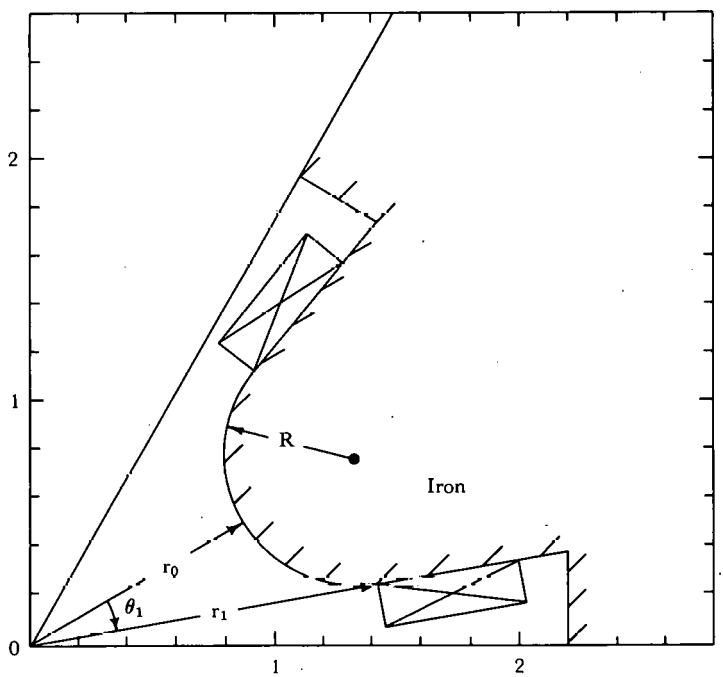

3.2-A. Sextupole with a circular pole.

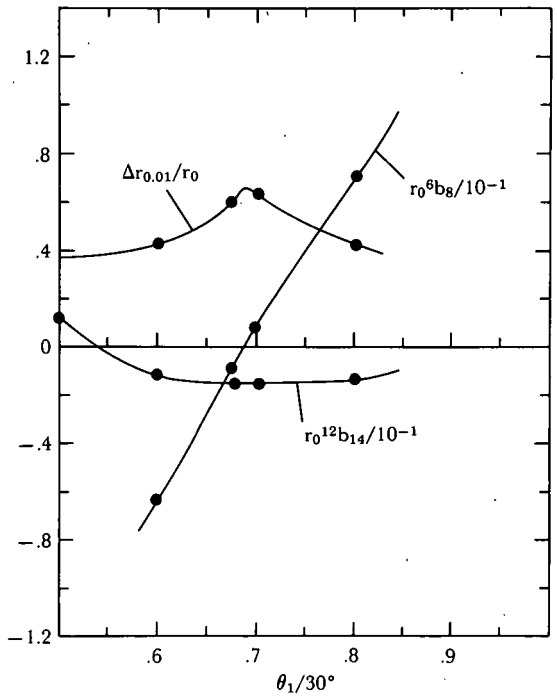

3.2-B. Field multipoles and good aperture for a sextupole with a circular pole.

the coil is closer to the center than r_1, the radial position of the circle at the cutoff angle θ_1.

The pole profile shown in Figure 3.2-A corresponds to the case in which b_8 vanishes.

3.3 Some Sextupole References

A sextupole was studied and built by Satti and Snowdon [3.3-a] at FNAL. The sextupole profile consisted of straight-line segments with $r_0 = 5.08$ cm, the magnet length was 76 cm, and the magnet produced a sextupole field of $B_0'' = 310$ G/cm^2. The design accuracy required was that B'' should not vary by $>0.5\%$ for $r/r_0 \leqslant 0.75$.

Measurements showed that the integrated field departed from a pure sextupole field by 0.22% at $r/r_0 = 0.8$. If it is assumed that this measured field departure was due to the presence of a b_8 multipole, then a good field aperture of $\Delta r_{0.01}/r_0 = 56\%$ was achieved for the integrated field.

A sextupole study was carried out by Ando, Endo, Kihara, Kasuga, Takasaki, and Igarashi [3.3-b] for the Japanese 12-GeV proton accelerator correcting sextupoles. The sextupole profile was made up of a series of circles and straight-line segments with $r_0 = 6.5$ cm. The required sextupole field was $B = 150$ G/cm^2. The design accuracy was $\Delta r_{0.01}/r_0 = 0.88$ in the horizontal direction.

Studies of sextupole magnets were also done by Calymaex [3.3-c].

REFERENCES, SECTION 3.3

3.3-a. J.A. Satti and S.C. Snowdon, *IEEE Trans. Nucl. Sci.* **NS-20**, No. 3, 713 (1973).

3.3-b. A. Ando, K. Endo, M. Kihara, T. Kasuga, E. Takasaki, and T. Igarashi, in *Proc. 5th Int. Conf. Magnet Technology, Rome, 1975*, p. 63, CONF-750444, 1975.

3.3-c. S. Calymaex, in *Proc. 3rd Int. Conf. Magnet Technology, Hamburg, 1970*, p. 187, G. Söhngen et al., Editors, Deutsches Elektronen-Synchrotron DESY, Hamburg, 1972.

4. OCTUPOLES

In an octupole, the desired magnetic field varies as r^3 across the aperture of the magnet on the median plane, where r is the distance from the magnet center. An octupole field can be generated by a magnet pole shape like that in Figure 4.1-A, in which the pole surface is given by $r^4 \cos 4\theta = \text{const}$, where θ is the azimuthal angle measured from the pole center. However, the $r^4 \cos 4\theta$ pole has to end somewhere to allow room for the exciting coils, and this limits the quality of the field achieved.

The octupole often has an 8-fold symmetry, as in Figure 4-A. In this case the ımetry requires that the only multipoles present are b_3, b_{11}, b_{19}, etc., and the ılian plane can be written as

$$B = \tfrac{1}{6} B_0'''(r^3 + b_{11}r^{11} + b_{19}r^{19} + \ldots),$$

$$B''' = B_0'''(1 + 165b_{11}r^8 + 969b_{19}r^{16} + \ldots), \tag{4-1}$$

where B_0''' is the field third derivative at the center of the octupole.

The remarks in Section 2 on quadrupoles apply here also. Because of the high symmetry, any octupole with 8-fold symmetry will have some region in which the field is cubic, no matter what pole shape is used, since the first undesired multipole is $b_{11}r^{11}$. It is usually possible to choose the pole dimensions to make b_{11} vanish, as shown below for the $r^4 \cos 4\theta$ pole and a circular pole.

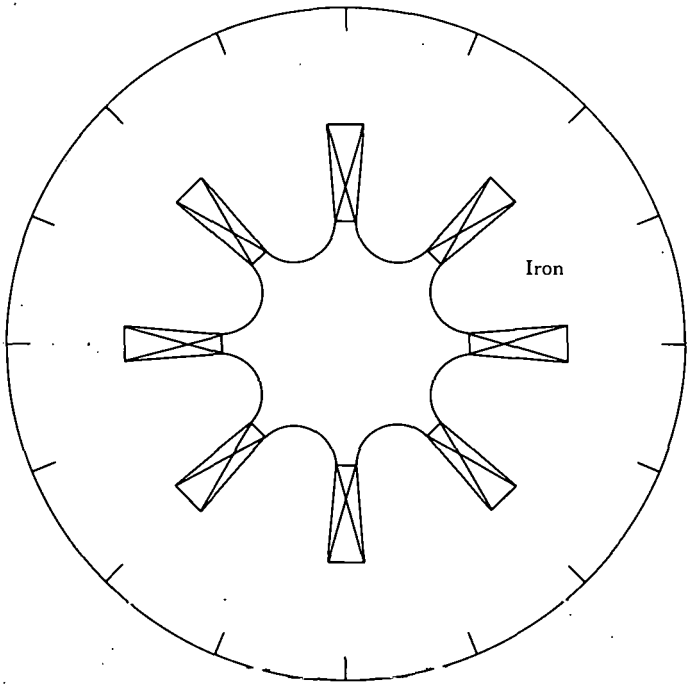

4-A. Octupole geometry.

4.1. Octupoles With $r^4 \cos 4\theta$ Poles

An octupole with an $r^4 \cos 4\theta$ pole is shown in Figure 4.1-A. The $r^4 \cos 4\theta$ part of the pole is cut off at the angle θ_1, where θ is measured relative to the center of the pole. At $\theta = \theta_1$, the pole is continued along a radius from the magnet center. The manner in which the pole is ended is usually not a sensitive factor. The equation for the pole surface may be written

$$r^4 \cos 4\theta = r_0^4 , \tag{4.1-1}$$

where r_0 is the radius to the center of the pole.

Figure 4.1-A shows how the size of the undesired multipoles b_{11} and b_{19} pends on the cutoff angle θ_1. The first undesired multipole, b_{11}, vanishes at

$$\theta_1 = 15.86° , \quad \theta_1/22.5° = 0.705 ;$$

$$r_1/r_0 = 1.223 . \tag{4.1-2}$$

In Figure 4.1-B, $r_0^8 b_{11}$ is the field at the pole due to the b_{11} multipole relative to that at the pole due to the cubic term, which is $\frac{1}{6} B_0''' r_0^3$. Similarly, $r_0^{16} b_{19}$ represents the field at the pole due to the b_{19} multipole.

Also shown in Figure 4.1-B is the good aperture achieved, $\Delta r_{0.01}$, which is defined by requiring that B''' not vary by $>1\%$ in any direction. When b_{11} vanishes, the size of $\Delta r_{0.01}$ is limited by the presence of the b_{19} multipole. It can be seen in Figure 4.1-B that for the cutoff angle θ_1 for which b_{11} vanishes, a good field aperture of 72% of r_0 can be achieved.

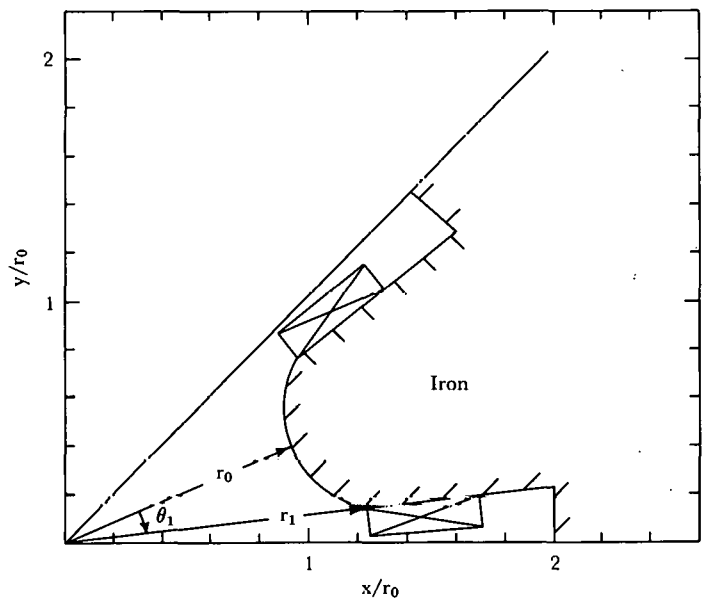

4.1-A. Octupole with an $r^4 \cos 4\theta$ pole.

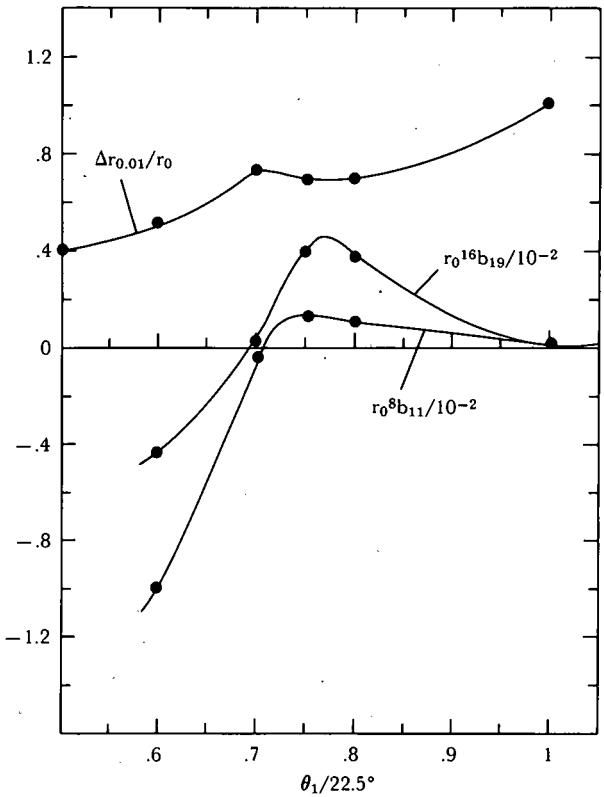

4.1-B. Field multipoles and good aperture for an octupole with an $r^4 \cos 4\theta$ pole.

Many of the remarks on quadrupoles with hyperbolic poles (Section 2.1) also apply to the octupole. It has been assumed in the above that the coil is sufficiently hidden by the iron pole that the field quality is not affected. This is the case if no part of the coil is closer to the magnet center than r_1, the radial position of the $r^4 \cos 4\theta$ curve at the cutoff angle θ_1.

Figure 4.1-A represents the case in which the choice of θ_1 causes b_{11} to vanish.

4.2 Octupoles With Circular Poles

An octupole with a circular pole of radius R is shown in Figure 4.2-A. The circle part of the pole surface is cut off at the angle θ_1, where the pole is continued along a radius tangent to the circle. Since the radius is tangent to the circle at $\theta=\theta_1$, R and θ_1 are related by

$$R=r_0\sin\theta_1/(1-\sin\theta_1)\,. \tag{4.2-1}$$

Figure 4.2-B shows how the multipoles b_{11} and b_{19} depend on the cutoff angle of the circle, θ_1. The first undesired multipole, b_{11}, vanishes at

$$\theta_1=15.3^\circ\,,\quad \theta_1/22.5^\circ=0.680\,;$$

$$r_1/r_0=1.3103\,;$$

$$R/r_0=0.3584\,. \tag{4.2-2}$$

Also shown in Figure 4.2-B is the good field aperture $\Delta r_{0.01}$, which is defined by requiring that B''' not vary by $>1\%$ in any direction. For the cutoff angle θ_1 that makes b_{11} vanish, a good aperture of 63% of r_0 is obtained. This is to be compared with 72% for the $r^4\cos4\theta$ pole.

It has again been assumed that the coil is sufficiently hidden by the pole that the field quality is not affected. This is the case if no part of the coil is closer to the center than r_1, the radial position of the circle at the cutoff angle θ_1.

The pole profile shown in Figure 4.2-A corresponds to the case in which b_{11} vanishes.

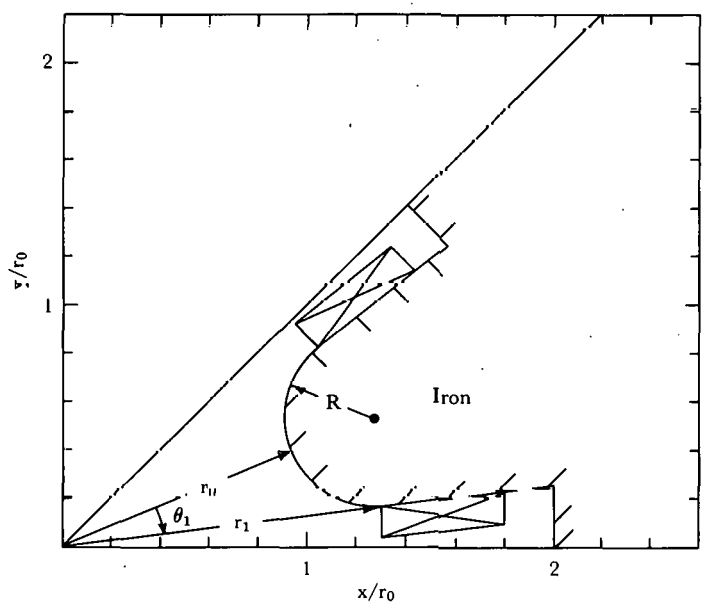

4.2-A. Octupole with a circular pole.

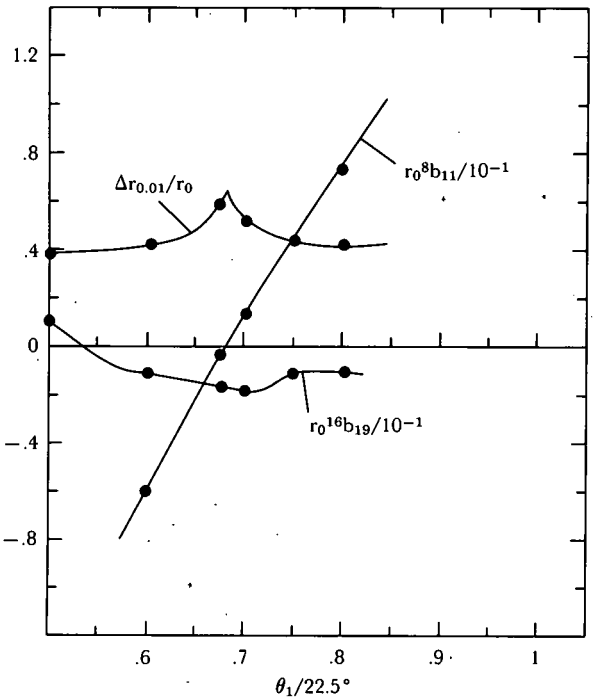

4.2-B. Field multipoles and good aperture for an octupole with a circular pole.

5. SEPTUM MAGNETS

Septum magnets are usually based on the known analytical result that the magnetic field distribution due to the iron and coil geometry shown in Figure 5-A has zero magnetic field outside the septum coil and that the field rises linearly inside the septum coil to a maximum value and is held at that level throughout the aperture. This is exactly true if the iron has infinite permeability and the septum coil is rectangular, completely filling the magnet gap and carrying a uniform current density. Any departure from these conditions produces a leakage field outside the septum coil.

In practice, the leakage field outside the septum is not zero for a numbe reasons, including (a) the iron has finite permeability; (b) a small space between the septum and the iron pole, called the pole clearance space, carries no current; and (c) the septum coil has to be cooled, which may require the presence of cooling holes in the septum.

5.1 Effect of Finite Permeability

The ideal septum is a septum of rectangular cross section that completely fills the gap and has a uniform current distribution. However, even an ideal septum will produce a leakage field if the iron permeability is not infinite. Even at low magnetic field levels, where the permeability of iron is of the order of several thousand, an appreciable leakage field may exist.

Computer studies indicate that the leakage field varies linearly with the inverse permeability, $\gamma\ (=1/\mu)$, and a rough empirical rule for the leakage field, B, at the surface of the septum on the median plane is

$$B/B_0 = -7.8\gamma\,, \tag{5.1-1}$$

where B_0 is the uniform field in the center of the magnet. Thus, for $\mu = 3000$ and $\gamma = 3.3\times10^{-3}$, the leakage field is 0.26%. Equation (5.1-1) is for lower fields, $B_0 \lesssim 10$ kG for conventional irons.

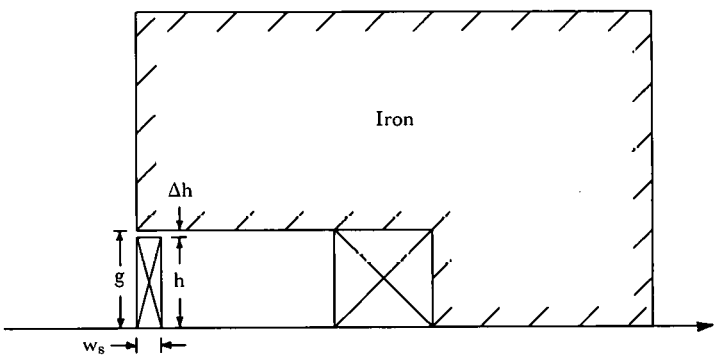

5-A. Septum magnet geometry.

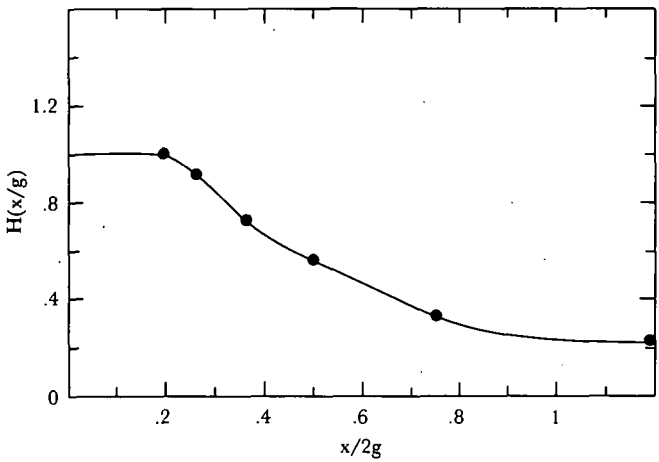

5.1-A. Plot of leakage field versus distance from the septum [see Eq. (5.1-2)]. $2g/w_s = 8$.

The leakage field has the reverse sign from that of the field inside the aperture of the septum magnet. With distance from the septum in the median plane, the leakage drops slowly to zero in about one gap length, or $2g$.

The maximum leakage field occurs off the median plane, at a distance of about $0.5g$, or 25% of the total gap, above the median plane. It is about 50% higher than the median-plane leakage field and depends on the choice of cooling-hole geometry.

For low-field septum magnets, the leakage field depends on the inverse permeability, $\gamma(B_0)$, and on the geometry or g/w_s, the ratio of the half-gap to the septum width. The leakage field is not very sensitive to the g/w_s ratio and thus does not appear in Eq. (5.1-1). The computer studies on which Eq. (5.1-1) is based were done with $2g/w_s = 8$ and $2g/w_s = 4$. The coefficient in Eq. (5.1-1) varies from 7.8 to 7.5 as $2g/w_s$ changes from $2g/w_s = 8$ to $2g/w_s = 4$.

The dependence of the leakage field on the distance from the septum at low magnetic fields may be represented by the empirical result

$$B/B_0 = -7.8\,\gamma H(x/g)\,, \tag{5.1-2}$$

where x is the distance from the septum and the function $H(x/g)$ is given in Figure A. Both the coefficient 7.8 and the function $H(x/g)$ depend on the relative width ne septum $w_s/2g$. However, neither quantity is very sensitive to the $2g/w_s$ ratio. Figure 5.1-A was computed for $2g/w_s = 8$.

The calculations on which the above is based assumed that the permeability was the same throughout the iron at the value corresponding to B_0. Similar results for the leakage field due to the finite permeability have been found by Umstätter [5.1-a].

REFERENCE, SECTION 5.1

5.1-a. H.H. Umstätter, CERN 65-35, 1965.

5.2 Effect of the Pole-Face Clearance Space

In practice, there will be a small clearance space, Δh, between the septum and the iron pole face. This pole-face clearance space has an appreciable effect on the leakage field. Since the ideal septum would produce no leakage field, the clearance space acts like a small current whose direction is opposite to that of the septum current, and produces a leakage field proportional to $\Delta h/g$. Computer studies show that the clearance space produces an additional leakage field, to be added to any leakage field present from other causes, which is given roughly by

$$B/B_0 = -0.22\Delta h/g\,. \qquad (5.2$$

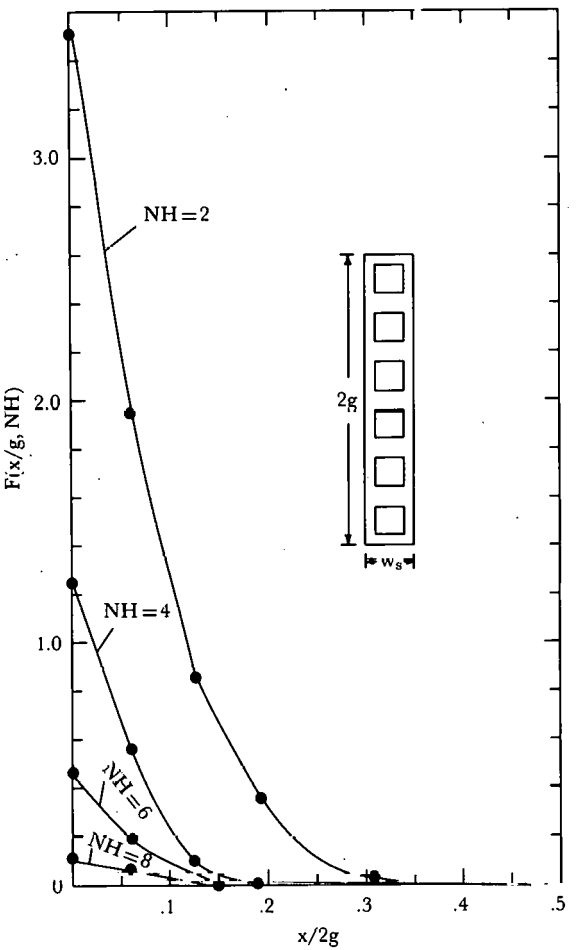

5.3-A. Plot of the leakage field versus distance from the septum for several choices of the total number of cooling holes, NH, for the septum thickness $2g/w_s = 8$ [see Eq. (5.3-1)].

Thus, for a clearance space of $\Delta h = 0.1$ mm and a septum half-gap of $g = 1$ cm, the additional negative leakage field is 0.22%.

5.3 Effect of the Cooling Holes

It is often necessary to depart from the ideal geometry of a rectangular septum in order to provide for the cooling of the septum. One method is to put cooling holes in the septum, as shown in Figure 5.3-A for the case of six holes across the septum. It is known [5.3-a] that the leakage field can be reduced by increasing the number of cooling holes. This can be understood by expressing the magnetic field as the sum of normal modes of the current-free case that are excited by the current distribution. If the current density is made to vary more rapidly across the septum, it will tend to excite the higher modes, which decrease more rapidly outside the septum.

Computer studies indicate that the leakage field depends most strongly on the total number of cooling holes across the septum and the total area of the cooling holes relative to the area of the septum.

The additional leakage field attributable to the cooling holes may be represented by the empirical result

$$\frac{B}{B_0} = -0.08 \frac{A_h}{A_s} F(x/g, NH) , \tag{5.3-1}$$

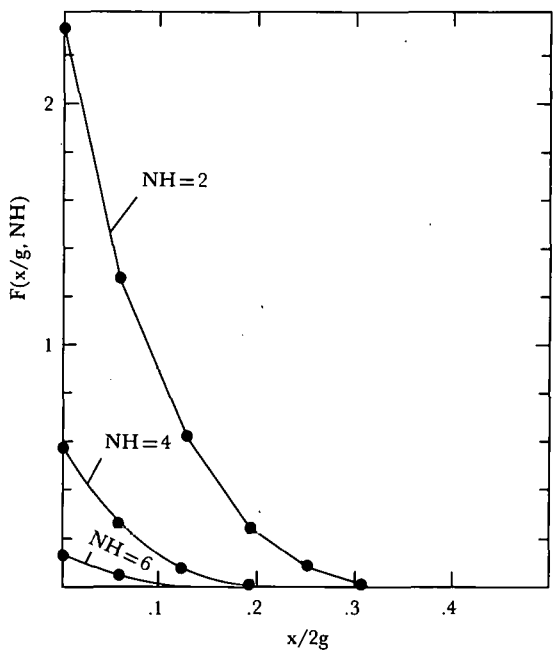

5.3-B. Plot of the leakage field versus distance from the septum for several choices of the total number of cooling holes, NH, for the septum thickness $2g/w_s = 4$ [see Eq. (5.3-1)].

where A_h is the total cross-sectional area of the cooling holes, A_s is the total cross-sectional area of the septum, NH is the total number of holes both above and below the median plane, and $F(x/g, NH)$ is a function given by Figure 5.3-B.

The function $F(x/g, NH)$ also depends to some extent on the relative width of the septum, $w_s/2g$. For this reason $F(x/g, NH)$ is given in Figure 5.3-A for $2g/w_s = 8$, and in Figure 5.3-B for $2g/w_s = 4$.

Assuming a relative area of the cooling holes of $A_h/A_s = 10\%$, the leakage field due to the cooling holes can be reduced to a few tenths of a percent by choosing 6 or 8 cooling holes across the septum.

Note that the leakage field due to other causes, such as the finite permeab[illegible] or the pole-face clearance space, must be added to the leakage field due to the c[illegible] ing holes [Eq. (5.3-1)], and when NH is large enough to eliminate the leakage field due to the holes, the leakage field due to other causes still remains.

The maximum leakage field occurs off the median near the cooling holes and may be about 50% more than the median-plane leakage field, depending on the choice of cooling-hole geometry.

The cooling holes can be arranged so that there is a half-hole at the top and the bottom of the septum. This arrangement was suggested by Umstätter [5.3-a], who pointed out that half-holes partially filled with the conducting material could be used to compensate for the leakage field due to the pole-face clearance space.

REFERENCE, SECTION 5.3

5.3-a. H.H. Umstätter, CERN 65-36, 1965.

5.4 Effect of Conducting Layers in the Septum

The septum may sometimes be constructed of layers of conducting material separated by even thicker layers of nonconducting material. An example is a septum wound from superconducting ribbon [5.4-a] consisting of a thin layer of superconductor between two layers of nonconducting material, with about 85% of the ribbon being nonconducting. Another example would be a septum constructed of a grid of wires, with relatively large nonconducting spaces between the wires.

In this case, most of the septum cross section carries no current. Nevertheless, the leakage field can be reduced to the same level as that of the ideal solid conducting septum by having a sufficient number, usually 50, of conducting layers [5.4

This problem is similar to that of the cooling holes treated in Section 5.3, [illegible] computer studies indicate that the additional leakage field at the surface of the septum caused by the nonconducting layers is given by an equation similar to Eq. (5.3-1):

$$\frac{B}{B_0} = -0.012 \frac{A_h}{A_s} F(NL), \tag{5.4-1}$$

where A_h is the total cross-sectional area of the nonconducting material, A_s is the total cross-sectional area of the septum, NL is the total number of conducting layers both above and below the median plane, and $F(NL)$ is a function given by Figure 5.4-A.

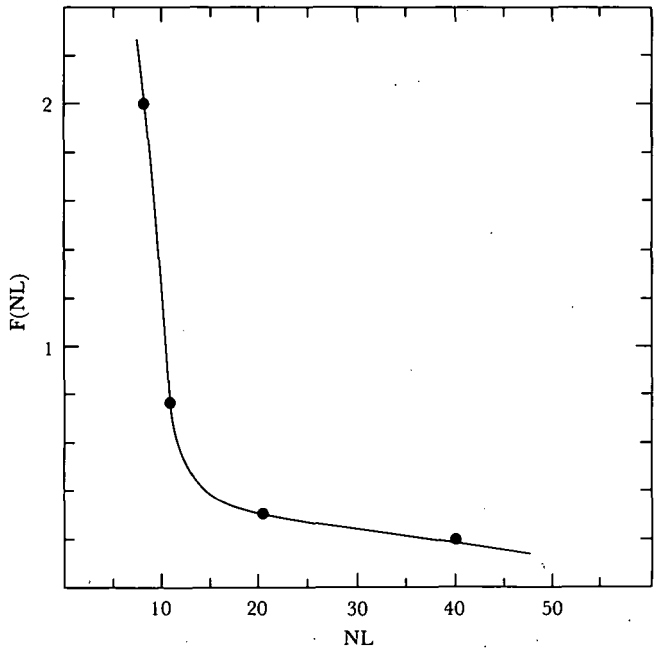

5.4-A. Plot of the leakage field at the surface of the septum versus the number of conducting layers in the septum, NL. [See Eq. (5.4-1).]

The function $F(NL)$ also depends to some extent on the relative width of the septum, $w_s/2g$. However, this dependence is not very strong. Figure 5.4-A was computed for $2g/w_s=5$. Runs done with $2g/w_s=10$ showed little change in the important regions of the curve.

It can be seen from Eq. (5.4-1) that a layered septum with 85% nonconducting material, $A_h/A_s=0.85$, will produce an additional leakage field of $B/B_0 \lesssim 10^{-3}$ if the number of conducting layers is $\gtrsim 40$.

REFERENCES, SECTION 5.4

. H. Hsieh, R. Britton, R. Gibbs, J. Grisoli, and H. Kapfer, in *Proc. 4th Int. Conf. Magnet Technology, Brookhaven, 1972*, p. 157, CONF-720908, 1972.

5.4-b. G. Parzen and K. Jellett, BNL Internal Report No. AADD-168, 1970.

5.5 Some Septum References

A detailed report was written by Umstätter [5.5-a] on two CERN septum magnets that were to operate at 10 and 20 kG and had septums that were either one turn or two turns of the same septum conductor. Each septum had eight cooling holes, computed to give an additional leakage field of $B/B_0 \simeq -0.4 \times 10^{-3}$. With use

of compensation currents and high-μ materials, the leakage field expected was quite small, about $B/B_0 \simeq 5 \times 10^{-4}$ for both magnets. However, because of end effects the integrated leakage field measured was considerably larger – at 20 kG, $B/B_0 \simeq 5 \times 10^{-3}$. This work was partially based on earlier calculations by Umstätter [5.5-b] and Fornel and Umstätter [5.5-c]. Leakages were estimated by analytical calculations that agree roughly with computer results presented in the previous sections. The two septum magnets have a gap of 2 cm and septum widths of 0.3 and 0.61 cm.

A septum magnet with a fairly elaborate system of compensation currents to correct for the leakage field was built and measured by Ratner, Lari, Bywater, and Berril [5.5-d]. The septum gap was 5 cm, the magnet length was 1.2 m, and the septum operated up to about 18 kG. The leakage fields without compensating current correction were computed to be, at 15 kG and at 18 kG, about -6×10^{-3} to -8×10^{-3}; with correction, they would be reduced to -2×10^{-5} and 0.6×10^{-3}. However, because of end effects, the integrated leakage field was measured at 15 kG and 18 kG as 0.3×10^{-3} and 0.6×10^{-3}. The correction system was previously reported on by Lari [5.5-j].

Two septum magnets built for the fast extraction system of the Serpukhov 70-GeV proton synchrotron were reported on by Van Breugel, Cuénot, Hérin, and Kuiper [5.5-e]. These magnets operated at 10 kG and 14 kG, were 1.5 m and 3 m long, and had a gap of 3 cm and septum widths of 0.3 and 0.5 cm. The measured integrated leakage field at the septum surface was found to be 8×10^{-3} at 10 kG and 4×10^{-3} at 14 kG. The emphasis here was on obtaining a uniform field inside the septum of $\Delta B \lesssim 10^{-3}$ over the usable aperture, and this was done by pole shaping. This work was partly based on previous work by Fabiani, Hérin, Indreas, Kuiper, and Milna [5.5-f].

A beam-splitter magnet built and measured at BNL was reported on by Hsieh, Britton, Gibbs, Grisoli, and Kapfer [5.5-g]. The septum was 0.35 in. wide and wound of a superconducting ribbon. The gap was 1 in. and the operating field, 15.5 kG. A model septum magnet using the same kind of septum was measured to have a leakage field of $B/B_0 = 3 \times 10^{-3}$ at 16 kG, compared with the computed value of 5×10^{-3}.

An extractor septum magnet for the Nimrod accelerator (Morgan, Gresham, and Dawson [5.5-h]) had a gap of 7.6 cm and a septum width of 5.7 cm and produced an integrated field of 710 kG-cm. In addition, a uniform gradient was required of about 0.22 kG/cm. The magnet had both an antireluctance correction winding, to correct the leakage field, and a pole-face correction winding, to obtain the desired gradient inside the aperture. An integrated leakage field was measured of 8×10^{-3} with no correction, or 2×10^{-3} when corrected.

Studies of septum magnets have also been carried out by Carrigan, Jagger, Michelassi, Pretzl, Sotti, Snowdon, and Wehman [5.5-i].

REFERENCES, SECTION 5.5

5.5-a. H.H. Umstätter, CERN 65-36, 1965.

5.5-b. H.H. Umstätter, CERN Report MPS/INT RF63-3, 1963.

5.5-c. B.B. Fornel and H.H. Umstätter, CERN Report MPS/INT RF64-18, 1964.
5.5-d. L.G. Ratner, R. J. Lari, J.A. Bywater, and E.C. Berrill, in *Proc. 4th Int. Conf. Magnet Technology, Brookhaven, 1972*, p. 167, CONF-720908, 1972.
5.5-e. H. Van Breugel, R. Cuénot, S. Hérin, and B. Kuiper, *Ibid.*, p. 144.
5.5-f. F. Fabiani, S. Hérin, G. Indreas, B. Kuiper, and S. Milna, in *Proc. 3rd Int. Conf. Magnet Technology, Hamburg, 1970*, p. 1518, G. Söhngen et al., Editors, Deutsches Elektronen-Synchrotron DESY, 1972.
5.5-g. H. Hsieh, R. Britton, R. Gibbs, J. Grisoli, and H. Kapfer, in *Proc. 4th Int. Conf. Magnet Technology, Brookhaven, 1972*, p. 157, CONF-720908, 1972.
5.5-h. R.H.C. Morgan, A.T. Gresham, and J.M. Dawson, in *Proc. 2nd Int. Conf. Magnet Technology, Oxford, 1967*, p. 291, H. Hadley, Editor, Rutherford Laboratory, 1967.
R. Carrigan Jr., J. Jagger, G. Michelassi, K. Pretzl, J. Sotti, S. Snowdon, and A. Wehmann, *IEEE Trans. Nucl. Sci.* **NS-20**, No. 3, 719 (1973).
R. J. Lari, ANL Particle Accelerator Division Internal Reports R JL-2 and R JL-3, 1962.

6. COMBINED-FUNCTION MAGNETS

It is sometimes convenient to combine the fields of a dipole and a quadrupole in the same magnet. Such a magnet is shown in Figure 6.1-A as a C-magnet whose pole face is shaped to give the desired field shape. The magnet can equally well be an H-magnet.

The desired median-plane magnetic field can be written as

$$B = B_0(1 + b_1 x + b_2 x^2) . \tag{6-1}$$

The b_1 multipole represents the desired field gradient and in accelerator usually about $b_1 \simeq 0.04/\text{cm}$; that is, the field is changing at the rate of 4% per centimeter. The b_2 multipole represents a small sextupole term, added to control the variation in the betatron oscillation frequency across the vacuum chamber of an accelerator, which may be about $b_2 \simeq 5 \times 10^{-5}/\text{cm}^2$.

6.1 Pole Profile Design

The pole surface may be divided into three regions: the central region, where the pole is essentially hyperbolic in shape and is designed as if it extended infinitely far in the x-direction; the low field end region, where the pole is terminated so as to extend the good field region as far as possible; and the high field end region, where the pole termination is also influenced by iron saturation effects.

If it is assumed that the pole extends infinitely and is not terminated and that the iron permeability is infinite, then, to reasonable accuracy, the surface of the pole is given by

$$y(1 + b_1 x + b_2 x^2) - \tfrac{1}{6}(b_1/\rho + 2b_2) y^3 = y_0 - \tfrac{1}{6}(b_1/\rho + 2b_2) y_0^3 , \tag{6.1-1}$$

where y_0 is the half-gap height at the magnet center, $x = 0$. Equation (6.1-1) also allows for the possibility that the magnet has a slight curvature in the longitudinal direction and that x in Eq. (6-1) is measured relative to a circle of radius ρ. It can be seen that, neglecting the y^3 and the b_2 terms, this equation is almost the equation for a hyperbole, $y = y_0/(1 + b_1 x)$.

The central part of the pole surface is described by Eq. (6.1-1) and will be called the hyperbolic part of the pole surface. The following questions then arise. How far should the hyperbolic part of the pole extend in order to get a certain good field region? How should the pole be terminated on both the high field side and low field side in order to get the largest good field region for a given pole width? How wide does the pole have to be to get a certain good field region?

The parameters involved are illustrated in Figure 6.1-A. The horizontal aperture required is $\pm a$ around $x = 0$, the magnet center. The required half-gap at $x = 0$ is y_0. The hyperbolic part of the pole, given by Eq. (6.1-1), extends from $x = -x_l$ on the low field side to $x = x_h$ on the high field side, and the corresponding vertical distances to the pole are y_l and y_h. The pole itself extends from $x = -w_l$ to $x = w_h$.

In terms of these parameters, the above questions may be reformulated as follows: What are x_l and x_h, the cutoff points of the hyperbolic part of the pole? What

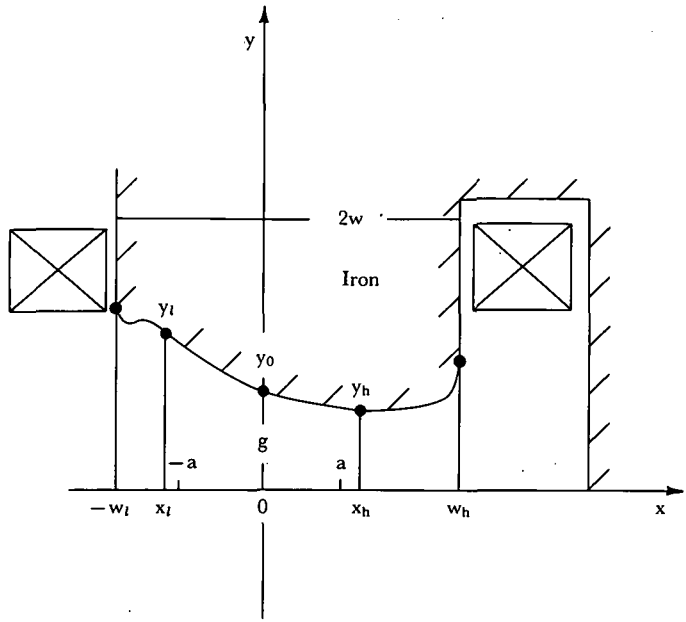

6.1-A. Geometry of a combined-function magnet.

are reasonable values for the ends of the pole, w_l and w_h? And what should be the pole shape in the two termination sections, $x=-x_l$ to $-w_l$ and $x=x_h$ to w_h?

Table 6.1-I summarizes the values of the parameters that were found in building several combined-function magnets, such as the Japanese KEK booster, the ISR at CERN, and the AGS at BNL.

A reasonable assumption about the dependence of x_l, the cutoff point of the hyperbolic region on the low field side, on the good field half-aperture, a, is that

$$x_l=a+\text{const}\,y_l\,, \tag{6.1-2}$$

where y_l is the half-gap at x_l. Similar assumptions can be made for the dependence of w_l, x_h, and w_h on a. Table 6.1-I illustrates how well equations like Eq. (6.1-2) hold for the combined-function magnets listed. The following empirical rule, which is an age of the results given in Table 6.1-I, can be proposed for the choice of the pole meters:

$$\begin{aligned} x_l&=a+0.3\,y_l\,,\\ w_l&=a+0.9\,y_l\,,\\ x_h&=a+0.6\,y_h\,,\\ w_h&=a+3\,y_h\,. \end{aligned} \tag{6.1-3}$$

It is clear that there is no unique choice of the pole parameters, and Eq. (6.1-3) should be regarded as simply a starting point for further study.

Table 6.1-I

Parameters of Several Combined-Function Magnets

	Magnet		
	KEK [6.1-a]	AGS [6.1-b]	ISR [6.1-c]
$(B_0)_{max}$, kG	11.0	13.	12
B_0'/B_0, m^{-1}	3.66	4.25	3.14
b_2, cm^{-2}	-3.1×10^{-5}	0	$-9.8\times$
a, cm	6.5	7.62	8
y_0, cm	3.8	4.44	5
x_l, cm	9.5	10.2	8
y_l, cm	7.4	7.95	6.63
w_l,cm	12.0	13.3	16.0
x_h, cm	8.3	11.4	8
y_h, cm	2.92	2.97	3.98
w_h, cm	15.0	17.8	20.0
x_l, see Eq. (6.1-3)	$a+0.6y_l$	$a+0.3y_l$	a
w_l, see Eq. (6.1-3)	$a+0.75y_l$	$a+0.7y_l$	$a+1.2y_l$
x_h, see Eq. (6.1-3)	$a+0.6y_h$	$a+1.5y_h$	a
w_h, see Eq. (6.1-3)	$a+3y_h$	$a+2y_h$	$a+3y_h$
$2w$, cm	27	31.8	36.0
w/a	2.1	2.1	2.2

Table 6.1-I also shows that the total width of the pole needs to be about twice the good aperture or, more accurately,

$$w/a=2.1\,, \tag{6.1-4}$$

where w is the half-width of the pole.

The remaining question, that of the pole shape in the two termination regions, clearly had to be answered for each of the magnets listed in Table 6.1-I, and the pole-face shape found for each case represents a possible solution [6.1-a to -c]. A study of the low field termination was carried out by Doke, Kihara, and Takeda [6.1-d], and of the high field region, by Kihara and Doke [6.1-e]. The details of the pole terminations may be found in refs. [6.1-a to -c]. A study of the magnet for the DESY electron-synchrotron was carried out by Hardt [6.1-f], and the magnet for the FNAL booster was studied by Billinge, Snowden, and Van Steenbergen [6.1-g]. In the pole design used by Hardt and Snowdon, the procedure of starting from a central hyperbolic region (described above) is not used. The entire pole is designed by an analytic procedure based on conformal mapping.

REFERENCES, SECTION 6.1

6.1-a. K. Takikawa, M. Kumada, and H. Sasaki, KEK Report KEK-75-3, 1975; H. Sasaki, K. Takikawa, M. Kumada, Y. Miyahara, T. Kurosawa, and H. Someya, in *Proc. 5th Int.*

Conf. Magnet Technology, Rome, 1975, p. 68, CONF-750444, 1975; H. SASAKI, K. TAKIKAWA, AND M. KUMADA, in *Proc. 4th Int. Conf. Magnet Technology, Brookhaven, 1972*, p. 372, CONF-720908, 1972.

6.1-b. *AGS Standards Book,* Brookhaven National Laboratory, 1960.

6.1-c. K.N. HENRICKSEN, R. PERIN, S. PICHLER, G. PLUYM, AND L. RESEGOTTI, CERN Report ISR-MAG/66-12, 1966.

6.1-d. T. DOKE, M. KIHARA, AND M. TAKEDA, *Jpn. J. Appl. Phys.* **6**, 403, 1967; KEK Report SJC-A-66-2, 1966.

6.1-e. M. KIHARA AND T. DOKE, KEK Report SJC-A-68-5, 1968.

6.1-f. W. HARDT, UCRL-Trans-1312, 1963.

6.1-g. R. BILLINGE, S.C. SNOWDON, AND A. VAN STEENBERGEN, *IEEE Trans. Nucl. Sci.* **NS-16**, No. 3, 969 (1969).

6.2 IRON SATURATION EFFECTS IN COMBINED-FUNCTION MAGNETS

Figure 6.2-A shows the effects of iron saturation on the uniformity of the field gradient across the aperture of the AGS combined-function magnet. This magnet has a half-gap at the center of $g = 4.44$ cm and a good field aperture of ± 7.5 cm. The magnetic field has been computed [6.2-a] at fields up to 15 kG and measured [6.2-b] at fields up to 13 kG. The AGS magnet has no built-in sextupole term, and the field gradient at low fields is uniform across the aperture. At 15 kG, the field gradient is changing so rapidly across the aperture that essentially no good field aperture is left [6.2-a].

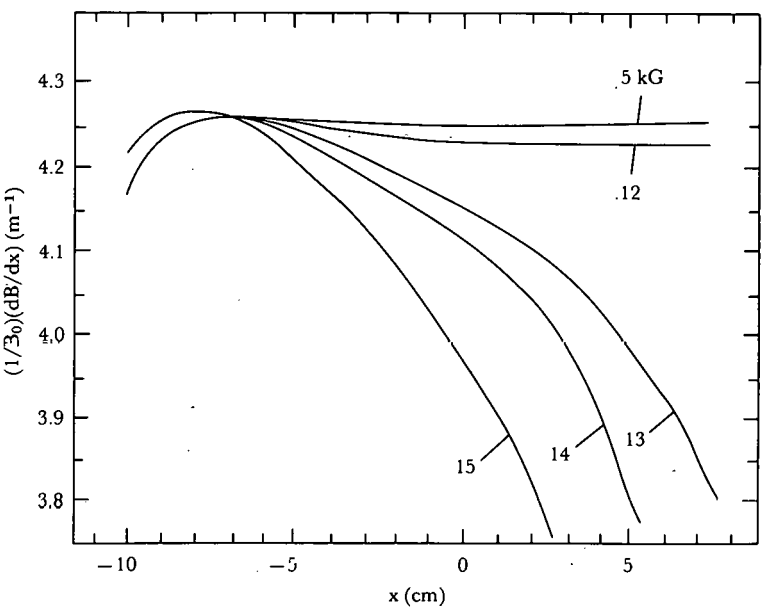

6.2-A. Plot of the field gradient in the AGS combined-function magnet across the aperture and on the median plane for several values of the central field.

Table 6.2-I

Computed Results for the AGS Combined-Function Magnet

[$g=4.44$, $w=15.9$, and $y_h=2.97$ cm; B_p is the effective field in the pole given by Eq. (6.2-3)]

	B_0, kG				
	0.12	5.0	13.0	14.0	15.0
$g\Delta b_1/10^{-2}$	0.00	0.1	−0.4	−0.5	−1.2
$g^2\Delta b_2/10^{-2}$	0.00	0.00	−0.24	−0.28	—
B_p, kG		7.4	19.4	20.9	?

At low fields, where there is no iron saturation effect, the median-plane field is

$$B=B_0(1+b_1x+b_2x^2)\,.$$

At higher field levels, where the iron saturation effect sets in, the median-plane field is

$$B=B_0[1+(b_1+\Delta b_1)x+(b_2+\Delta b_2)x^2+(b_3+\Delta b_3)x^3+\ldots]\,, \qquad (6.2\text{-}1)$$

where Δb_1, Δb_2, etc. indicate the change in these multipoles due to iron saturation effects.

In Table 6.2-I, Δb_1 and Δb_2 are computed for the AGS magnet for fields up to 15 kG. Over most of the field aperture of interest, the effects of iron saturation are described fairly well by just the two multipoles Δb_1 and Δb_2.

It was pointed out in Section 1.4 that for bending magnets the sextupole term due to iron saturation effects was described by the same empirical result as that found for H-magnets. It may also be true here that the sextupole term due to iron saturation effects, Δb_2, in combined-function magnets is given by the same empirical rule as was found for H-magnets, Eq. (1.2.3-2). Thus an empirical rule for Δb_2, good within a factor of ~2, is

$$g^2\Delta b_2 \simeq -F(B_p)\left(\frac{5g}{w}\right)^2 \frac{g}{w+g}\,, \qquad (6.2\text{-}2)$$

where w is the pole half-width, B_p is the effective field in the iron pole, and $F(B_p)$ is a function of B_p only and is given in Table 1.2.3-III.

In this case, B_p is considerably larger than B_0 because of the field gradient. empirical result of B_p indicated by the computed results given in Table 6.2-I is

$$B_p=B_0(g/y_h)\,, \qquad (6.2\text{-}3)$$

where y_h is the half-gap of the pole at the point where the hyperbolic part of the pole terminates at the high field end. For the AGS magnet $g/y_h=1.49$.

In Table 6.2-II, Δb_1 and Δb_2 are computed for the ISR combined-function magnet for fields from 3 to 13 kG, for which the magnet has been measured [6.2-c] and computed [6.2-d]. This magnet has a half-gap at the magnet center of $g=5$ cm and a good field aperture of ± 8 cm. The results are similar to those found for the

Table 6.2-II

Computed Results for the ISR Combined-Function Magnet

[$g=5.0$, $w=18$, and $y_h=3.98$ cm; B_p is the effective field in the pole given by Eq. (6.2-3); Δb_1 and Δb_2 are the changes in these multipoles due to iron saturation]

	B_p, kG				
	3	10	11	12	13
$/10^{-2}$	0	−0.040	−0.055	−0.10	−0.41
$_2/10^{-2}$	0.00	0.00	−0.01	−0.065	−0.15
$_p$, kG	3.8	12.6	13.8	15.1	16.3

AGS magnet. Results are not available at very low fields for this magnet, which introduces a small inaccuracy in the computation of Δb_1 and Δb_2. The ISR has a smaller sextupole, $g^2\Delta b_2$, at 13 kG, which may be partly due to its lower field gradient ($b_1=0.0314$/cm compared with 0.0425/cm for the AGS magnet). The lower gradient produces a lower field in the pole iron and thus a smaller iron saturation effect.

Results are also given in Tables 6.2-I and 6.2-II for Δb_1, the change in gradient due to iron saturation. Because the data available are for magnets having similar gap to pole-width (g/w) ratios, it is not possible to establish an empirical rule for Δb_1. However, Δb_1 is probably given by a relationship of the form

$$g\Delta b_1 = f_1(g/w) f_2(B_p)\,, \tag{6.2-4}$$

where $f_1(g/w)$ is probably some power of g/w, and $f_2(B_p)$ is essentially given by the results for $g\Delta b_1$ in Table 6.2-I. For any magnet that has $w/g \simeq 3.6$, the results in Table 6.2-I should apply.

A careful study of saturation effects was also carried out by Hirose and Sasaki [6.2-e]. Results for the Bonn 2.3-GeV synchrotron magnet are given by Drees [6.2-f]. Studies of combined-function magnets have been carried out by Dorst [6.2-g] and by Colonias and Dorst [6.2-h], Macpherson and Wilson [6.2-i], Bronca, Hamelin, and Jaidane [6.2-j], Jaidane [6.2-k], Hardt [6.2-l], Perin [6.2-m], and Asner, Holsinger, and Iselin [6.2-n].

REFERENCES, SECTION 6.2

6.2-a. P.F. Dahl and G. Parzen, in *Proc. 5th Int. Conf. High Energy Accelerators, Frascati, Italy, 1965*, p. 165, M. Grilli, Editor, Comitato Nazionale per l'Energia Nucleare, Rome, 1966.

6.2-b. J. Palmer and R.H. Phillips, BNL Internal Memorandum, 1959; R.H. Phillips, BNL Internal Memorandum, 1959; M.H. Blewett, BNL Internal Memorandum, 1958; M.H. Blewett, BNL Internal Memorandum, 1959.

6.2-c. K.N. Henricksen, R. Perin, S. Pichler, G. Pluym, and L. Resegotti, CERN Report ISR-MAG/66-12, 1966.

6.2-d. R. Perin and S. van der Meer, CERN 67-6, 1967.

6.2-e. T. Hirose and H. Sasaki, KEK Report S JC-A-69-3, 1969.

6.2-f. J. Drees, in *Proc. 2nd Int. Conf. Magnet Technology, Oxford, 1967*, p. 276, H. Hadley, Editor, Rutherford Laboratory, 1967.
6.2-g. J.H. Dorst, in *Proc. Int. Symp. Magnet Technology, SLAC, Stanford University, 1965*, p. 182, H. Brechna and H.S. Gordon, Editors, CONF-650922, 1965.
6.2-h. J.S. Colonias and J.H. Dorst, *Ibid.*, p. 188.
6.2-i. G. Macpherson and E. J.N. Wilson, in *Proc. 2nd Int. Conf. Magnet Technology, Oxford, 1967*, p. 114, H. Hadley, Editor, Rutherford Laboratory, 1967.
6.2-j. G. Bronca, J. Hamelin, and S. Jaidane, in *Proc. Int. Symp. Magnet Technology, SLAC, Stanford University, 1965*, p. 96, H. Brechna and H.S. Gordon, Editors, CONF-650922, 1965.
6.2-k. S. Jaidane, SACLAY Report GES. 65-09 AI 22, 1965.
6.2-l. W. Hardt, DESY Report DESY-A1.5, 1954.
6.2-m. R. Perin, CERN Report AR/INT. SG/64-12, 1964.
6.2-n. A. Asner, R. Holsinger, and Ch. Iselin, *IEEE Trans. Nucl. Sci.* **NS-20**, No. 3, 703 (1

6.3 End Effects in Combined-Function Magnets

End effects in combined-function magnets can contribute appreciably to the effective value of the various field multipoles. The relevant magnetic quantity in determining the orbits of the particles passing through the magnets is usually the integrated value of the magnetic field over the longitudinal length of the magnet. If

$$\bar{B}(x,y)=\int_{-\infty}^{\infty} dz B(x,y,z)\ ,$$

then we write in the median plane ($y=0$)

$$\bar{B}=\bar{B}_0(1+\bar{b}_1 x+\bar{b}_2 x^2+\ldots) \tag{6.3-1}$$

and

$$\bar{B}'=\bar{B}_0(\bar{b}_1+2\bar{b}_2 x+\ldots)\ , \tag{6.3-2}$$

where $\bar{B}_0$ is the integrated field along the central axis of the magnet ($x=0$).

The effect of the magnet ends is often described by measuring the effective dipole length ΔL_B of the ends, which is defined by

$$\bar{B}(x,0)=B(x,0)(L_M+\Delta L_B)\ , \tag{6.3-3}$$

where $B(x,y)$ is the two-dimensional field valid near the longitudinal center of the magnet and L_M is the length of the magnet iron. ΔL_B is measured on the median plane, $y=0$, and for various values of x so that $\Delta L_B=\Delta L_B(x)$. The contribution of the ends to $\bar{b}_1$ can be computed from $\Delta L_B(x)$. If Eq. (6.3-1) is expanded in powers of x

$$\begin{aligned}\bar{B}&=B_0(1+b_1 x+b_2 x^2+\ldots)[L_M+\Delta L_B(0)+\Delta L_B' x\ldots]\\&=B_0[L_M+\Delta L_B(0)][1+(b_1+\Delta L_B'/L_M)x+\ldots]\ ,\end{aligned} \tag{6.3-4}$$

where b_1 and b_2 are the two-dimensional multipoles valid near the longitudinal center of the magnet and $\Delta L_B'=d(\Delta L_B)/dx$. Note that $\bar{B}_0=B_0[L_M+\Delta L_B(0)]$. Thus if we write $\bar{b}_1=b_1+\Delta b_1$, where Δb_1 is the contribution of the ends to $\bar{b}_1$, we find

$$\begin{aligned}\Delta b_1&=\Delta L_B'/L_M\ ,\\ \Delta b_2&=\tfrac{1}{2}\Delta L_B''/L_M+b_1\Delta L_B'/L_M\ .\end{aligned} \tag{6.3-5}$$

Another measurement often made to describe the effect of the magnet ends is that of the effective gradient length ΔL_G of the ends, which is defined by

$$\bar{B}'(x,0) = B'(x,0)(L_M + \Delta L_G) \,. \tag{6.3-6}$$

ΔL_G is also measured as a function of x on the median plane, and the contribution of the ends to $\bar{b}_1$ and $\bar{b}_2$ can be computed from $\Delta L_G(x)$. If Eq. (6.3-6) is expanded in powers of x,

$$\begin{aligned}
\bar{B}' &= B_0(b_1 + 2b_2x + \ldots)[L_M + \Delta L_G(0) + \Delta L_G' x + \ldots] \\
&= B_0[L_M + \Delta L_B(0)](b_1 + 2b_2x + \ldots)[1 + (\Delta L_G - \Delta L_B)/L_M + \Delta L_G'/L_M x + \ldots] \\
&= B_0[L_M + \Delta L_B(0)]\{b_1[1 + (\Delta L_G - \Delta L_B)]/L_M \\
&\quad + 2b_2[1 + (\Delta L_G - \Delta L_B)]/L_M x + b_1 \Delta L_G'/L_M x + \ldots\} \,.
\end{aligned} \tag{6.3-7}$$

Thus if we write $\bar{b}_1 = b_1 + \Delta b_1$ and $\bar{b}_2 = b_2 + \Delta b_2$, where Δb_1 and Δb_2 are the contributions of the ends to $\bar{b}_1$ and $\bar{b}_2$, we find

$$\begin{aligned}
\Delta b_1 &= b_1(\Delta L_G - \Delta L_B)/L_M \,; \\
\Delta b_2 &= b_2(\Delta L_G - \Delta L_B)/L_M + \tfrac{1}{2} b_1 \Delta L_G'/L_M \,.
\end{aligned} \tag{6.3-8}$$

Table 6.3-I lists the results for ΔL_B, ΔL_G, Δb_1, and Δb_2 for the AGS and ISR combined-function magnets at 5 kG. For the AGS, Δb_1 and Δb_2 were measured [6.3-a] by using long coil measurements, and L_B was also measured. ΔL_G, $\Delta L_G'$, and $\Delta L_B'$ were then computed by using Eqs. (6.3-7) and (6.3-8). For the ISR, ΔL_B, ΔL_G, $\Delta L_B'$, and $\Delta L_G'$ were measured [6.3-b] and Δb_1 and Δb_2 were computed by using the same equations. In computing Δb_1 and Δb_2, the ISR magnet was assumed to be 200 cm long.

Table 6.3-I

Results for the End Effects in Two Combined-Function Magnets at Low Fields

	Magnet	
	AGS [6.3-a]	ISR [6.3-b]
L_M, cm	190	200
g, cm	4.44	5.0
b_1, cm^{-1}	0.0425	0.0314
$b_2/10^{-5}$, cm^{-2}	0	−9.8
$\Delta b_1/b_1$, cm^{-1}	−0.02	−0.04
$\Delta b_2/10^{-5}$, cm^{-2}	−2.6	−3.9
$\Delta L_B/2g$, cm	1.22	1.5
$\Delta L_G/2g$, cm	0.8	0.7
$\Delta L_B'/2$	−0.08	−0.12
$\Delta L_G'/2$	−0.25	−0.23

Note that ΔL_B and ΔL_G include the effects of both ends. If both ends contribute about equally, then $\Delta L_B/2$ and $\Delta L_G/2$ give the effects of one end.

Using the results in Table 6.3-I, one may propose the following empirical rule for ΔL_B, ΔL_G, Δb_1, and Δb_2:

$$\Delta L_B/2 = 1.4g\ ;$$

$$\Delta L_G/2 = 0.75g\ ;$$

$$\Delta b_1/b_1 = -0.65g/L_M\ ;$$

$$\Delta b_2 = -0.25\, b_1/L_M\ . \tag{6.3-9}$$

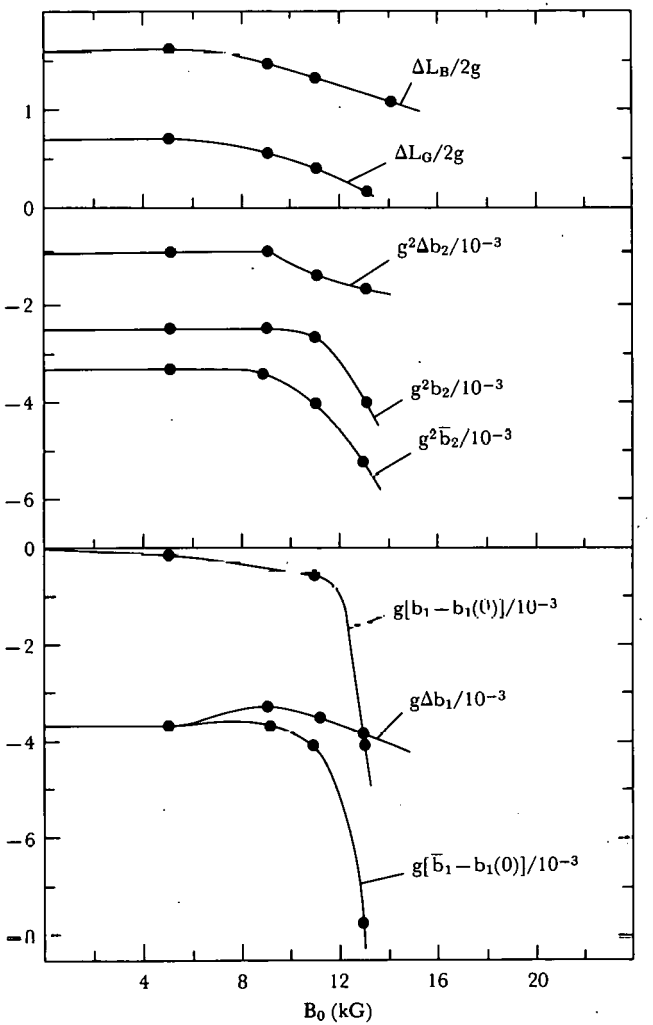

6.3-A. End effect on the multipoles b_1 and b_2 and on the effective lengths ΔL_B and ΔL_G for the ISR combined-function magnet.

It is clear that ΔL_B, the effective dipole length, must depend on the thickness of the coils at the magnet ends. However, this dependence does not seem very strong in the case of the AGS magnet. The coil extends past the end of the iron by 15.2 cm or by $3.4g$, yet the coil increases the effective length by only 40%. A coil of zero thickness gives an effective length $\Delta L_B/2 = g$.

The empirical results obtained for Δb_1 and Δb_2 are for two rather similar magnets, the AGS and ISR combined-function magnets, and thus can be expected to be valid for magnets similar to these two.

It is of interest that a very appreciable sextupole term is introduced by the ends of the magnet.

Effect of iron saturation. The above results for the end effects, ΔL_B, ΔL_G, Δb_1, Δb_2, are valid at low field levels. At higher fields, the end effects will change because of iron saturation.

For the ISR combined-function magnet, $\Delta L_B/2$, the contribution of one end of the magnet to the effective length, varies from 1.5 to $1.16g$, from low fields to 13 kG, or a change of 23%. For the same magnet $\Delta L_G/2$ varies from 0.68 to $0.14g$, from low fields to 14 kG, or a change of 80%.

Figure 6.3-A shows the effect of iron saturation on Δb_2 and Δb_1, the contribution of the ends to the integrated multipoles $\bar{b}_2$ and $\bar{b}_1$ for the ISR magnet which has $L_M = 200$, $g = 5$, and $w = 15.9$ cm. This figure also shows the contribution of the central part of the magnet, which is given by the two-dimensional multipoles b_1 and b_2; $b_1(0)$ is the low field gradient built into the magnet profile.

The results for Δb_2 and Δb_1 in Figure 6.3-A can be used for other combined-function magnets with a similar g/w ratio by scaling the results according to the factor g/L_M. If the g/w ratio changes, then Δb_1 and Δb_2 probably get smaller by some power of (g/w), as found in Section 1 for bending magnets, where the relevant factor was $(g/w)^2$. However for combined-function magnets, the power of (g/w) involved has not yet been established.

$\Delta L_B/2g$ and $\Delta L_G/2g$ are also shown in Figure 6.3-A as a function of field.

REFERENCES, SECTION 6.3

6.3-a. J. Palmer and R.H. Phillips, BNL Internal Memorandum, 1959; R.H. Phillips, BNL Internal Memorandum, 1959; M.H. Blewett, BNL Internal Memorandum, 1958; M.H. Blewett, BNL Internal Memorandum, 1958; P.F. Dahl and G. Parzen, in *Proc. 5th Int. Conf. High Energy Accelerators, Frascati, Italy, 1965*, p. 165, M. Grilli, Editor, Comitato Nazionale per l'Energia Nucleare, Rome, 1966; P.F. Dahl and G. Parzen, BNL Internal Report AADD-49, 1964.

6.3-b. K.N. Henricksen, R. Perin, S. Pichler, G. Pluym, and L. Resegotti, CERN Report ISR-MAG/66-12, 1966.

7. ELECTROSTATIC SEPTUMS

If a very thin septum is required, one solution is to use an electrostatic rather than a magnetic septum. The electrostatic septum (see Figure 7-A) is often made of a thin conducting wire like tungsten, and the septum and box are at ground potential, whereas the cathode is at a potential V below ground, generating a horizontal electric field between the septum and the cathode.

The problem is to choose the dimensions of cathode and box that will give sufficiently uniform electric field between septum and cathode and a sufficiently large vertical aperture in which the field shape is acceptable. It appears desirable to keep the vertical dimensions small so that the tension required to keep the wires straight vertically will not be too great.

7.1 A Simple Cathode

A possible cathode, shown in Figure 7-A, consists of a flat surface of half-height A, terminated by a circular surface of radius R. The cathode is a distance g from the septum and a distance B from the box in the vertical direction.

Tables 7.1-I and 7.1-II give the results of a computer study on the effect of the choice of A/g, R/g, and B/g on the field quality. The field properties listed are $\Delta E/E_0$, the percentage variation in the electric field between the septum and cathode on the median plane; $\Delta y_{0.01}$, the vertical half-aperture defined by requiring the electric field not to vary by $>1\%$; $\Delta y_{0.05}$, the vertical half-aperture allowing a 5% variation in the electric field; and E_{max}/E_0, the largest electric field found in the box.

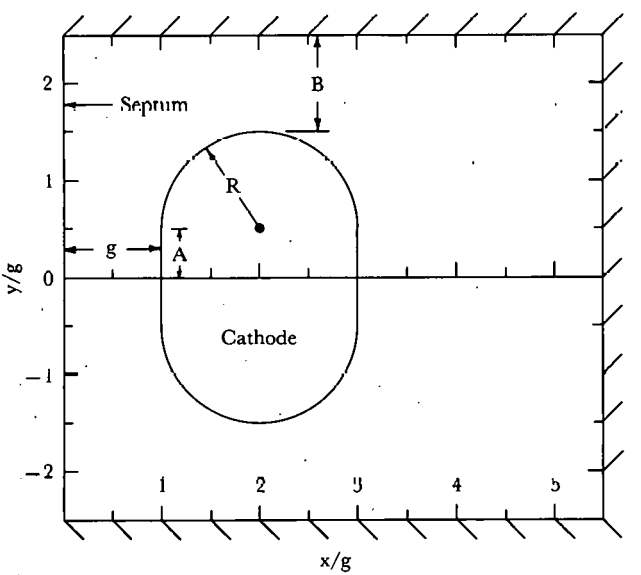

7-A. Electrostatic septum geometry.

Table 7.1-I

Computed Results for Electrostatic Septums

	R/g:	1	1	1	1	1
	B/g:	3	3	3	3	2
	A/g:	3	2	1.5	1	3
$\Delta E/E_0/10^{-2}$		0.002	0.06	0.3	1.6	0.002
$\Delta y_{0.01}/g$		2.3	1.3	0.8	0.5	2.3
$\Delta y_{0.05}/g$		2.9	1.9	1.4	0.94	2.9
x/E_0		1.14	1.14	1.14	1.14	1.14
	R/g:	0.5	0.5	0.5	0.5	0.5
	B/g:	3	3	3	2	2
	A/g:	2	1.5	1	2	1.5
$\Delta E/E_0/10^{-2}$		0.11	0.52	2.5	0.11	0.53
$\Delta y_{0.01}/g$		1.2	0.74	0.4	1.2	0.73
$\Delta y_{0.05}/g$		1.7	1.2	0.8	1.7	1.2
E_{max}/E_0		1.22	1.22	1.22	1.22	1.22
	R/g:	0.25	0.25			
	B/g:	3	3			
	A/g:	2	1			
$\Delta E/E_0/10^{-2}$		0.16	3.6			
$\Delta y_{0.01}/g$		1.06	0.34			
$\Delta y_{0.05}/g$		1.69	0.69			
E_{max}/E_0		1.45	1.52			

Table 7.1-II

Computed Results for Electrostatic Septums, Showing Effect of Varying B/g

	R/g:	1	1	1	1
	A/g:	2	2	2	2
	B/g:	3	2	1	0.5
$\Delta E/E_0/10^{-2}$		0.06	0.07	0.08	0.09
$\Delta y_{0.01}/g$		1.33	1.32	1.29	1.24
$\Delta y_{0.05}/g$		1.90	1.88	1.04	1.78
$/E_0$		1.14	1.14	1.15	2.05

Figure 7.1-A plots $\Delta y_{0.01}$, $\Delta y_{0.05}$, and $\Delta E/E_0$ against A, the half-height of the flat region, for various values of the radius R of the circular region. All lengths are in terms of g, the septum-to-cathode horizontal distance, since the solutions found can be scaled to any choice of g.

As shown later, the field results are almost independent of the choice of B, the vertical distance from the cathode to the box, provided that $B/g \geqslant 1$. The results in Figure 7.1-A assume that $B/g \geqslant 1$.

As an example of the use of the data in Table 7.1-I and Figure 7.1-A, let us assume that a field uniformity from septum to cathode of $\Delta E/E_0 = 0.01$ is required.

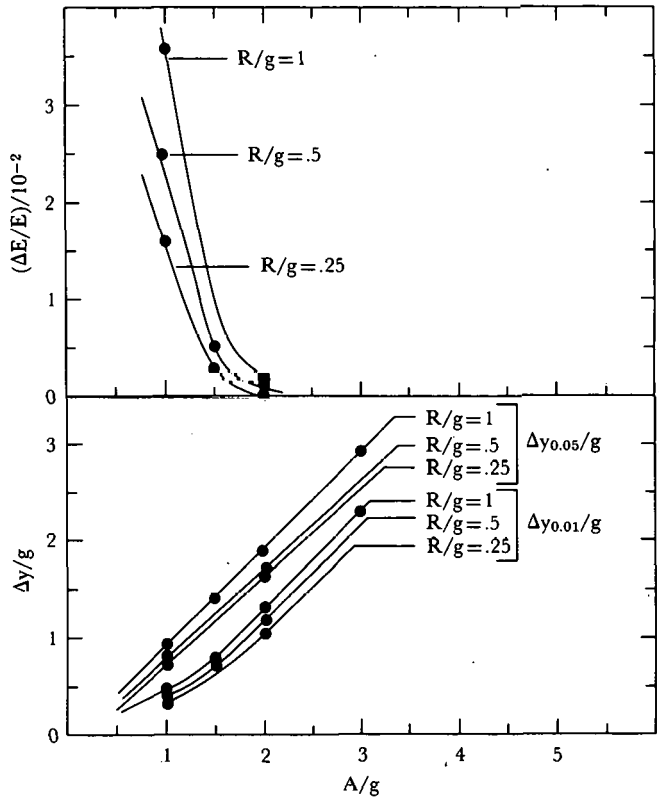

7.1-A. Dependence of the field variation and good aperture on the choice of geometry for an electrostatic septum. $B/g \geqslant 1$.

Using Figure 7.1-A for each value of R/g, the smallest A/g that gives $E/E_0 = 0.01$ is found. In Figure 7.1-B the $(R+A)/g$ so found is plotted versus R/g. $(R+A)/g$ is plotted rather than A/g because $(R+A)/g$ indicates the vertical dimension of the cathode.

If a further requirement is a vertical good field aperture of $\Delta y_{0.01}/g = 0.8$ the required parameters of $R/g = 1$, $A/g = 1.5$, and $(R+A)/g = 2.5$ can be found in Figure 7.1-B. Choosing $B/g = 1$, the vertical half-height of the septum is $2.5g$.

In Figure 7.1-C, E_{max}/E_0 and $\Delta y_{0.01}$ are plotted against B/g for the case in which $A/g = 2$, $R/g = 1$. It can be seen that the results are independent of B/g if $B/g \geqslant 1$. Below $B/g = 1$, E_{max}/E_0 starts to increase steeply.

7.2 A Shimmed Cathode

The region of uniform field can be increased in the vertical direction by shimming the cathode, as was done in Section 1 for the H-magnet. One such solution,

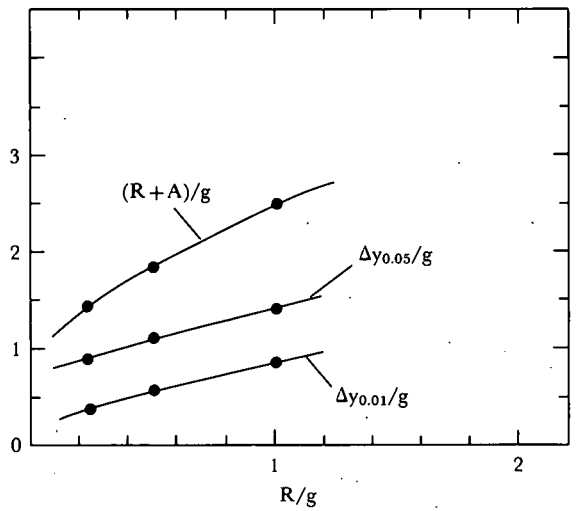

7.1-B. Plot of the cathode length and the vertical good aperture versus the cathode radius to give a field variation of $\Delta E/E_0 = 0.01$; $B/g \geqslant 1$.

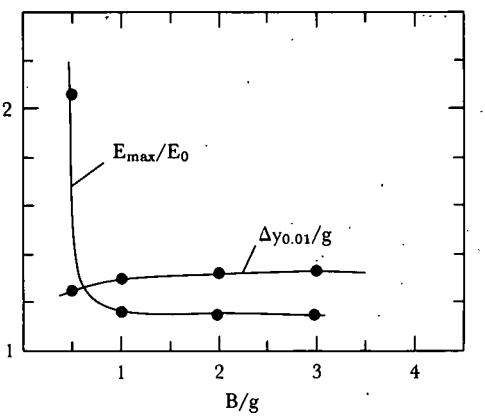

7.1-C. Dependence of the maximum electric field and the vertical good aperture on the choice of B, the cathode-to-ground-shield distance. $A/g = 2$; $R/g = 1$.

proposed by Snowdon [7.2-a], is shown in Figure 7.2-A. All dimensions are in units of g. This cathode has a vertical half-height of $1.6g$, and the vertical good half-aperture is $\Delta y_{0.05} = 1.25g$.

Whether or not it pays to shim the cathode depends on how much vertical aperture is required. For example, if for a cathode size of $1.5g$, the vertical half-aperture of $\Delta y_{0.01}/g = 0.8$ is acceptable, then the simple cathode designed in Section

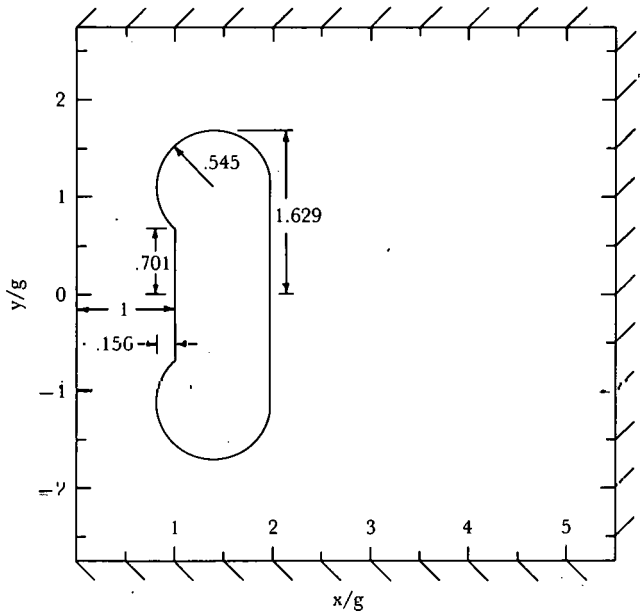

7.2-A. Geometry of a shimmed cathode for an electrostatic septum.

7.1 will do. If more vertical aperture is needed without an increase in the cathode size, then shimming may be necessary.

REFERENCE, SECTION 7.2

7.2-a. S.C. Snowdon, Private communication, 1974.